

**Characterization of
Ambra1 heterozygous mice as
genetic mouse model
of female-specific autism**

Dissertation

for the award of the degree

“**Doctor of Philosophy**”

Division of Mathematics and Natural Sciences

of the Georg-August-Universität Göttingen

within the doctoral program (GGNB program)

of the Georg-August University School of Science (GAUSS)

submitted by

Anes Ju

born in

Seoul, Republic of Korea

Göttingen 2016



Members of the thesis committee

Prof. Dr. Dr. Hannelore Ehrenreich, Reviewer
Clinical Neuroscience
Max Planck Institute of Experimental Medicine, Göttingen

Dr. Kamal Chowdhury, Reviewer
Department of Molecular Developmental Neurobiology
Max Planck Institute for Biophysical Chemistry, Göttingen

Prof. Dr. Thomas Bayer
Division of Molecular Psychiatry
University Medical Center Göttingen, Göttingen

Dr. Oliver Schlüter
Molecular Neurobiology
European Neuroscience Institute, Göttingen

Further members of the examination board

Prof. Dr. Nils Brose
Department of Molecular Neurobiology
Max Planck Institute of Experimental Medicine, Göttingen

Prof. Klaus-Armin Nave, Ph.D.
Department of Neurogenetics
Max Planck Institute of Experimental Medicine, Göttingen

Prof. Dr. Ralf Heinrich
Department of Cellular Neurobiology
Institute of Zoology, Georg-August-University, Göttingen

Date of the oral examination: 12th.September.2016

DECLARATION

I hereby declare that this thesis entitled “**Characterization of *Ambra1* heterozygous mice as genetic mouse model of female-specific autism**” has been written independently, with no other aids than those quoted.

Anes Ju
July, 2016
Göttingen, Germany

Table of Contents

Table of Contents	IV
Summary	VII
1 Introduction	1
1.1 Autism spectrum disorder	1
1.1.1 Genetics of autism spectrum disorder	1
1.1.2 Sex differences in autism spectrum disorder	2
1.1.3 ASD and Brain enlargement	3
1.1.4 Comorbidity of seizure in autism	3
1.1.5 Genetic mouse model of autism	4
1.2 Ambra1	4
1.2.1 Mutation of <i>Ambra1</i>	5
1.2.2 Function of Ambra1	6
1.2.2.1 Role of Ambra1 on the autophagic pathway	6
1.2.2.2 Role of Ambra1 on mitophagy	7
1.2.2.3 Role of Ambra1 on apoptosis	7
1.2.2.4 Role of Ambra1 on cell proliferation	7
1.2.3 <i>Ambra1</i> ^{+/-} mice – Genetic mouse model of autism spectrum disorder	8
1.3 Characteristics of neurons; in the prospective of hippocampal pyramidal neurons	9
1.3.1 The structure of the hippocampus	9
1.3.2 Hippocampal pyramidal neuron	10
1.4 Functional characteristics of neurons	11
1.4.1 Synaptic plasticity	11
1.4.1.1 Short-term synaptic plasticity: Paired-pulse ratio	11
1.4.1.2 Long-term synaptic plasticity: Early-phase long term potentiation (E-LTP)	12
1.4.2 Neuronal oscillation	12
1.4.2.1 Gamma oscillations	13
1.5 Aim of the present study	14
2 Method & Materials	15
2.1 Methods	15
2.1.1 Animals	15
2.1.2 Genotyping	15

2.1.2.1	Extraction of DNA from tail-tip biopsies	15
2.1.2.2	PCR for genotyping	15
2.1.3	Behavior experiments	16
2.1.3.1	Observation of neonatal development.....	16
2.1.3.2	Ultrasound vocalizations.....	18
2.1.3.3	Pentylenetetrazol (PTZ)-Induced Seizure	19
2.1.4	Biochemical analyses	20
2.1.4.1	Real-time quantitative reverse transcription-PCR (RT-qPCR)	20
2.1.4.2	Protein extraction and Western blot	21
2.1.5	Magnetic resonance imaging (MRI).....	22
2.1.5.1	MRI Volumetry	22
2.1.6	Histological and immunohistochemical analyses	23
2.1.6.1	Perfusion.....	23
2.1.6.2	X-galactosidase (X-gal) staining.....	23
2.1.6.3	Immunohistochemistry (Colocalization of β -Gal with different cellular markers & counting CTIP2+, GAD67+ and PV+ cells).....	23
2.1.6.4	Image acquisition.....	24
2.1.7	Electrophysiological analysis of hippocampal pyramidal neurons	24
2.1.7.1	Synaptic plasticity	24
2.1.7.2	Gamma oscillation in CA3 pyramidal layer of hippocampus	26
2.1.8	Morphological analysis of hippocampal pyramidal neurons	28
2.1.8.1	In utero electroporation (IUE)	28
2.1.8.2	Immunohistochemistry for dendritic morphology and spine number	29
2.1.9	Statistical analysis	31
2.2	Materials.....	32
2.2.1	Chemicals.....	32
2.2.2	Equipment.....	33
2.2.3	Software.....	34
2.2.4	Consumable.....	35
2.2.5	Buffers and solutions	35
2.2.6	Primers	37
2.2.7	Antibodies	37

3	Result	39
3.1	Assessment of developmental milestones and early ultrasonic communication	39
3.2	Ambra1 mRNA and protein expression	40
3.3	Brain enlargement.....	41
3.4	Expression of Ambra1 protein in postnatal brain	42
3.5	Functional study of neuron.....	45
3.5.1	Synaptic plasticity	45
3.5.1.1	Input-Output relationship	46
3.5.1.2	Paired-pulse ratio (PPR).....	47
3.5.1.3	Early-phase LTP	48
3.5.2	Gamma oscillation	50
3.6	Seizure propensity	51
3.7	Neuronal number and morphology	53
3.7.1	Neuronal number (Counting of CTIP2+, GAD67 and PV+ cells)	54
3.7.2	Neuronal morphology	55
3.7.3	Dendritic arborization.....	56
4	Discussion	58
4.1	Neonatal development and communication function	58
4.2	mRNA and protein expression of Ambra1	59
4.3	Very mild brain enlargement, neuronal expression & neuronal counting	60
4.4	The effect of Ambra1 on synaptic plasticity	62
4.5	Seizure phenotype, gamma oscillations and E/I balance	63
4.6	Dendritic arborization & spine number	65
4.7	Female-specific ASD.....	67
5	References	69
6	List of Abbreviations	80
7	Acknowledgement	85
8	Curriculum Vitae	86
9	List of Publications	89

Summary

Autism is known as a heritable neurodevelopmental disorder, diagnosed prior to the age of three years in humans based on three major domains: (1) impairment in social interaction (2) communication deficits (3) restricted interests and repetitive behaviors. Since it is a very heterogeneous disorder with various causes and different combinations of phenotypes, it is also called autism spectrum disorder (ASD). Monogenic heritable forms of ASD enable us to develop genetic mouse models of autism in order to obtain mechanistic insight in this disorder.

Ambra1 is a positive regulator of Beclin1, a major player in the formation of autophagosomes during the process of autophagy. While *Ambra1* null mutation leads to embryonic lethality, we could show that *Ambra1* heterozygous mice (*Ambra1*^{+/-}) display autism-like behavior only in females. Purpose of this thesis was therefore to characterize this mouse line further.

It turned out that communication deficits, measured by ultrasound vocalization, start in the neonatal stage of females, while physical or neurological development is normal in *Ambra1*^{+/-}. Female *Ambra1* mutants had a stronger reduction in *Ambra1* expression than male mutants, which gives first hints of the female-specific autism-like behavior in this mouse line. Mild enlargement of whole brain and hippocampus was detected in both *Ambra1*^{+/-} males and females, with no change of ventricle size. Since β -galactosidase, used as reporter expressed under the *Ambra1* promoter, was found only in neuronal cells, I focused on understanding the neural mechanism of its phenotype.

Short-term and long-term synaptic plasticity in the hippocampus was normal for males and females of both genotypes. However, the power of gamma oscillations (γ -power), indicative of change in the balance of excitation and inhibition, was age-dependently altered in *Ambra1*^{+/-} females only. However, this difference was not detected in male. Moreover, increased susceptibility to seizures, a known comorbid condition of ASD was restricted to females, suggesting an association between autism-like behavior, gamma oscillation and seizure propensity in female *Ambra1*^{+/-} mice.

Next, I approached the neuronal substrate of these three phenotypes by morphological analysis of hippocampal pyramidal neurons, such as dendritic arborization and synapse number. A genotype-associated difference of dendritic arborization was detected in neither males nor females. The quantification of spines or synapses and cellular electrophysiology are still on-going. First signals point to an imbalance between excitation and inhibition as a cause of the female autism-like behavior in *Ambra1*^{+/-} mice.

1 Introduction

1.1 Autism spectrum disorder

"The Diagnostic and Statistical Manual of Mental Disorders, fifth edition (DSM-V)" defined autism spectrum disorder (ASD) as a group of heterogeneous neurodevelopmental disorders which is diagnosed prior to the age of three years in humans based on three main domains: (1) deficits in social interaction, (2) a lack of appropriate language and communication skills, and (3) repetitive behaviors and stereotypies (Association, 2013).

1.1.1 Genetics of autism spectrum disorder

Epidemiological research on twin and family studies has provided evidence of a strong genetic component in ASD etiology. Epidemiological studies estimated that more than 1% of the world's population have received a diagnosis of ASD (Christensen et al., 2016; Elsabbagh et al., 2012). The recurrence risk in families with infants having an affected older sibling was approximately 20% (Ozonoff et al., 2011). One twin study revealed the concordance rate in monozygotic twins to be 82-92%, in dizygotic twins as the rate was more than 20%, supporting ASD as genetic neuropsychiatric disorder. The heritability of autism has been estimated to be 70-80%, implying that a possibility of environmental effect but still a strong genetic cause in ASD (Bailey et al., 1995; Colvert et al., 2015; Frazier et al., 2014; Hallmayer et al., 2011; Schendel et al., 2014).

In the 1990s, genetic factors of ASD were first reported in monogenic disorders, such as fragile X and Rett syndromes (Pieretti et al., 1991; Zoghbi et al., 1999) and later as chromosomal abnormalities in family studies (Vorstman et al., 2006). Several candidate genes encoding for synaptic proteins, such as *NLGN3*, *NLGN4X*, *NRX1* and *SHANK3*, were identified to be mutated in patients diagnosed with ASD (Durand et al., 2007; Jamain et al., 2003; Szatmari et al., 2007). Another group of genes encoding for translational proteins, such as *TSC1/TSC2*, *NF1* or *PTEN*, were recently found mutated in a number of ASD patients (Goffin et al., 2001; Gutierrez et al., 1998). Exploring the role of mutated genes may lead to mechanistic insight into etiology or pathological features of ASD.

1.1.2 Sex differences in autism spectrum disorder

The prevalence of sexually dimorphic diseases is well known, but poorly understood. While several disorders related with autoimmunity, like multiple sclerosis and systemic lupus erythematosus, are female-dominant (Whitacre, 2001), neurodevelopmental disorders such as attention deficit hyperactivity disorder and language impairment show male-dominance (Barbaresi et al., 2002; Szatmari et al., 1989; Viding et al., 2004). ASD has been described as a sexually dimorphic disease, since they are diagnosed more often in males than females (4:1, male to female ratio). This observation of sex-specific biological factors in ASD etiology has been consistent across time and populations. There has been no sex-dependent difference found in overall severity of ASD measured by a variety of assessment tools (Kopp and Gillberg, 2011; Lai et al., 2012, 2011). Among many possible hypotheses about the male-dominance in autism, two biological connections have been implicated: genetic perturbation and hormonal regulation.

It is widely accepted that children who are exposed to high levels of testosterone in the womb show similar results in psychological tests to people with ASD, called the fetal testosterone (fT) theory. And it is the major explanation of sexual hormonal effect on the sex bias in ASD (Baron-Cohen et al., 2004). In the general population, sexual dimorphism of social domains has been associated with fT level, implying an effect of fT on the development of social behaviors (Knickmeyer et al., 2005, 2006, Lutchmaya et al., 2001, 2002). fT has not been the only hormone implicated in ASD phenotypes. Estrogen and oxytocin have been discussed as causes of ASD (Auyeung et al., 2015; Crider et al., 2014; Hoffman et al., 2016; Jones and Okere, 2008; Liu et al., 2015; Sarachana et al., 2011; Sharpe et al., 2013; Yatawara et al., 2015).

The main alternatives to the fT theory are the X and Y chromosome theories. Fragile X mental retardation 1 (*FMR1*) gene, where 46% of male and 16% of females carrying the full mutation were also diagnosed with ASD, is the best example of X chromosome effect on ASD (Bailey et al., 2008). One study reported higher autistic traits score in girls with Turner syndrome (characterized by the XO karyotype) (Tartaglia NR, Hansen RL, Reynolds A, Hessl D, 2006). As the XXY and XXYY syndromes have increased incidence of ASD (Bruining et al., 2009; Geerts et al., 2003; Tartaglia et al., 2008), it is also important to consider if the male bias in ASD result from the male-limited expression of genes on the Y chromosome. One study has reported a missense variant in *NLGN4Y* in a single patient with

autism and his father with learning difficulties (Jamain et al., 2003). All three theories might not be mutually exclusive, because all those factors can regulate or influence each other (Baron-Cohen et al., 2011).

1.1.3 ASD and Brain enlargement

Studies of neuroimaging and postmortem examinations in human autists have reported the structural abnormalities in whole brain or sub-regions of the brain (Chen et al., 2016; Courchesne and Pierce, 2005; Hazlett et al., 2011; Haznedar et al., 2000; Piven et al., 1998; Saitoh et al., 1995; Schumann et al., 2004). In spite of inconsistency across all studies, a majority of research has shown an increase in whole brain or sub-regions, such as cortex or hippocampus, in autist brains (Courchesne and Pierce, 2005; Courchesne et al., 2003, 2011; Hazlett et al., 2011; Schumann et al., 2004).

One study showed that at the age of two or three years, 90% of autist toddlers had enlarged brain volumes, especially cerebral gray and white matter and cerebellar white matter, than average of normal toddlers (Courchesne et al., 2001). This enlargement of brain and cerebrum in young autists was replicated independently in a study of 3 to 4-year old children, showing larger volume of whole brain, cerebrum, cerebellum and amygdala in autists compared to normal children (Sparks et al., 2002). The growth rate of the brain was slower in older autists than normal children, especially in gray matter (Courchesne et al., 2001), which result in normal or reduced volumes in limbic or cerebral structures in autistic adults (Bigler et al., 2003; Courchesne et al., 2001; Herbert et al., 2003; Kates et al., 2004; Lotspeich et al., 2004). Although the cellular bases of the early growth pathology in autism are unclear, this enlargement might be due to excess number of neurons in the prefrontal cortex (Courchesne et al., 2011) or increased number of synapses (Tang et al., 2014).

1.1.4 Comorbidity of seizure in autism

One of the relatively common comorbid conditions in autism is epilepsy. Epilepsy is defined as a brain disorder characterized by the predisposition to generate epileptic seizures due to abnormal, excessive, or synchronous neuronal activity in the brain and by neurobiological, cognitive, psychological and social consequences of this condition (Fisher et al., 2005).

The risk of epilepsy in patients with ASD is increased but variable. A wide range of prevalence rates have been reported, from 5 to 40%, probably due to the heterogeneity in the clinical study with respect to diagnosis, age, and mental level (Elia et al., 1995; Giovanardi Rossi et al., 2000). Comparison the prevalence of epilepsy in autistic children and all children, approximately 2-3%, indicates high association of epilepsy in autism. Around 60% of human autists without history of epilepsy showed abnormal electroencephalogram (EEG) activity during sleep (Chez et al., 2004).

Previous studies suggested two peaks in the onset of seizures in autism; early childhood and adolescence (Volkmar and Nelson, 1990). The rate of epilepsy in pre-adolescent autists was less than 10% (Fattal-Valevski et al., 2007; Hoshino et al., 1987; Voigt et al., 2000), while in adolescent or adult autists were as high as 39% (Giovanardi Rossi et al., 2000; Kawasaki et al., 1997).

A common genetic basis has been proposed to speculate on the comorbidity of seizure and autism. In humans *SYN1*, an X-linked gene encoding a neuron-specific phosphoprotein which regulates neurotransmitter release and synaptogenesis, is a predisposing gene to ASD as well as epilepsy (Fassio et al., 2011). Furthermore, the R451C missense mutation in the *NLGN3* gene was identified in two siblings with ASD, one with comorbid epilepsy (Jamain et al., 2003).

1.1.5 Genetic mouse model of autism

The etiology of ASD has been still unclear, since this disorder has heterogeneous severity as well as causes. Previously, the animal models based on face validity were used in ASD studies searching for pharmacological therapy (predictive validity), but there was no effective treatment paradigm for the core symptom of human ASD (Hulbert and Jiang, 2016). Recently, monogenic heritable forms of ASD enable us to develop the genetic mouse model of autism with construct validity (Betancur et al., 2009; Jamain et al., 2008; Tabuchi et al., 2007). Most of the described mechanisms of ASD phenotypes come from detailed characterization of mouse models of syndromic autism, where the genetic cause is clearly defined.

1.2 Ambra1

Ambra1 is an activating molecule in Beclin-1-regulated autophagy (Ambra1) and plays a crucial role in the regulation of Beclin1 which is a key modulator of autophagosome formation during autophagic processes. Ambra1 is a protein comprising 1300 amino acid residues including WD40, proline- and

serine-rich domains and dynein binding domains. Importantly, protein containing WD40-domains function as coordinators of multi-protein complex assembly and provide a rigid scaffold for protein-protein interactions. Ambra1 was first found as a binding partner of Beclin1. More recently, other interaction partners of Ambra1 such as mitochondrial Bcl-2, ULK1, PP2, and DLC1/2 have been described, indicating multiple, distinct functions of Ambra1 in eukaryotic cells (Cianfanelli et al., 2015a). The *Ambra1* gene is located on mouse chromosome 2 and human chromosome 11 and is composed of 18-19 exons (Maria Fimia et al., 2007).

1.2.1 Mutation of *Ambra1*

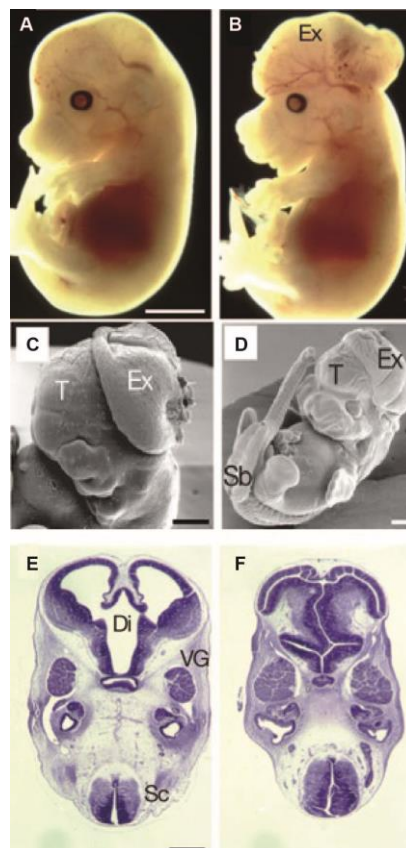


Figure 1. Neural tube defects in *Ambra1*^{-/-} embryos

A, B: Embryos of *Ambra1*^{+/+} (**A**) and *Ambra1*^{-/-} (**B**) at E14.5; the homozygosity of the *Ambra1* mutation is characterized by prominent exencephaly (Ex) in the embryos, which results in embryonic lethality. **C, D:** Electron scanning microscopic analysis of *Ambra1*^{-/-} embryos at E11.5 (**C**) and E12.5 (**D**); failure of the neural tube closures, extensive midbrain/hindbrain exencephaly with a closed telencephalon (T), and lumbosacral spina bifida (Sb) were detected. **E, F:** Histological analysis of *Ambra1*^{+/+} (**E**) and *Ambra1*^{-/-} (**F**) cross-section of embryonic brains at E12.5; *Ambra1*^{-/-} embryos exhibits the absence of a normal ventricular system due to the extensive overgrowth of the proliferative neuroepithelium in the diencephalon (Di) and spinal cord (Sc). Presence of an enlarged fifth ganglia (VG) was also evident in the *Ambra1*^{-/-} embryo. Scale bars; A, 2 mm; C-E, 500 μ m. Adapted with permission from Nature Publishing Group with license number #3912480801468 (Maria Fimia et al., 2007)

The mouse mutation of *Ambra1* was generated by gene trapping mutagenesis. This is done by inserting a gene trap vector containing a *lacZ* reporter gene into intron 11, which produces a truncated, non-functional Ambra1 protein. However, the homozygous *Ambra1* mouse mutant (*Ambra1*^{-/-}) is embryonic lethal in outbred or inbred genetic backgrounds. At embryonic day (E)10-14.5, most of the *Ambra1*^{-/-} embryos had neural tube defects such as midbrain/hindbrain exencephaly and/or spina bifida. In the forebrain of embryonic *Ambra1*^{-/-} mice, closed but displaced vesicles, extensive overgrowth of neuroepithelium, and enlarged spinal cords were found (Fig 1. A-F). Neural tube defect in the deficiency of Ambra1 in mouse embryos might be associated with autophagy impairment, excessive cell proliferation and apoptosis and accumulation of ubiquitinated proteins in the neuroepithelium. The embryonic expression of Ambra1 was found throughout the neuroepithelium at E8.5 and detected in the ventral-most part of the spinal cord, the encephalic vesicles, the neural retina, the limbs, and the dorsal root ganglia at E11.5. Ambra1 is later expressed throughout the entire developing nervous system (Maria Fimia et al., 2007).

1.2.2 Function of Ambra1

As previously mentioned, recent binding assays discovered more potential binding partners of Ambra1, implicating the possibility of multiple functions of Ambra1.

1.2.2.1 Role of Ambra1 on the autophagic pathway

Under basal conditions, Ambra1 is bound to the dynein light chains 1/2 (DLC12) of the dynein motor complex, together with Beclin1 and PI3KIII. After autophagy induction, Ambra1 is released from the dynein complex by ULK1-mediated phosphorylation, resulting in translocation of Ambra1 still bound to Beclin1 and Class III Phosphoinositol-3-kinase complex (PI3KIII), to the endoplasmic reticulum (ER) where the formation of autophagosomes are initiated (Cianfanelli et al., 2015a). Recently, Ambra1 was shown to regulate the activity and stability of ULK1, suggesting strong evidence of Ambra1's role on the autophagic pathway. After autophagy induction, Lys63-linked ubiquitin of ULK1 by Ambra1 helps the self-association of ULK1. Additionally, this ubiquitination can be prevented by mTORC1-mediated phosphorylation of Ambra1, which is an inactive state of Ambra1 proteins (Nazio et al., 2013). This mechanism is regarded as a positive-feedback loop, in which Ambra1 functions to 'fine-tune' the autophagic process by enhancing the activity of ULK1 (Cianfanelli et al., 2015a).

1.2.2.2 Role of Ambra1 on mitophagy

Additionally, interaction between Ambra1 and LC3 was revealed as another evidence of the role of Ambra1 in autophagy, especially in mitophagy (selective autophagy of mitochondria) (Strappazon et al., 2015). Under the basal conditions, Ambra1 binds to mitochondrial Bcl-2 (mBcl-2) on the mitochondrial membrane (Strappazon et al., 2011). After the induction of mitophagy, Ambra1 binds to the LC3 interacting region (LIR) motif of LC3, the autophagosome adaptor, leading to mitochondrial clearance.

1.2.2.3 Role of Ambra1 on apoptosis

A functional deficiency of Ambra1 might cause cellular apoptosis during the embryonic development (Maria Fimia et al., 2007). When tested, reduction in Ambra1 expression lead to an increased susceptibility to different apoptotic stimuli (Pagliarini et al., 2012). The cells become more resistant to apoptosis, in the presence of caspase-resistant form of Ambra1, compared than wild-type *Ambra1*, indicating a cellular pro-survival effect of Ambra1. Due to the interaction between Ambra1 and mBcl-2, anti-apoptotic factor, a crosstalk between autophagy and apoptosis via Ambra1 has been proposed (Cianfanelli et al., 2015b).

1.2.2.4 Role of Ambra1 on cell proliferation

Cell proliferation during embryonic development was increased in *Ambra1* functional mutants (Maria Fimia et al., 2007). Recently, Ambra1 was reported as an effector of mTORC1 signaling. mTORC1 inhibition activates Ambra1 function in autophagy and down-regulates cell proliferation by anti-proliferative effect of Ambra1 (Cianfanelli et al., 2015b; Nazio et al., 2013). The direct binding of PXP motif of Ambra1 to the serine/threonine-protein phosphatase 2A (PP2A) has been found to dephosphorylate c-Myc, leading to its degradation. Mutation in the PxPxxxR (PXP) motifs of Ambra1 had no effect on the autophagic pathway indicating these two functions may depend on different regions of Ambra1 (Cianfanelli et al., 2014). Moreover, in the sub-ventricular zone (SVZ) of the adult brain, Ambra1 remains highly expressed promoting the survival of neural precursor cells by controlling the level of immature neurons (Yazdankhah et al., 2014).

1.2.3 *Ambra1*^{+/-} mice – Genetic mouse model of autism spectrum disorder

A number of human genetic studies have connected *AMBRA1* gene mutations with psychiatric disorders, especially schizophrenia. Schizophrenia is a group of psychotic disorders characterized by severely impaired thinking, emotions, and behaviors. A genome-wide association study (GWAS) demonstrated an association between schizophrenia and genetic variation on the human chromosome which contains the *AMBRA1* gene (Rietschel et al., 2012). Another genetic study showed an association between *AMBRA1* and various aspects of impulsivity (Heinrich et al., 2013)

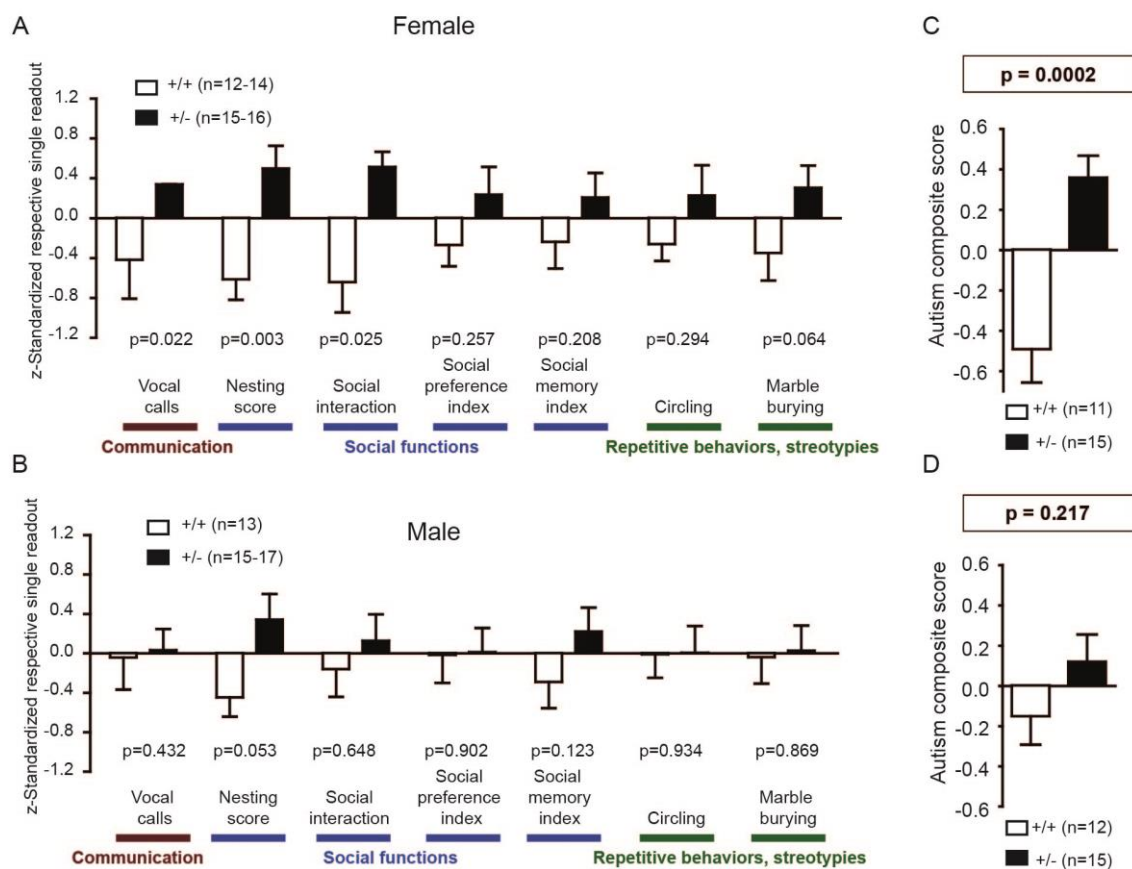


Figure 2. Composition of the autism severity score and autism composite score in *Ambra1*^{+/-} and *Ambra1*^{+/+} mice of both males and females

The upper row (A, C) shows results for females, the lower row (B, D) for male mice. A, B: Z-standardized autism-relevant readouts from mouse behavior experiments which represent three main domains in ASD; C, D: Autism composite score calculated by averaging z-standardized score from Figure A and C. The comparison of mutant and control groups was analyzed by Mann-Whitney *U*-tests. Mean±SEM presented; n numbers of each group are presented in the figures. Adapted from *Frontiers in Behavioral Neuroscience* (Dere et al., 2014).

Recently, we performed a comprehensive behavioral analysis of *Ambra1*^{+/-} mice and reported autism-like phenotypes in females including compromised social interactions, a tendency to exhibit

stereotypies or repetitive behaviors and impaired cognitive flexibility (Dere et al., 2014). Fig 2. A and B show z-standardized scores of behavioral readouts which cover all three main diagnostic domains (communication, social interaction and stereotypies/repetitive behaviors). Here, the scores of *Ambra1*^{+/-} females were higher than control females in most of the parameters, while there was no significant difference between the two genotypes in males. Thus, the average of all z-standardized scores, reflecting the autism composite score, was profoundly higher in female *Ambra1*^{+/-} mice compared to control females whereas it was not significantly different in male mice (Fig 2. C and D). And this indicates the female-specific autism-like behavior in *Ambra1*^{+/-} mice.

1.3 Characteristics of neurons; in the prospective of hippocampal pyramidal neurons

1.3.1 The structure of the hippocampus

The hippocampus has been a major region of the brain for characterization of neurons in different contexts, from electrophysiological properties and morphological features to synaptic plasticity as a mechanism of information processing and storage in the brain. The hippocampus is composed of the dentate gyrus and the Ammon's horn field which contains four parts of the *Cornu Ammonis* 1-4 (CA1-4).

The hippocampus is composed of simple laminar patterning of a neuronal pathway, called the trisynaptic loop, which enables extracellular recording techniques to record synaptic events in vivo or in vitro. Fig 3. A and B represent the wiring system of hippocampus as a trisynaptic loop. Sensory information of neurons in layer II of the entorhinal cortex conveys excitatory input to the dendrites of granule cells via perforant path (PP). Granule cells project to the proximal apical dendrite of CA3 pyramidal cells via the mossy fiber pathway. Axons of CA3 pyramidal neurons project to ipsilateral CA1 pyramidal neurons through Schaffer collaterals and to contralateral CA3 and CA1 pyramidal cells through commissural connections. CA3 pyramidal neurons also receive direct input from layer II cells of the entorhinal cortex. Layer III cells of the entorhinal cortex innervate the distal apical dendrites of CA1 pyramidal neurons (Neves et al., 2008).

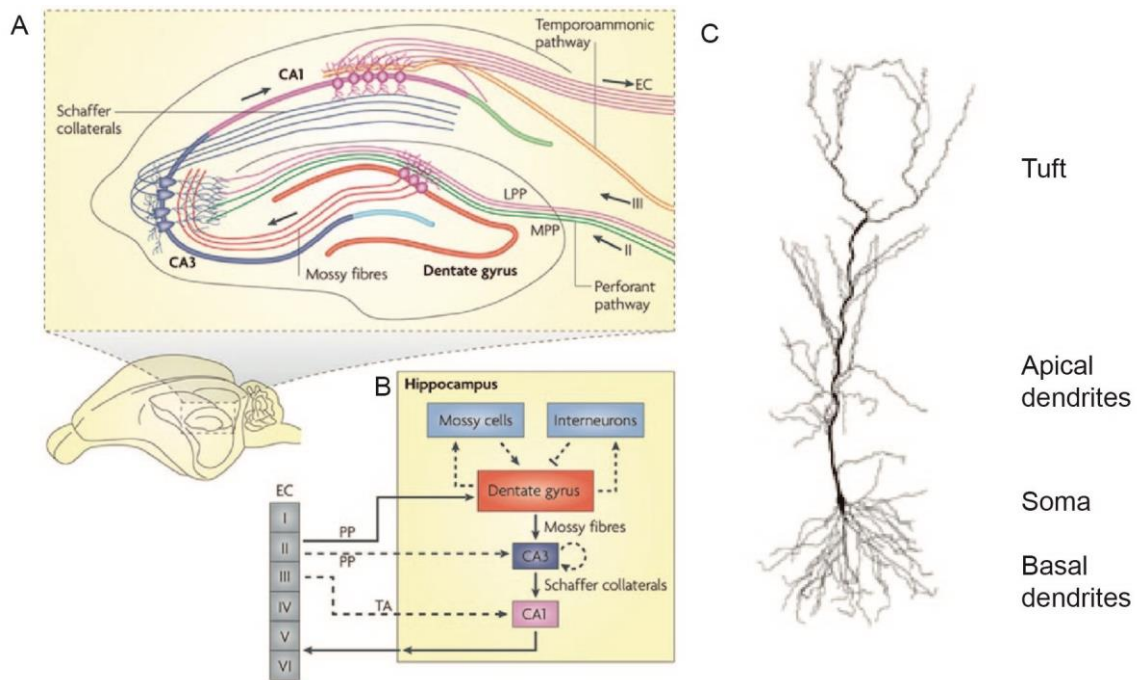


Figure 3. The illustration of hippocampal trisynaptic loop and hippocampal CA1 pyramidal neuron

A, B: Illustrations of hippocampal neural network. The traditional trisynaptic pathway (entorhinal cortex (EC)–dentate gyrus–CA3–CA1–EC) is shown by solid arrow. The axons of layer II neurons in the entorhinal cortex project to the dentate gyrus through the perforant pathway (PP), including the lateral perforant pathway (LPP) and medial perforant pathway (MPP). The dentate gyrus sends projections to the pyramidal cells in CA3 through mossy fibers. CA3 pyramidal neurons relay the information to CA1 pyramidal neurons through Schaffer collaterals. CA1 pyramidal neurons send back-projections into deep-layer neurons of the EC. CA3 also receives direct projections from EC layer II neurons through the PP. CA1 receives direct input from EC layer III neurons through the temporoammonic pathway (TA). The dentate granule cells also project to the mossy cells in the hilus and hilar interneurons, which send excitatory and inhibitory projections, respectively, back to the granule cells. Adapted with permission from Nature Publishing Group with license number #3912761270009 (Deng et al., 2010) **C:** The structures of pyramidal neuron in CA1 of the hippocampus. It is consisted of short basal and one long apical dendrites and an apical tuft at the end. Adapted with permission from Nature Publishing Group with license number # 3912771321428 (Spruston, 2008)

1.3.2 Hippocampal pyramidal neuron

Pyramidal neurons are found in several regions of the CNS including the hippocampus have one distinct large apical and short basal dendritic trees and the pyramidal shape of their soma, as shown in Fig 3. C (Spruston, 2008). The activation of pyramidal neuron is able to excite the interneurons. Excitatory inputs onto the pyramidal cells occur on the dendritic spines, whereas the inhibitory inputs target the soma, axon or dendritic shaft. Parvalbumin (PV) positive basket cells preferentially form synapses onto the soma of the pyramidal cells, whereas somatostatin positive interneurons preferentially synapse onto the axon initial segment of pyramidal neurons causing a modularity effect on neuronal response to a stimulus (Freund, 2003; Mann and Paulsen, 2007).

1.4 Functional characteristics of neurons

1.4.1 Synaptic plasticity

Synaptic plasticity refers to the activity-dependent changes of the strength or efficacy of synaptic transmission at preexisting synapses. In other words, neuro-adaptation to a wide range of environmental stimuli is a requirement that the synaptic transmission can be either enhanced or depressed. This modification can persist from milliseconds to hours or even longer, indicating a role in incorporating transient experiences into persistent memory traces and modifying thoughts, feelings and behavior. Recently, it has been reported that synaptic plasticity is involved in the early development of neuronal circuitry and has been linked to several neuropsychiatric disorders (Citri and Malenka, 2008).

Due to the laminar structure of hippocampus, the technique of extracellular recording acute hippocampal slices is widely used for long-term plasticity (LTP) measurements. Transverse hippocampal slices with intact Schaffer collateral projections enable extracellular recordings to measure field excitatory postsynaptic potentials (fEPSPs) in the apical dendritic part of CA1 in the *Stratum radiatum* upon stimulation of the Schaffer collateral projections.

1.4.1.1 Short-term synaptic plasticity: Paired-pulse ratio

Several forms of short-term synaptic plasticity, lasting from milliseconds to several minutes, have been observed in synapses of different organisms, ranging from simple invertebrates to mammals (Zucker and Regehr, 2002). These short-term adaptations to sensory inputs have been considered to be a short-lasting form of memory by inducing transient changes in behavioral states. At the experimental level, short-term plasticity can be measured through a paired-pulse ratio (PPR). PPR is upon two stimuli within a short-time interval which will lead the response to the second stimuli to be either enhanced or depressed compared to the response to the first stimulus. Paired pulse depression is observed at short inter-stimulus intervals (ISI < 20 msec) and most likely caused by inactivation of voltage-dependent sodium and calcium channels or by a transient depletion of the readily-releasable pool of vesicles docked at the presynaptic terminal. Paired-pulse facilitation can be detected at longer ISI (20-500 msec). The major explanation of this phenomenon is that the residual calcium from the first

action potential contributes to additional release during the second stimulation, but additional mechanisms are likely to be involved such as activation of protein kinases that modulate the activity of presynaptic phosphoproteins (Citri and Malenka, 2008).

1.4.1.2 Long-term synaptic plasticity: Early-phase long term potentiation (E-LTP)

Among different forms of plasticity, LTP in the CA1 region of the hippocampus has been studied the most extensively. It refers to the activity-dependent and long-lasting modifications of synaptic strength and is involved in rapid information storage and various forms of long-term memory.

LTP can be measured in acute hippocampal slices by recording fEPSPs generated upon stimulation of presynaptic fibers during a short-duration train of high-frequency electric stimuli typically at 100 Hz for 1 sec (D V Madison et al., 2003). LTP is characterized by two phases; baseline before the induction of LTP and maintenance phase of sustaining potentiation after the induction of LTP (Sacktor, 2008).

There are two major types of ionotropic glutamate receptors which are important for LTP: α -amino-3-hydroxy-5-methyl-4-isoxazolepropionic acid (AMPA) receptors (AMPA receptors) and N-methyl-D-aspartate (NMDA) receptors (NMDARs). During basal synaptic transmission, glutamate binds to the NMDA and AMPARs. AMPARs contains a channel permeable to monovalent cations (Na^+ and K^+), and activation of AMPARs will generate inward current which provides the excitatory post-synaptic response when the cell is close to its resting membrane potential. In contrast to AMPARs, the NMDAR channels allow Na^+ and Ca^{2+} into the postsynaptic dendritic spines. During basal synaptic transmission, it contributes little to the postsynaptic response due to blockage of its channel by extracellular Mg^{2+} (Citri and Malenka, 2008). High frequency stimulation (e.g. 100Hz) of the presynaptic fibers results in a large depolarization of the postsynaptic membrane and glutamatergic inputs simultaneously, leading to dissociation of Mg^{2+} from NMDAR channel and calcium influx into the postsynapses (Raymond, 2007).

1.4.2 Neuronal oscillation

Neuronal oscillations refer to rhythmic and repetitive fluctuation resulting from a generation of temporally coordinated spikes within the neuronal circuits. A single action potential in regular manner generates rhythmic activation of postsynaptic neurons, resulting in a periodic fluctuation in the intracellular membrane potential. Several action potentials in regular and synchronous manner will

amplify the output signal and produce a fluctuating field potential signal, which will be easily measured by extracellular recording (Bartos et al., 2007).

Oscillations can be characterized by their frequency (Hz), peak amplitudes ($\text{Power}=\text{Amplitude}^2$). Based on their frequencies, they can be categorized as delta oscillations (0.5-3 Hz), theta oscillations (3-8 Hz), alpha oscillations (8-13 Hz), gamma oscillations (30-90 Hz), and ultrafast oscillations (90-200 Hz). Oscillatory activities take place in different regions of the brain and are correlated with higher brain functions (Mann and Paulsen, 2007; Mathalon et al., 2015). Different forms of neuronal oscillations have been extensively studied in human EEG, recorded on the scalp (Buzsáki et al., 2012). For example, the theta range is usually detected during an exploratory behavior as well as rapid eye movement (REM) sleep. Disruption of gamma oscillations could underlie some psychiatric disorders, such as schizophrenia and ASD (Bartos et al., 2007).

1.4.2.1 Gamma oscillations

Among different types of neuronal oscillations, gamma oscillations (30-80 Hz) have been extensively investigated since they have been involved in cognitive functions, recall of memory, sensory processing and memory formation. Gamma oscillations have been studied in different areas of the brain; neocortex (Fries et al., 2001; Gray et al., 1989; Murthy and Fetz, 1992; Sirota et al., 2008), entorhinal cortex (Chrobak and Buzsáki, 1998), amygdala (Halgren et al., 1977; Popescu et al., 2009), hippocampus (Bragin et al., 1995; Buzsáki et al., 1983; Mann et al., 2005), striatum (Berke et al., 2004), thalamus (Pinault and Descheˆnes, 1992) and other areas. The major explanation about the generation of gamma oscillation is the regulation of neuronal network by PV-positive basket cells. They are present in the pyramidal cell layer of CA1 and CA3 (Miles et al., 1996) and they have fast spiking properties at the similar frequency of gamma oscillations (Jonas et al., 2004).

Gamma oscillations in the hippocampus have been studied via extracellular recording acute brain slices upon application of electric stimulation (Whittington et al., 1995) or chemical stimulation such as 3,5 dihydroxyphenylglycine (DHPG) for metabotropic glutamate receptors (mGluRs), carbachol for muscarinic acetylcholine receptors (mAChRs), or kainate for kainate receptors (Fisahn et al., 1998, 2004; Mann et al., 2005). Application of different chemical stimulants together with different antagonists enables the exploration of different mechanisms of gamma oscillations. For example,

induction by kainate receptor or mGluRs can be blocked by bicuculline but not by AMPA receptor antagonists, indicating that kainate-induced or DHPG-induced oscillations are mainly dependent on inhibition (Fisahn et al., 2004; Whittington et al., 1995). In contrast, induction by Carbachol can be blocked by both AMPA receptor antagonist and GABA_A receptor antagonist, indicating that these oscillations are dependent on both excitatory and inhibitory pathways (Fisahn et al., 1998).

1.5 Aim of the present study

The aim of the present study was to identify how reduced expression of Ambra1 protein changes the characteristic of neurons in *Ambra1*^{+/-} mice in order to explain the autism-like phenotype only in *Ambra1*^{+/-} female mice.

Therefore, quantification and localization of protein in the brain was studied. Other symptoms or comorbidity of autism, such as brain enlargement or epileptic seizure were also observed in this mouse line. Moreover, change of the neuronal network and neuronal morphology in *Ambra1*^{+/-} mice was studied in the hippocampus.

Overall, this is the first study to investigate the involvement of Ambra1 in the neuronal features associated with female-specific autism in mouse model.

2 Method & Materials

2.1 Methods

2.1.1 Animals

Ambra1 mutation was made by inactivation of *Ambra1* gene which has been described in detail previously (Maria Fimia et al., 2007). *Ambra1* wild-type (WT, *Ambra1*^{+/+}) and *Ambra1*^{+/-} (Het) littermates of both genders with a >99% C57BL/6N genetic background were used for *in vivo* study. They were obtained from male *Ambra1*^{+/-} and female WT C57BL/6N breeding pairs. This investigation was carried out in agreement with the guidelines for the welfare of experimental animals issued by the Federal Government of Germany and the Max Planck Society.

2.1.2 Genotyping

2.1.2.1 Extraction of DNA from tail-tip biopsies

Genomic DNA for genotyping was extracted from tail tips of 2-3 week-old offsprings or embryos using NucleoSpin Tissue kit. The tail tips were lysed by incubation in 180 µl T1 buffer and 25 µl Proteinase K for more than 3 hr at 56°C. After application of 200 µl B3 buffer and 210 µl ethanol, the lysate was transferred to a column followed by centrifugation at 11,000 rpm for 1 min at room temperature (RT). The column was washed by 500 µl BW buffer and 600 µl B5 buffer with centrifugation at 11,000 rpm for 1 min at RT between each step. After drying membrane by same centrifugation method as previous, the DNA sample was eluted in 100 µl of pre-warmed BE buffer (70°C).

2.1.2.2 PCR for genotyping

Ambra1 WT type gene, *Ambra1* mutated gene and Y chromosome of offsprings or embryos were detected by PCR of genomic DNA. The primers were synthesized in MPI-EM DNA Core Facility for this experiment indicated in the material part (Page No. 37).

Ambra1 mutated gene can be detected using primers #24509/#24510 to yield a 3 kilo basepair (kb) product in *Ambra1* mutated gene and #5063/#5064 to produce 350 basepair (bp) product of Interleukin-2 (IL-2) as internal control with Failsafe enzyme with PreMix D. PCR of *Ambra1* WT allele was carried out using #24508/#24509 to produce a 0.5 kb product of *Ambra1* wild type gene with

GoTaq® G2 Flexi DNA polymerase. For the sex determination of embryo, PCR of Y chromosome was performed using #23366/#23367 to detect 270 bp in Y chromosome with GoTaq® G2 Flexi DNA polymerase. All the PCR cycle information is summarized in Table 1. Final PCR products were run on a 1.5% agarose gel in TAE buffer and stained with HDGreen® Plus Safe DNA Dye.

Temperature	Time	Number of cycle
<i>Ambra1 mutated allele</i>		
94°C	3 min	 x 40
94°C	30 sec	
57°C	2 min 30 sec	
72°C	5 min	
72°C	5 min	
<i>Ambra1 wild type allele</i>		
95°C	5 min	 x 35
95°C	30 sec	
57°C	45 sec	
72°C	1 min 45 sec	
72°C	10 min	
<i>Y chromosome</i>		
94°C	1 min	 x 33
94°C	1 min	
63°C	30 sec	
72°C	30 sec	
72°C	7 min	

Table 1. Cycle information of PCR for genotyping

Cycle information of PCR for the detection of *Ambra1* mutated and *Ambra1* WT genes and Y chromosome is shown in this table.

2.1.3 Behavior experiments

2.1.3.1 Observation of neonatal development

Females were individually housed approximately 2 weeks after pairing and observed twice a week for pregnancy and delivery. The day of delivery can be regarded as postnatal day (P) 0 for that litter. The litter was not disturbed in their home cage with their mothers until 3 days old when the paws of pups were tattooed by injecting non-toxic animal tattoo ink using a 30 gauge hypodermic needle tip.

Observation of neonatal development was carried out by a trained observer, who is blinded to the genotype and sex. The size of litters was restricted to 6-10 pups per litter. The battery of tests consisted of a daily assessment of physical and neurodevelopmental as well as neuromotor coordination throughout the neonatal period and each readout has different time window of observation and performed as described earlier (Ju et al., 2014). Neonatal assessments include (i) maturation measures targeting physical development, (ii) neurodevelopmental measures targeting the development of neurological reflexes, and (iii) the development of neuromotor coordination.

2.1.3.1.1 Maturation measures targeting physical development

Body weight was measured daily and the day of opening both eyes and ears was checked.

2.1.3.1.2 Neurodevelopmental Measures targeting development of neurological reflexes

Placing response: Pups were gently grasped around trunk and suspended in the air to make none of the paws on ground. A thin metal bar was placed on the top of forepaw and the day when the pups raised both fore-paw for two consecutive days was measured. It starts from P4 and was performed one trial per day.

Surface righting reflex: Pups were placed with their back on ground and then released. The time needed for pups to right themselves was measured. It was performed twice a day, starting from P4 until the measured time was within 2 sec in both trials for two consecutive days.

Cliff avoidance: Forepaws of pups were placed at the edge of cliff and observe the retraction reflex (cliff avoidance reflex) within 10 sec by one trail from P6 until they showed the reflex within 10 sec for two consecutive days. Both eyes should be closed.

Negative geotaxis reflex: Pups were placed on an inclined plane (30° angle) with its head facing downwards and the time needed for pups to change its orientation in order to face up the incline (proper response) was measured. Criterion was reached when the proper response appeared before 30 sec for two consecutive days. This observation was carried out daily from P7 until the criteria was reached.

Tactile startle: A puff of air (e.g. experimenter's breath) was gently applied to the pups, starting on P10. The criteria were reached when the proper response (jumping or running) was observed on 3 consecutive days.

Ear twitch: The fine filament pulled out from cotton tip was gently brushed on the tip of the ear for 3 times. The criteria can be reached when the pups showed the ear twitch which is flattening the ear against the side of head for 3 consecutive days.

Air righting reflex: This experiment starts from P10. The pup was held upside down holding both side of the head and the hind quarters approximately 10 cm above a cage. The pup was released and whether the pup was able to turn right to position upon landing by one trial for 3 consecutive days.

2.1.3.1.3 Neuromotor Coordination Measures

Open field traversal: The pup was placed in the center of 13 cm circle and the time needed to escape from the circle was recorded, starting from P10. This performance was terminated when the pup still stayed within the circle after 30 sec. The criteria were reached when the measured time was less than 30 sec for two consecutive days.

Wire suspension: The animals were forced to grip a 3 mm wire starting from P10 onward until the pups were able to hang on the wire for 30 sec. The criteria were reached when the pup was able to hold the wire for 30 sec for two consecutive days.

2.1.3.2 Ultrasound vocalizations

Ultrasonic vocalizations (USVs) of pups were recorded between P8-9 by inducing the vocalization after the isolation from their mothers and nest (isolation test) in collaboration with Dr. Kurt Hammerschmidt in DPZ, Göttingen (Ju et al., 2014).

Pups were randomly selected and placed in a soundproofed custom-made plastic box (diameter 13.5 cm). An ultrasound microphone (UltraSoundGate CM16) in the lid of the box, 12 cm above the bottom, was connected to a preamplifier (UltraSoundGate 116) coupled to a notebook computer. The total number of calls and calling duration were measured during an observation period of 3 min. USVs were separated from other sounds based on the whistles detection algorithm of Avisoft-SASLab 5.2 using

following selection criteria: Possible changes per step=4 (4687 Hz), minimal continuity=5 and 8 msec for neonatal and juvenile recording, possible frequency range=35 – 150 kHz.

2.1.3.3 Pentylenetetrazol (PTZ)-Induced Seizure

The protocol was performed as described before in a publication where I was co-author (Wojcik et al., 2013). Seizure activity was induced in awake mouse by a single intraperitoneal (i.p) injection of 50 mg of Pentylenetetrazol (PTZ), per 1 kg of body weight. After injection, the mouse was observed closely for 30 min in a small and clear home cage. This experiment was carried out in 23-25 day-, 12-13 week- and 13 month-old *Ambra1* WT and Het mice in both sexes.

Four phases of behavioral response to PTZ injection were defined as follows: 1) Hypoactivity; Decrease in mobility until the animal take a rest in a crouched or prone position by contacting the abdomen at the bottom; 2) Partial clonus (PC); Clonic seizure activity in face, head, and forelimbs; 3) Generalized clonus (GC); Sudden loss of upright posture, whole body clonus including all four limbs and tail, rearing and autonomic signs; and 4) Tonic-Clonic (TC) (maximal) seizure; Generalized seizure with tonic hind-limb extension followed by death. Latencies to PC, GC and TC seizures were used to produce from each mouse a seizure score as a quantitative trait measure for mapping by the following equation:

$$Seizure\ score = \frac{1}{(0.2 * PC\ latency + 0.3 * GC\ latency + 0.5 * TC\ latency)} \times 1000$$

Since GC is a more significant event than PC and TC is regarded as the strongest phenotype, the weighting factors (0.2, 0.3, and 0.5) were used in this equation as a measure of the progressive nature of the PTZ-induced seizure phenotype into the rate of severity (Bodda et al., 2013; Ferraro et al., 1999; Wojcik et al., 2013).

2.1.4 Biochemical analyses

2.1.4.1 Real-time quantitative reverse transcription-PCR (RT-qPCR)

2.1.4.1.1 Extraction of total RNA

Isolation of total RNA was carried out from cortex tissue of 60-week old mice with miRNeasy Mini Kit according to manufacturer's protocol. For details, cortex tissues were homogenized with homogenizer in 700 µl QIAzol followed by passing through a syringe with 27G needle for three times. The lysates were incubated for 5 min at RT and 140 µl of chloroform were applied. After centrifugation at 12,000 rpm at 4°C for 15 min, the aqueous phase was collected and mixed with 1.5 times of 100% ethanol. This mixture was applied on the miRNeasy Mini column and flew through by centrifugation at 8,000 rpm for 15 sec at RT. The column was washed once by 700 µl RWT buffer and twice by 500 µl RPE buffer together with same centrifugation as previous in each step. After centrifugation at 14,500 rpm for 1 min, the total RNA was collected in 50 µl RNase free water at 8,000 rpm for 1 min at RT. The RNA concentration was measured after dilution of sample into 1:25 in RNase free water by GeneQuant II spectrometry at 260 nm.

2.1.4.1.2 Synthesis of cDNA

Reverse transcription of purified RNA was performed using the SuperScript III Reverse Transcriptase, following manufacturer's manual. For detail, each reaction, 1 µg of total RNA together with 120 pmol N9 random primers and 0.6 pmol oligo(dT)-mix in a volume 12 µl was incubated at 70°C for 2 min followed by adding 8 µl of master mix including 1 µl 200 U/µl SuperScript III, 4 µl 5x first strand buffer, 2 µl 0.1 M DTT and 1 µl 10 mM dNTPs. The mixtures went through the cycle consisting of 10 min at 25°C, 45 min at 50°C and 45 min at 55°C. Afterwards, the samples were diluted into 1:10 with ultra-pure water and stored at -20°C.

2.1.4.1.3 qPCR

For qPCR, 4 µl cDNA, 6 µl of Power SYBR Green PCR Master Mix (Life Technologies) and 5 pmol of primers in a total volume of 10 µl was pipetted into 384 well-plates by the Epmotion robot 7075. The primers were synthesized from MPIEM DNA Core Facility for this experiment and are listed in the material section (Page No. 36-37). The primers #31502/#31503 for *Ambra1* allele in C-terminal where

the difference between *Ambra1* WT and mutant allele is coming from and #9146/#9147 for β -actin. The qPCR reactions were held on LightCycler 480 System with 3 technical replicates under the following cycle: Initiation; 50°C, 2 min / Denaturation; 95°C, 2 min / 45 cycles; 95°C, 15 sec & 60°C, 1 min. The cycle threshold method (LightCycler® 480 Software release 1.5.0 SP3) was used for calculation of relative expression levels of *Ambra1* normalized to β -actin.

2.1.4.2 Protein extraction and Western blot

2.1.4.2.1 Extraction of protein

Homogenization of total protein was performed from cortex tissue of 60-week old mice in RIPA-lysis buffer with Halt Protease Inhibitor Single-Use Cocktail using homogenizer. The supernatant was used for protein analysis after centrifugation at 12,000 rpm for 45 min at 4°C.

2.1.4.2.2 Measurement of protein concentration

The protein concentration was measured by Lowry assay. Briefly, the protein samples were diluted in a total volume of 200 μ l. In parallel, BSA solution in 1 mg/ml was diluted for standard curve (0, 2.5, 5, 7.5, 10, 12.5, 15, 20 μ g/200 μ l). After adding 1 ml of copper solution to each sample, these mixtures were vortexed and incubated for 15 min at RT. 100 μ l of Folin-Ciocalteu reagent were added followed by vortex and incubation for 45 min at RT. The absorbance at 595 nm from triplicates of 200 μ l/well in 96 well-plate was measured and the concentration of protein sample was calculated from the standard curve.

2.1.4.2.3 Western Blots

Protein lysates were denatured by incubation at 95°C for 5 min in a Laemmli buffer and stored at -80°C. 50 μ g of protein was loaded on two-layered polyacrylamide gel consisting the upper stacking gel and lower 8% separating gel (Bio-Rad Mini-PROTEAN® Electrophoresis) and electrophoresis was performed by being soaked in running buffer under a constant voltage of 80 V in upper stacking gel and 120 V in lower separating gel. The PageRuller or PageRuler Plus Prestained Protein Ladders were used as protein markers. Separated proteins from SDS-PAGE were transferred onto nitrocellulose membrane inside a blocking tank unit with transfer buffer under a constant current of 80 mA for 10 hr. After transfer, membranes were incubated with MemCode Reversible Protein Kit

according to manufacturer's protocol in order to stain proteins. After destaining and washing membranes were blocked in a blocking buffer which is 5% non-fat milk in Tris-buffered saline-Tween (TBST; 50 mM Tris, 150 mM NaCl, 0.5% Tween 20, pH 7.4) for 1h at RT. This blocking buffer was used for dilution of primary and secondary antibodies. The membranes were incubated with primary antibodies including anti-Ambra1 and anti-actin at 4°C overnight followed by incubation with horseradish peroxidase conjugated secondary antibody diluted in 5% non-fat milk in TBST for 1 hr at RT with washing three times for 15 min in TBST between each step. Antibody information is described in the material section (Page No. 37). The signal on the membrane was exposed to Amersham Hyperfilm enhanced chemiluminescent (ECL) by Immobilon Western chemiluminescent horseradish peroxidase (HRP) substrate and measured by Image J. Ambra1 bands were all normalized to their respective actin signals and were expressed in % of average value in male WT. In order to compare difference between WT and Het in male and female, all the values were normalized by the average WT value in each sex as 100% and this normalized Het value was subtracted from 100%.

2.1.5 Magnetic resonance imaging (MRI)

Female and male *Ambra1* WT and Het mice were investigated in juvenile period (P23-25, *Ambra1* WT; n=15/10, *Ambra1* Het; n = 15/9 (Female/Male)). For MRI, animals were initially anesthetized using a chamber pervaded with 5% isoflurane. Subsequently, the mice were intubated, artificially ventilated and maintained under anesthesia with 1.75% isoflurane in ambient air. The animals were then placed in a prone position on a purpose-build palate holder. Respiratory movement and rectal temperature were monitored. A heated water bed was used to maintain the rectal temperature at $36\pm 1^{\circ}\text{C}$. MRI was performed at 7 and 9.4 T. Radiofrequency excitation and signal reception were accomplished with the use of a birdcage resonator (inner diameter, 72 mm) and a four-channel phased-array surface coil, respectively. T2-weighted MRI data were acquired with a three-dimensional fast spin-echo MRI sequence (repetition time TR = 3.5 sec, effective echo time TE_{eff} = 55 msec, 12 differently phase-encoded echoes, 56 min measuring time) at an isotropic spatial resolution of 100 μm.

2.1.5.1 MRI Volumetry

Surface reconstructions and volume-rendered visualizations of the brain were computed from T2-weighted 3D MRI data sets at 100 μm isotropic spatial resolution. Polygonal surface models of

selected brain structures were generated by importing DICOM images into AMIRA which offers 3D reconstruction and visualization tools. Structures of interest such as the whole brain, cerebellum, olfactory bulb, hippocampus and ventricles (the lateral and third ventricles) were manually as well as semi-automatically labeled with the use of the program's segmentation editor. All brain areas were segmented on three-dimensional label fields (80 horizontal, 192 coronal, and 144 sagittal slices). All objects could be visualized independently, rotated in space, and overlaid onto anatomical images, while maintaining spatial relationships. The experimenter performing the analyses was not aware of the genotype of the mice.

2.1.6 Histological and immunohistochemical analyses

2.1.6.1 Perfusion

Mice were anesthetized by i.p. injection with 0.276 mg Avertin per g of body weight and perfused transcardially with Ringer solution followed by 4% paraformaldehyde (PFA) in PBS. Brains were taken out and post-fixed at 4°C in 4% PFA in PBS for 2 hr for X-galactosidase (X-gal) histochemical staining and for overnight followed by cryo-protectant step until sinking down in 30% sucrose solution in PBS and cryopreserved in liquid nitrogen for immunohistochemistry.

2.1.6.2 X-galactosidase (X-gal) staining

X-gal histochemical staining was performed in 9 week-old *Ambra1* WT and Het male mice. The 50 µm coronal brain sections were cut using Leica VT1000S vibrotome and incubated for overnight in the dark at 37°C in X-gal solution which is described in the material part (Page No. 36), rinsed in PBS (3 times), and mounted with Aqua-Poly/mount medium. Digital images were obtained using Axiophot microscope.

2.1.6.3 Immunohistochemistry (Colocalization of β-Gal with different cellular markers & counting CTIP2+, GAD67+ and PV+ cells)

Colocalization of β-Gal with different cellular markers (NeuN, Olig2, GFAP and IBA-1) and counting CTIP2+, GAD67+ and PV+ cells were carried out in 23-day old *Ambra1* WT and Het female mice. Coronal sections in 30 µm thickness were cut by Leica CM1950.

The sections including hippocampal regions were blocked with 10% normal horse serum (NHS) and 0.2% Triton X-100 in PBS for 1 hr at RT. 5% NHS and 0.2% Triton X-100 in PBS was also used for the primary and secondary antibody dilution. The information of primary and secondary antibodies that were used in this study is indicated in the material section (Page No. 37-38). Incubation of the primary antibodies was carried out at 4°C for 1-3 nights, followed by incubation of secondary antibodies for 2 hr and DAPI for 5 min at RT with dilution factor as 1:500 for primary antibodies and 1:1000 for secondary antibodies. Washing using PBS for 5 min x 3 times was performed between every step. Lastly, sections were mounted using Aqua-Poly/mount.

2.1.6.4 Image acquisition

Confocal laser scanning microscopy (Leica TCS SP5) was used to scan for co-localization of β -Gal with different cellular markers and counting CTIP2+ and GAD67+ cells in anatomically matched sections using 0.5 μ m intervals and 20x glycerol objective lens. Images of PV+ cells in the hippocampal pyramidal layer (CA1+CA2+CA3) were obtained using a 20x objective in epifluorescence microscopy (Leica DMI6000).

For counting CTIP2+, GAD67+ and PV+ cells, every 10th section obtained from the dorsal part of hippocampus (Bregma -1.34 to -2.54 mm posterior) was analyzed bilaterally in each animal (3 sections per animal). Cell density was obtained by dividing the number of CTIP2+ and GAD67+ in hippocampal CA1 pyramidal layer and PV+ cells in hippocampal pyramidal layer per animal by the total volume of hippocampal region in mm³. Stacks were further processed by Image J. The final quantification of CTIP2+, GAD67+ and PV+ cells was done using Imaris 7.5.1.

2.1.7 Electrophysiological analysis of hippocampal pyramidal neurons

2.1.7.1 Synaptic plasticity

2.1.7.1.1 Preparation of acute hippocampal slice

3 and 4 week-old *Ambra1* WT and Het mice in male and female were used for input-output curve, paired-pulse ratio (PPR) and early phase-long term potentiation (E-LTP). The mice were anesthetized with Isoflurane and decapitated by cervical dislocation and skull was open. The whole brain was quickly and carefully removed from the skull and immediately transferred in the cold slicing solution.

The hippocampi were isolated carefully and cut in 300 μm using a McILWAIN tissue chopper. These transverse hippocampal slices were immediately transferred and recovered in a chamber filled with carbogen (95% oxygen and 5% carbon dioxide)-supplied artificial cerebrospinal fluid (ACSF) at 37°C (3 week-old animal: for 1 hr, 4 week-old animal: for 1 hr 40 min). After the recovery, the slices were kept at RT.

For the measurement, the slice was placed on a recording chamber with carbogen-supplied ACSF and maintained at 30°C. The recording electrode (2-3 M Ω) was pulled from thin-walled borosilicate glass capillaries using a pipette puller, filled with ACSF. To evoke fEPSPs, electric stimulations on the *Stratum radiatum* at CA3/CA1 junction for the activation of Schaffer collaterals were applied using a concentric metal bipolar electrode with a 100 μs duration time. The recording pipet was positioned in the *Stratum radiatum* of the CA1 area and the recordings were performed using a Multiclamp 700B amplifier and a Digidata 1440A. For the analysis, the data were analyzed using AxographX.

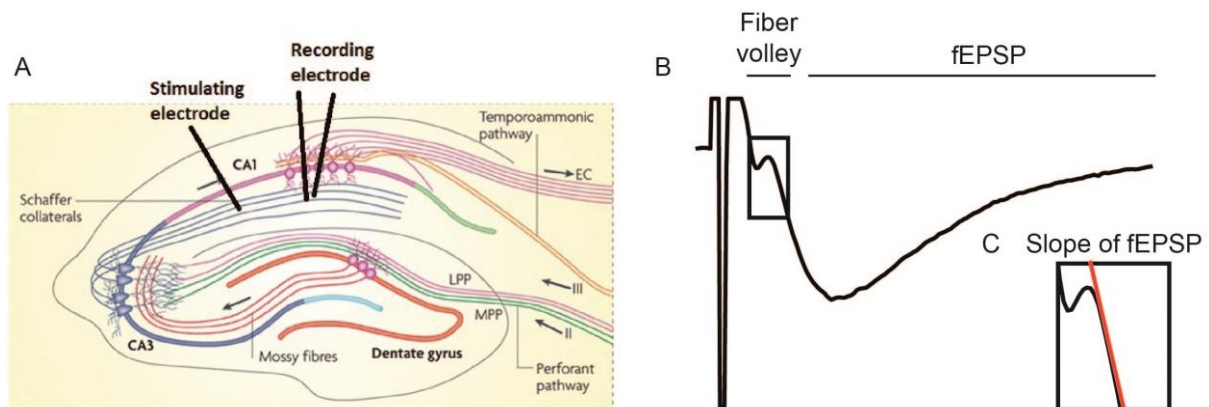


Figure 4. Illustration of extracellular recording of fEPSP at CA1 *Stratum radiatum* by stimulation of Schaffer collateral

A: Illustration of positioning stimulating and recording electrode for extracellular recording of CA1 LTP; Adapted by permission from Nature Publishing Group with license number #3912761270009 (Deng et al., 2010). **B:** An exemplar trace of evoked fEPSP in CA1 *Stratum radiatum*, consisting of a fiber volley caused by the inward current of the action potential and fEPSP (Bortolotto et al., 2011) **C:** Enlarged picture of initial part of fEPSP. Slope of fEPSP was depicted in red color.

2.1.7.1.2 Input-Output curve

For input-output relationship, fEPSPs were evoked with different stimuli at 1/30 Hz and an average of two consecutive responses was used for analysis. Slopes of fEPSPs taken at the initial linear parts of fEPSPs (0.1 msec duration) were plotted in the y-axis of input output curve, and amplitudes of fiber

volley (FV) measured at the negative peaks of FV were used at the x-axis of the curve. Linear regression was performed on the individual slices to calculate the linear fit slope as the slope of the linear input-output relationship.

2.1.7.1.3 Paired pulse ratio (PPR)

The stimulation intensity was determined as 40-50% of the maximal fEPSP slope. Pairs of stimuli were given with various interstimulus intervals (ISI) between 10-1000 msec (10, 25, 50, 100, 200, 500, and 1000 msec). The ratio of the second fEPSP slope to the first fEPSP slope was analyzed. Average of two or three repetitive trials were used for each point per slice.

2.1.7.1.4 Early phase long-term potentiation (E-LTP)

The stimulation strength was adjusted to yield 40-50% of the maximal fEPSP slope. The fEPSP was continuously monitored every 30 second. After measurement of a stable baseline at least for 20 min, E-LTP was induced by a single train of high frequency stimulation (HFS) consisted of 100 pulses at 100 Hz. 1 min after LTP induction, fEPSP was measured for 40 min. If fEPSP after LTP induction was lower than baseline level, the recording was discarded.

2.1.7.2 Gamma oscillation in CA3 pyramidal layer of hippocampus

2.1.7.2.1 Preparation of acute brain slices

3 and 4 week-old mice were anesthetized with Isoflurane and decapitated. Skull was open and each hemisphere was cut 5° tilted from the midline. The cutting side was placed on the Leica VT1200S vibrotome inside a cold slicing solution at 4°C with application of carbogen gas. Tilted sagittal sections in 300 µm thickness were obtained using a vibratome. During the cutting procedure, the tissue was immersed in carbogen-supplied cold slicing solution. The sections were transferred to a chamber carbogen-supplied ACSF at 37°C for 20 min due to recovery. After then, the sections in a chamber with ACSF saturated with carbogen gas were kept at RT.

2.1.7.2.2 Gamma oscillations under interface conditions

Network activity was evaluated by recording extracellular field potentials. Hippocampal slices were placed in a recording chamber. Slices were placed on a nylon mesh in a stream of warm ACSF at

33°C supplied by carbogen gas. The recording electrode (2-3 MΩ) was pulled from thin-walled borosilicate glass capillaries using a pipette puller, filled with ACSF and placed in the hippocampal pyramidal cell layers of CA3. Extracellular field potentials were recorded with a 700B amplifier and the Digidata 1440 A data acquisition system with application of a Bessel filter at 3 kHz and a gain of 100. For each slice, field potentials were recorded for 30 min during ACSF application as baseline, followed by recording of gamma-oscillation field-potentials during application of 100 nM kainate in ACSF for 30 min. After recording, the electrode was slightly moved and measured to acquire the maximum power of gamma oscillations for 10 more minutes. Data were analyzed using Axograph X software.

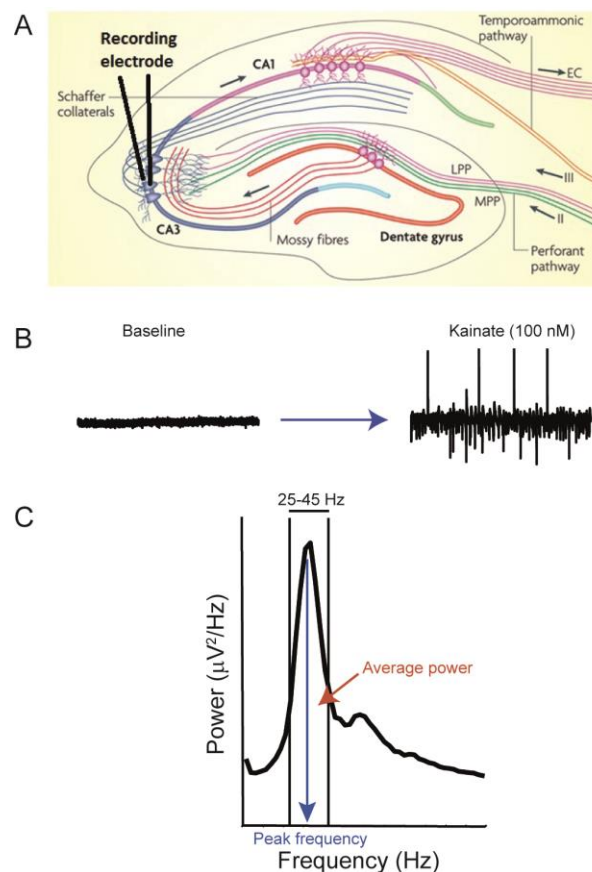


Figure 5. Illustration of extracellular recording of kainate-induced gamma oscillation at CA3 *Stratum pyramidale*

A: Illustration of positioning recording electrode at the CA3 *Stratum pyramidale* for recording gamma oscillation. Adapted and modified by permission from Nature Publishing Group with license number #3912761270009 (Deng et al., 2010). **B:** Representative trace of baseline and after induction of gamma oscillation at CA3 *Stratum pyramidale*. **C:** Exemplar power spectrum after subtraction of power spectrums of baseline and after induction of gamma oscillation. The peak frequency and average power within gamma range (25-45 Hz), which was also used in the present study, are indicated in the picture.

The power spectrum was calculated for 10-min epochs (last 10 min of each recording) of field activity recorded from baseline and kainate application. The baseline power spectrum was subtracted from the power spectrum induced by kainate. Frequency of the maximum peak and average power were calculated within the gamma oscillatory frequency range (25 – 45 Hz) from the power spectrum.

2.1.8 Morphological analysis of hippocampal pyramidal neurons

2.1.8.1 In utero electroporation (IUE)

Micropipettes for IUE were prepared from 1.5–1.8 X 100 mm borosilicate glass capillaries (Kimble and Chase) using HEKA PIP5 temperature controlled pipette puller. To ensure the appropriate tip diameter, the filament was heated to 1000°C, and pulling of glass capillary was controlled manually, allowing for slow expansion of heated glass.

E14.5 mouse embryos were subjected to IUE according to permit number 33.19-42502-04-13/1052 (Hiroshi Kawabe), and previously published work (dal Maschio et al., 2012; Matsui et al., 2011). *Ambra1* WT pregnant female mice, crossed with *Ambra1* Het males, were deeply anesthetized with isoflurane (Ecuphar)/oxygen diffusor (Plexx, HNG6), and placed on warm heating pad (32°C). Before surgery, the heart rate or the breathing frequency was noted, and the toe pinch-reflex enabled to assess the surgical plane. A layer of Vidisc gel was applied onto each cornea to prevent their damage. To ensure post-operative analgesia, 3 mg buprenorphine was administered subcutaneously. Abdominal wall was thoroughly washed with 70% ethanol, and 50 mg/mL povidon-iodine. Incision of about 2 cm in the abdominal cavity was made to expose entire uterus with embryos, which were subsequently moistened with warm PBS supplied with penicillin 2000 U/mL, and 2 mg/mL streptomycin. Micropipette with the DNA solution with pFUGW (0.1mg/mL) (Lois et al., 2002) and pCX::myrVENUS (0.1mg/mL) (Rhee et al., 2006) for myrVenus construct was carefully injected to the lateral ventricle of the embryonic brain, and exhausted by expiratory pressure through a pneumatic pump. Those DNA constructs were kindly provided by the authors of cited papers. The forceps-type electrode was placed around the embryo head accordingly to the targeted brain region (Kolk et al., 2011), and electric current was applied with ElectroSquare. For electroporation, 38 V pulses were applied six times with 50 msec duration for each pulse with 950 msec intervals. After pulsing, embryo head was thoroughly washed with warm PBS with antibiotics. Next, the uterus with embryos was

carefully placed back to the abdominal cavity, and the body wall was closed with absorbable surgical sutures (Safil, Aesculap; 4/0, 28"; HR17), and the skin with 9 mm Autoclips. The animals were kept on the warm pad until back to consciousness. The mouse was monitored post-operatively until deceased.

2.1.8.2 Immunohistochemistry for dendritic morphology and spine number

2.1.8.2.1 Perfusion & section preparation

At P28, *Ambra1* WT and Het mice in both sexes went through intracardiac perfusion with PBS and 4% PFA in PBS for 15 min. Afterwards, brains were post-fixed in 4% PFA in PBS for overnight, washed with PBS thoroughly and subjected to sucrose gradient (15%-30% w/v sucrose in PBS). Coronal brain sections in 230 µm thicknesses were collected by the Leica VT1000S vibrotome and stored in PBS with 0.01% sodium azide, and kept at 4°C until further processing.

Imaging of brain coronal cross sections after in utero electroporation was performed at -1.06 mm to -2.46 mm from Bregma. For immunofluorescence staining, PFA was quenched from brain sections by application of 1mg/1mL NaBH₄ in PBS for 5 min and sections were thoroughly washed with PBS. The brain sections were blocked in blocking solution (5% Normal goat serum and 0.5% Triton-X-100 in PBS) for 1 hr at RT followed by 0.2% Tween-20 and 10 µg/mL heparin in PBS for 1.5 hr on the purpose of penetration of antibody in the thick brain section. This blocking solution was also used for the primary and secondary antibody incubation with dilution factor, 1:1000 (Page No. 37-38). The incubation of polyclonal rabbit GFP antibody was carried for 4 days at 4°C with gentle agitation. Sections were incubated in Alexa Fluor 488 goat anti-rabbit for overnight at RT with washing for 8 hr after incubation of each antibody. The information of antibody and dilution is described in Material part. The incubation of DAPI, diluted as 1:10000 in PBS, was followed for 1hr at RT. After washing, sections were on slide and coverslip was mounted using Immu-Mount.

2.1.8.2.2 Image acquisition and analysis

For dendritic morphology, images were acquired from Leica SP2 confocal microscopes (Leica) with oil immersion 20x objectives and 2 optical zoom. Image stacks of pyramidal cells in the middle of CA1 area were acquired at 1.02 µm intervals and the dendritic morphology was reconstructed and shall analysis was done in 3-D using NeuronStudio software. NeuronStudio is a program designed to allow

automatic tracing and 3D reconstruction of neuron structures from confocal image stacks (Rodriguez et al., 2008). It is able to handle morphologic details on the scale of local spine geometry via complex tree topology to the multi-neuron networks.

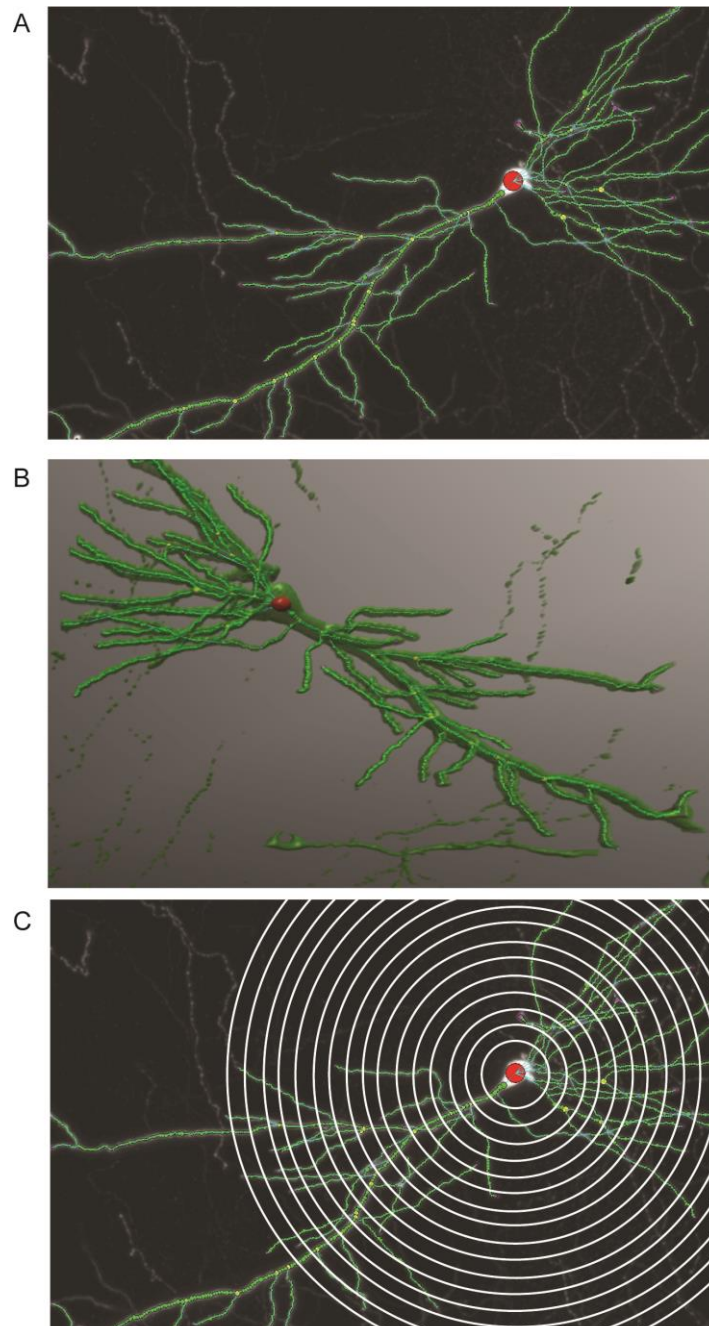


Figure 6. Dendritic reconstruction and 3D shell analysis by NeuronStudio program

A, B: Representative picture of dendritic reconstruction of CA1 pyramidal neuron in 2D and 3D picture.

C: Based on the dendritic reconstruction, 3D shell analysis was performed.

2.1.9 Statistical analysis

All data were analyzed separately for males and females. Between group-comparisons were made by t-test for independent sample. Survival analysis was performed for the data in Fig 16. F. All statistics were performed in Prism Graph Pad software. Data presented in the figures and test are expressed as mean \pm SEM and p-values $<$ 0.05 were considered as being significant.

2.2 Materials

2.2.1 Chemicals

Product	Company
30% Acrylamide	Merck KGaA, Darmstadt, Germany
Agarose	Life Technologies GmbH, Darmstadt, Germany
Ammonium persulfate (APS)	Sigma-Aldrich, Taufkirchen, Germany
Aqua-Poly/Mount	Polyscience, Philadelphia, USA
Bromophenol blue	Sigma-Aldrich, Taufkirchen, Germany
BSA 10mg/ml (100x)	Neu England Biolabs (NEB), Hitchin, UK
Buprenorphine (Temgesic)	
Chloroform	Merck KGaA, Darmstadt, Germany
CuSO ₄	Merck KGaA, Darmstadt, Germany
EDTA	Sigma-Aldrich, Taufkirchen, Germany
Ethylene glycol	Sigma-Aldrich, Taufkirchen, Germany
Folin-Ciocalteu reagent	Merck KGaA, Darmstadt, Germany
Formaldehyde	Merck KGaA, Darmstadt, Germany
Glacial acetic acid	Merck KGaA, Darmstadt, Germany
Glycerol	Merck KGaA, Darmstadt, Germany
Glycine	Merck KGaA, Darmstadt, Germany
HDGreen Plus Safe DNA Dye	Intas, Göttingen, Germany
Heparin	Sigma-Aldrich, Taufkirchen, Germany
37% HCl	Merck KGaA, Darmstadt, Germany
Immuno-Mount	Thermo Fisher Scientific, Bonn, Germany
Isopropanol	Merck KGaA, Darmstadt, Germany
Isofurane	Actavis Deutschland GmbH & Co. K, München, Germany
K-Na-tartrate	Merck KGaA, Darmstadt, Germany
β-Mercaptoethanol	Sigma-Aldrich, Taufkirchen, Germany
MgCl ₂	Sigma-Aldrich, Taufkirchen, Germany
Na ₂ CO ₃	Merck KGaA, Darmstadt, Germany
NaOH	Merck KGaA, Darmstadt, Germany
Normal horse serum	Jackson ImmunoResearch Laboratories, Inc. USA
Nonfat dried milkpowder	AppliChem, Darmstadt, Germany
Pentylentetrazol (PTZ)	Sigma-Aldrich, Taufkirchen, Germany
Povidon-iodine	Vetasept,
Power SYBR Green	Thermo Fisher Scientific, Bonn, Germany
Pyronin Y	Sigma-Aldrich, Taufkirchen, Germany
Ringer solution	B.Braun Melsungen AG, Melsungen, Germany
Sodium dodecyl sulfate (SDS)	Merck KGaA, Darmstadt, Germany
Sodium tetraborohydride	Sigma-Aldrich, Taufkirchen, Germany
Streptomycin	Thermo Fisher Scientific, Bonn, Germany

Sucrose	Merck KGaA, Darmstadt, Germany
TEMED	SERVA Electrophoresis GmbH, Heidelberg, Germany
Tribromoethanol	Sigma-Aldrich, Taufkirchen, Germany
Trizma base	Sigma-Aldrich, Taufkirchen, Germany
Tissue-Tek	VWR International GmbH, Darmstadt, Germany
Triton-X-100	Sigma-Aldrich, Taufkirchen, Germany
Tween-20	Sigma-Aldrich, Taufkirchen, Germany
Vidisc gel	Buasch + Lomb, Rochester, USA

Ladders

Product	Company
PageRuler Plus Prestained protein ladders	Thermo Fisher Scientific, Bonn, Germany
1kb DNA ladder	Life Technologies GmbH, Darmstadt, Germany
100 bp Plus DNA ladder	Thermo Fisher Scientific, Bonn, Germany

Kit

Product	Company
Failsafe enzyme with PreMix D	Epicentre, Madison, USA
SuperScript III Reverse Transcriptase	Life Technologies, Darmstadt, Germany
Power SYBR Green PCR Master Mix	Life Technologies, Darmstadt, Germany
NucleoSpin Tissue Kit	MACHERY-NAGEL GmbH & Co. KG, Düren, Germany
Immobilion Western chemiluminescent HRP substrate	Merck Millipore, Germany
GoTaq® G2 Flexi DNA polymerase	Promega, Mannheim, Germany
miRNeasy Mini Kit	Qiagen, Hilden, Germany
MemCode Reversible Protein Kit	Thermo Scientific, Darmstadt, Germany

2.2.2 Equipment

Vibrotome or Cryostat	Company
Leica VT 1000S Vibrotome	Leica Biosystems, Wetzlar, Germany
Leica VT 1200S Vibrotome	Leica Biosystems, Wetzlar, Germany
Leica CM1950 Cryostat	Leica Biosystems, Wetzlar, Germany

Microscopy	Company
Axiophot microscope	Carls Zeiss Microscopy GmbH, Göttingen, Germany
Leica TCS SP5 confocal microscopy	Leica Biosystems, Wetzlar, Germany
Leica TCS SP2 confocal microscopy	Leica Biosystems, Wetzlar, Germany
Leica DMI6000 epifluorescence microscopy	Leica Biosystems, Wetzlar, Germany

Equipment	Company
------------------	----------------

7T MRI	Bruker Biospin MRI GmbH, Ettlingen, Germany
9.5T MRI	Bruker Biospin MRI GmbH, Ettlingen, Germany
Axon Digidata 1440A	Molecular devices, LLC., Sunnyvale, USA
Axon MultiClamp 700B amplifier	Molecular devices, LLC., Sunnyvale, USA
BioRad Mini Trans-Blot Cell system	Bio-Rad, München, Germany
Bio-Rad Mini-PROTEAN Electrophoresis	Bio-Rad, München, Germany
Birdcage resonator (inner diameter, 72mm)	Bruker Biospin MRI GmbH, Ettlingen, Germany
Concentric bipolar electrode	FHC, Bowdoin, USA
Digidata 1440A	Molecular devices, LLC., Sunnyvale, USA
EpMotion robot 5075	Eppendorf AG, Hamburg, Germany
Four channel phased array surface coil	Bruker Biospin MRI GmbH, Ettlingen, Germany
GeneQuant II Spectrometry	Pharmacia Biotech, Piscataway, USA
HEKA PIP temperature-controlled pipette puller	HEKA, Lambrecht/Pfalz, Germany
HERA-cell240 incubator	Thermo Fisher Scientific, Bonn, Germany
Heraeus Biofuge haemo	Thermo Fisher Scientific, Bonn, Germany
Heraeus Megafuge 16R	Thermo Fisher Scientific, Bonn, Germany
Homogenizer	KINEMATICA AG, Luzern, Switzerland
Interface recording chamber (BSC-BU Base Unit with BSC-HT Haas Top)	Harvard apparatus, Freiburg, Germany
Light Cycler 480	Roche, Mannheim, Germany
MclLWAIN tissue chopper	Molecular devices, LLC., Sunnyvale, USA
Mini-peristaltic pump	HARVARD apparatus, Holliston, USA
Multiclamp 700B amplifier	Molecular devices, LLC., Sunnyvale, USA
Pipette puller P-80/PC	Sutter Instrument Co., Novato, USA
Recording chamber 64-1525,	HARVARD apparatus, Holliston, USA
Thermomixer Compact	Eppendorf AG, Hamburg, Germany
UltraSoundGate 116	Avisoft Bioacoustics, Glienicke, Germany
UltraSoundGate CM16	Avisoft Bioacoustics, Glienicke, Germany

2.2.3 Software

Software	Company/Supplier
AMIRA	Bisage Imaging, Berlin, Germany
Avisoft-SASLab 5.2	Avisoft Bioacoustics, Glienicke, Germany
AxographX	Axograph, Berkeley, USA
Axon instruments Digitizer 1322A (and pClamp9.2)	Molecular Devices, Sunnyvale, USA
Graphpad Prism 4	GraphPad Software Inc., La Jolla, USA
Image J	Free open source software
LightCycler 480 software 1.5.0 SP3	Roche, Mannheim, Germany
NeuronStudio	CNIC, Mount Sinaï School of Medicine, Newyork, USA
Patchmaster 2 program	HEKA, Lambrecht/Pfalz, Germany

2.2.4 Consumable

Product	Company
1.5-1.8 x 10mm borosilicate glass capillaries	Kimble and Chase
Amersham Hyperfilm ECL	GE Healthcare, buckinghamshire, UK
Borosilicate glass capillaries GC150TF-10	HARVARD apparatus, Holliston, USA
Microwell Plate 96	Thermo Fisher Scientific, Roskilde, Denmark
Millex Syringe Filter Unit, 0.22µm	Merck KGaA, Darmstadt, Germany
Multiwell plate 384	Roche Diagnostics, Mannheim, Germany
Nitrocellulose membrane	GE Healthcare, buckinghamshire, UK
SuperFrost ultra plus slide	Menzel GmbH, Braunschweig, Germany

2.2.5 Buffers and solutions

1x TAE

4.84g Tris base
 1.142ml glacial acetic acid
 2ml 0.5M EDTA,
 Fill ultra-pure water upto 1l, pH8.0

Fresh Copper solution

20ml 2% Na₂CO₃ (10g Na₂CO₃ in 500ml 0.1M NaOH)
 0.2ml 2% K-Na-tartrat (10g K-Na-tartrat in 500ml ultra-pure water)
 0.2ml 1% CuSO₄ (5g CuSO₄·5H₂O in 500ml ultra-pure water)

RIPA-lysis buffer

50mM Tris
 150mM NaCl
 1.0% Triton X-100
 0.5% sodium deoxycholate
 0.1% SDS, pH 7.4

4x Laemmli buffer

2.5ml 1M Tris HCl (pH8.3)
 0.8g SDS
 4ml Glycerin
 2ml β-mercaptoethanol
 4mg Pyronin Y
 1.5ml ultra-pure water

1x PBS

0.2g NaCl
 8g KCl
 1.44g Na₂HPO₄
 0.24g KH₂PO₄
 Filled up with ultra-pure water, pH7.4

Ethylene glycol cryoprotectant solution

498ml Glycerol (85%)
588ml Ethylene glycol
912ml 1x PBS

8% lower gel

10ml 30% acrylamide
0.59g Tris base
390µl 10% SDS
13.13ml ultra-pure water
125 µl 10% APS
30µl TEMED

Upper gel

1.3ml 30% acrylamide
0.151g Tris base
100µl 10% SDS
6.1ml H₂O
50µl 10% APS
10µl TEMED

1x Running buffer

3g Tris base
18.78g Glycine
1g SDS
Fill ultra-pure water upto 1l

1x Transfer buffer

2.42g Tris base
11.64g Glycine
Fill ultra-pure water upto 1l

1x TBS

50mM Tris base
150mM NaCl, pH7.4

1x TBST

1l 1x TBS
0.5mL Tween-20

Avertin

1g Tribromoethanol
74.49ml Pre-warmed H₂O (40°C)
0.81ml Amyl alcohol

X-Gal solution

5mM K₃[Fe(CN)₆]
5mM K₄[Fe(CN)₆]
2mM MgCl₂
1.2mg/mL 5-bromo-2-chloro-3-indoyl-b-D-galactopyranoside in PBS

Slicing solution

230 mM Sucrose
26 mM NaHCO₃
2 mM KCl
1 mM KH₂OP₄
2 mM MgCl₂·6H₂O

10 mM Glucose
0.5 mM CaCl₂

ACSF

120 mM NaCl
26 mM NaHCO₃
1 mM KH₂PO₄
2 mM KCl
2 mM MgCl₂·6H₂O
10 mM Glucose
2 mM CaCl₂
320 mOsmol/l, pH7.3

2.2.6 Primers

The primers were synthesized in MPI-EM DNA Core Facility for this experiment and mentioned in the method part.

Primer #	Detection of gene	Sequences
<i>Genotyping</i>		
24508	<i>Ambra1</i> wild type allele	5'-AAC TGA ACC TGG GTT CTT TGA A -3'
24509	<i>Ambra1</i> wild type & mutated allele	5'-GAA AAG CTC CCC ATC TTT TCT T-3'
24510	<i>Ambra1</i> mutated allele	5'-ATC CCA AGG GCA GTA GAG TTC-3'
5063	Interleukin-2	5'-CTA GGC CAC AGA ATT GAA AGA TCT-3'
5064	Interleukin-2	5'-GTA GGT GGA AAT TCT AGC ATC ATC C-3'
23366	Y chromosome	5'-GGT GTG GTC CCG TGG TGA GAG-3'
23367	Y chromosome	5'-GAG GCA ACT GCA GGC TGT AAA ATG-3'
<i>cDNA synthesis</i>		
4542	N9	5'-NNN NNN NNN-3'
9578	Oligo (dT)-Mix	5'-TTT TTT TTT TTT TTT TTT TTV N-3'
<i>qPCR</i>		
31502	<i>Ambra1</i>	5'-AGG CTC CAG TGG TGG GAC TTC AC-3'
31503	<i>Ambra1</i>	5'-GCC AGG AGC TGA CCA TCT GCA G-3'
9146	β-actin	5'-CTT CCT CCC TGG AGA AGA GC-3'
9147	β-actin	5'-ATG CCA CAG GA+A1:C17T TCC ATA CC-3'

2.2.7 Antibodies

1°antibody	Full name	Company	Catalog No.	Host	Poly / Clone
Ambra1	Activating molecule in Beclin-1-regulated autophagy	Millipore	ABC131	rabbit	polyclonal
β-gal	β-galactosidase	Promega	Z3781	mouse	monoclonal
NeuN	Neuronal nuclei	Synaptic systems	266006	chicken	polyclonal
IBA-1	Ionized calcium binding adaptor molecule 1	Wako	019-19741	rabbit	polyclonal
Olig2	Oligodendrocyte transcription factor 2	Chemicon	AB9610	rabbit	polyclonal
GFAP	Glial fibrillary acidic protein	Promega	G5601	rabbit	polyclonal

GFP	Green fluorescent protein	MBL	598	rabbit	polyclonal
CTIP2	COUP-TF-interacting protein 2	Synaptic Systems	325 005	guinea pig	polyclonal
GAD 67	Glutamic Acid Decarboxylase 67	Chemicon	MAB5406	mouse	monoclonal
PV	Parvalbumin	Sigma	P3088	mouse	monoclonal, PARV-19

2° Antibody

2° Antibody	Company	Catalog Number
Alexa Fluor 488 donkey anti-mouse IgG	Invitrogen	A21202
Alexa Fluor 488 donkey anti-rabbit IgG	Life Technologies	A-21206
Alexa Fluor 488 donkey anti-chicken IgG	Jackson ImmunoResearch	703-546-155
Alexa Fluor 594 goat anti-mouse IgG	Jackson ImmunoResearch	115-587-186
Alexa Fluor 594 donkey anti-rabbit IgG	Invitrogen	A21207
Cy3 goat anti-mouse IgG	Jackson Immuno Research	115-165-146
HRP-conjugated anti-rabbit	Sigma Aldrich	A-0545

3 Result

3.1 Assessment of developmental milestones and early ultrasonic communication

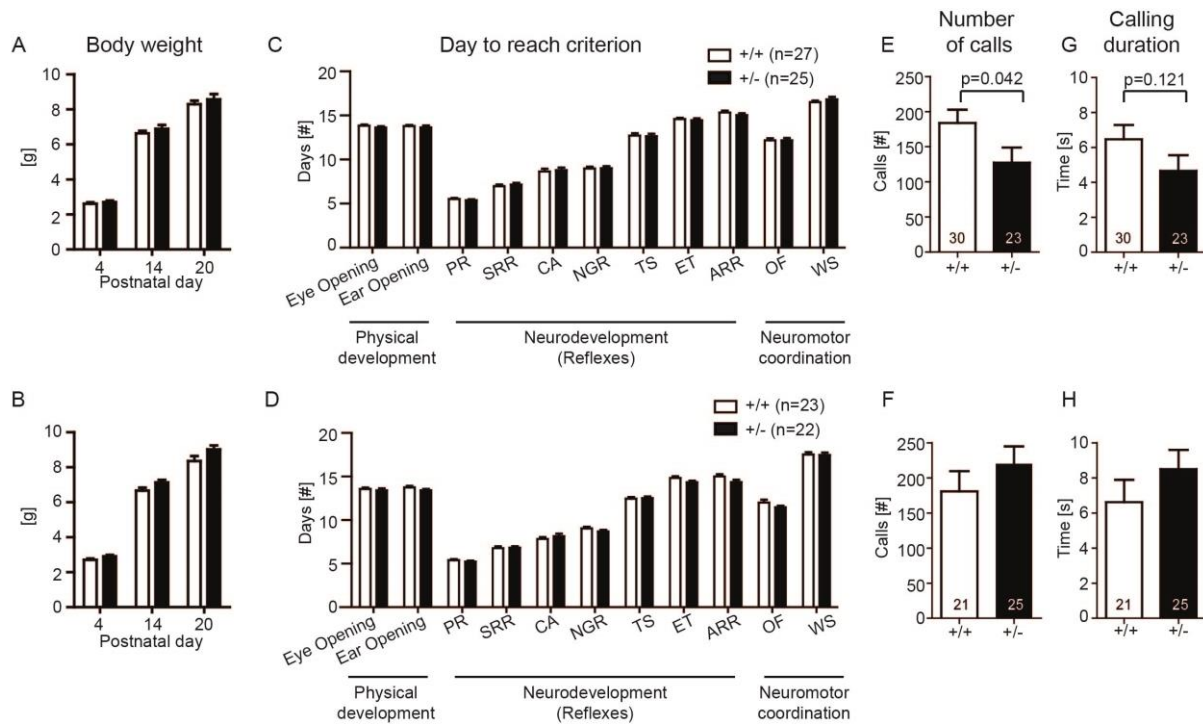


Figure 7. Neonatal development and pub vocalization in *Ambra1*^{+/-} versus *Ambra1*^{+/+} mice of both sexes

The upper row shows results for female, the lower row for male mice. **A, B:** Body weight at P4, P14 and P20; **C, D:** The day to reach criterion in physical development, neurodevelopment (PR: placing response; SRR: surface righting reflex; CA: cliff avoidance; NGR: negative geotaxis reflex; TS: tactile startle; ET: ear twitch; ARR: air righting reflex) and neuromotor coordination (OF: open field traversal; WS: wire suspension) **E-H:** Ultrasound vocalization of pups induced by separation from their mother or nest on postnatal day 8 or 9. Mean±SEM presented; n numbers of each group are presented in the figures. Adapted from *Frontiers in Behavioral Neuroscience* (Dere et al., 2014).

Given the fact that remarkable autistic phenotypes are evident in *Ambra1*^{+/-} females from an early stage, the observation of neurobehavioral developmental milestones and early ultrasonic communication in neonatal mice up to the age of 3-4 weeks is necessary. In order to use *Ambra1*^{+/-} mice as a mouse model of autism, neurological and physical development can be additionally characterized for these mice to indicate a phenotypic onset during any developmental time point. Physical development including body weight, eye opening and ear opening, the development of neurological reflexes and the development of neuro-motor coordination such as open field traversal and wire suspension were comparable in pups of both genders and genotypes ($p > 0.05$) (Fig 7. A-D).

There was a significant reduction in the number of calls induced by separation from mother or nest in female *Ambra1*^{+/-} pups at P8 or P9 compared to control (Number; F_WT: 183.8±19.08, F_Het: 127.3±21.58, p=0.042; Duration; F_WT: 6.467±0.8219 s, F_Het: 4.654±0.9012 s, p=0.121) (Fig 7. E and G), however there was no difference in male mice (Number; M_WT: 180.7±28.77, M_Het: 220.2±24.75, p>0.05; Duration; F_WT: 6.626±1.265 s, F_Het: 8.500±1.092 s, p>0.05) (Fig 7. F and H).

3.2 *Ambra1* mRNA and protein expression

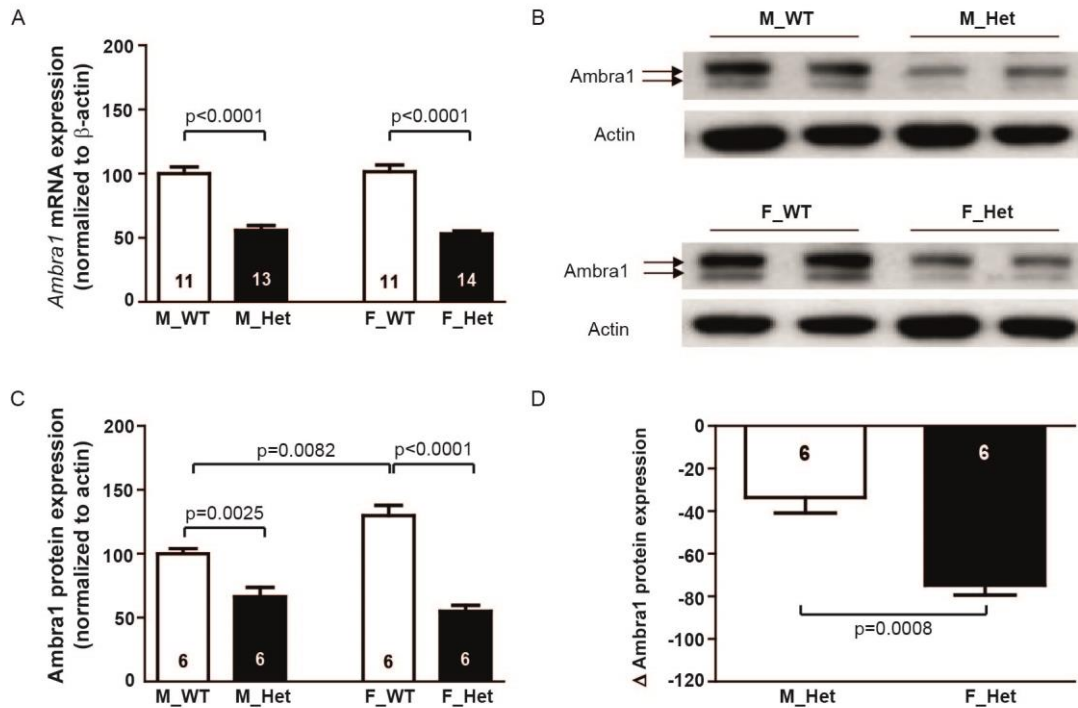


Figure 8. *Ambra1* mRNA and protein expression level in cortex of male and female *Ambra1*^{+/-} and *Ambra1*^{+/+} mice

A: RT-qPCR; **B:** Sample Western blot; **C:** Western blot quantification. **D:** The relative reduction between *Ambra1* WT and heterozygous was produced by subtracting the mean value of WT from all value of heterozygous in each sex. M=male; F=female; Mean±SEM presented; n numbers of each group are shown in the figures. Adapted from *Frontiers in Behavioral Neuroscience* (Dere et al., 2014).

To understand the sexual dimorphism of autistic behavior, the expression levels of *Ambra1* mRNA and protein in the cortex of both genotypes and sexes were measured by RT-qPCR and Western Blot. Levels of both mRNA (M_WT: 100±5.243, M_Het: 55.94±3.643, p<0.0001; F_WT: 101.5±5.234, F_Het: 53.15±2.260, p<0.0001) and protein were significantly lower in *Ambra1*^{+/-} mice, compared to WT controls of both males and females (M_WT: 100±4.085, M_Het: 66.46±7.334, p=0.0025; F_WT: 129.9±8.110, F_Het: 55.11±4.655, p<0.0001), shown in Fig 8. A-C. Interestingly, while *Ambra1* mRNA

levels of *Ambra1*^{+/+} were comparable between males and females ($p>0.05$), *Ambra1* protein levels in female WT mice was higher compared to male WT ($p=0.0082$), a drastic reduction upon heterozygosity was seen in females (Male: -33.54 ± 7.334 , Female: -74.74 ± 4.655 , $p=0.0008$) (Fig 8. D). There may be a connection of *Ambra1* protein expression and the female-specific autism phenotype.

3.3 Brain enlargement

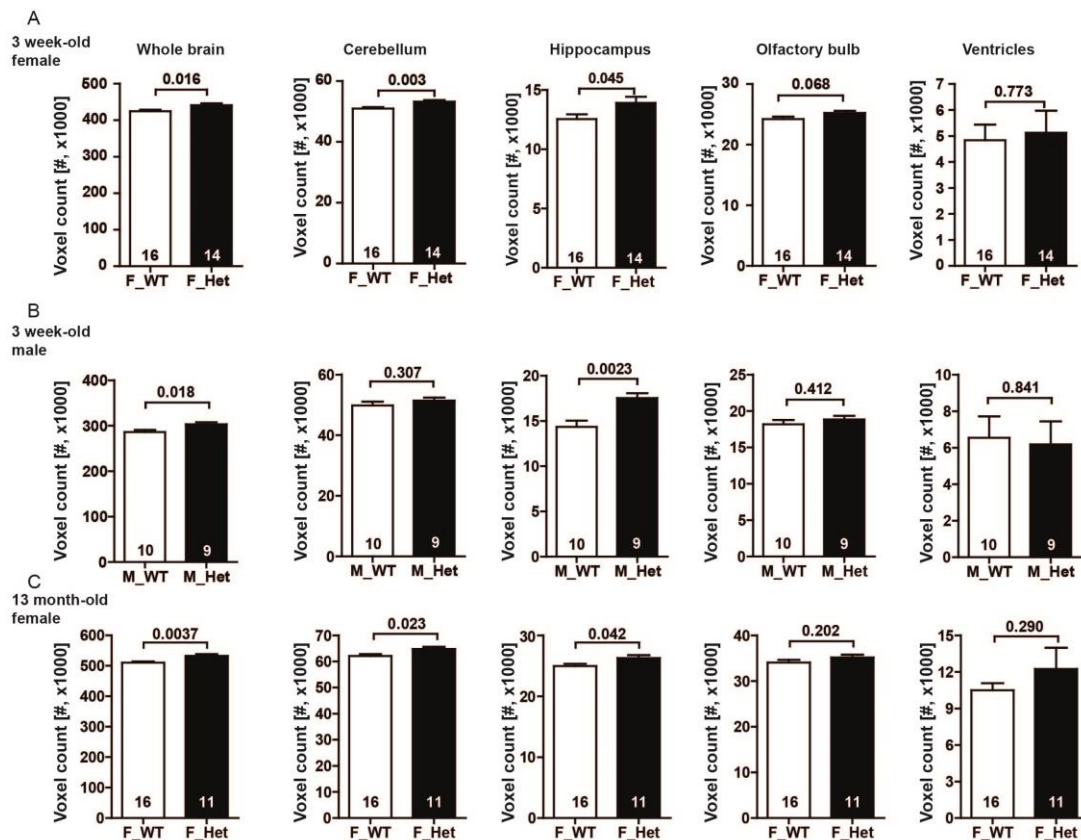


Figure 9. Voxel-based volumetry (T2-weighted MRI) of sub-region and whole-part of brain in *Ambra1* WT and Het mice

Bar graphs of brain dimension ROI (Whole brain, Cerebellum, Hippocampus, Olfactory bulb and Ventricles) in both genotype of **A**: 3 week-old females (F), **B**: 3 week-old males (M) and **C**: 13 month-old females; Mean \pm SEM presented; n numbers of each group and p-value by t-test are shown in the figures.

Several studies have identified the presence of brain enlargement during childhood in autism (Courchesne and Pierce, 2005; Courchesne et al., 2003; Fidler et al., 2007; Hazlett et al., 2011). While the neuroanatomical basis of ASD is not yet known, numerous lines of evidence suggest that abnormalities in brain volume may be a characteristic of autism. Several MRI studies of very young children with autism reported a 5-10% abnormal enlargement in total brain volume that persists into

early childhood (Courchesne et al., 2001; Hazlett et al., 2011). Therefore, in collaboration with Prof. Jens Frahm in MPI-BPC in Göttingen and Prof. Susann Boretius in Kiel, the brains of *Ambra1^{+/-}* and *Ambra1^{-/-}* mice of both sexes in P22-25 and 13 month-old females were imaged by T2-weighted MRI. And this allowed for voxel-based volumetry of different region of interest (ROI), including whole brain, cerebellum, hippocampus, olfactory bulb and ventricles.

Fig 9. A depicts an enlargement of the whole brain (F_WT: 424460±4011 voxels, F_Het: 440630±4921 voxels, p=0.0157), cerebellum (F_WT: 50921±451 voxels, F_Het: 53157±539 voxels, p=0.0034) and hippocampus (F_WT: 12540±403 voxels, F_Het: 13897±518 voxels, p=0.0455) in females while there was no difference in the size of olfactory bulb (F_WT: 24217±396 voxels, F_Het: 25224±342 voxels, p=0.0684) and ventricles (F_WT: 4832±605 voxels, F_Het: 5192±841 voxels, p=0.7731) in comparison to WT females. Whole brain (M_WT: 286030±4541 voxels, M_Het: 302960±4573 voxels, p=0.0179) and hippocampus (M_WT: 14343±675.2 voxels, M_Het: 17510±550 voxels, p=0.0023) were also bigger in male *Ambra1^{+/-}* mice when compared to control males (Cerebellum; M_WT: 49797±1211 voxels, M_Het: 51445±952 voxels, p=0.3074; Olfactory bulb; M_WT: 18153±617.3 voxels, M_Het: 18834±512.8 voxels, p=0.4138; Ventricles; M_WT: 6538±1180 voxels, M_Het: 6186±1258 voxels, p=0.8407) as shown in Fig 9. B. This enlargement of whole brain (F_WT: 510111±4209 voxels, F_Het: 532625±5871 voxels, p=0.0037), cerebellum (F_WT: 62079±716.0 voxels, F_Het: 64760±836.2 voxels, p=0.0231) and hippocampus (F_WT: 24952±376.9 voxels, F_Het: 26258±488 voxels, p=0.0416) in *Ambra1^{+/-}* females persisted after 12 months (Olfactory bulb; F_WT: 34063±557.7 voxels, F_Het: 35151±586.5 voxels, p=0.2023; Ventricles; F_WT: 10499±585.8 voxels, F_Het: 12234±1745 voxels, p=0.2885) (Fig 9. C).

3.4 Expression of *Ambra1* protein in postnatal brain

Given the fact that brain and sub-brain regions were enlarged in juvenile *Ambra1^{+/-}* mice as is seen with autistic children, the next experiment was to figure out the cellular substrate of this enlargement. In order to study this aim, we would like to know in which region of the brain this protein is expressed. Since there is no commercially produced *Ambra1* antibody for immunofluorescence staining, and β -gal activity in a gene-trap line mimics the expression of the tagged endogenous gene (Skarnes et al., 1995), β -gal protein was used as a marker of *Ambra1* expression in the postnatal brain of *Ambra1^{+/-}* mice.

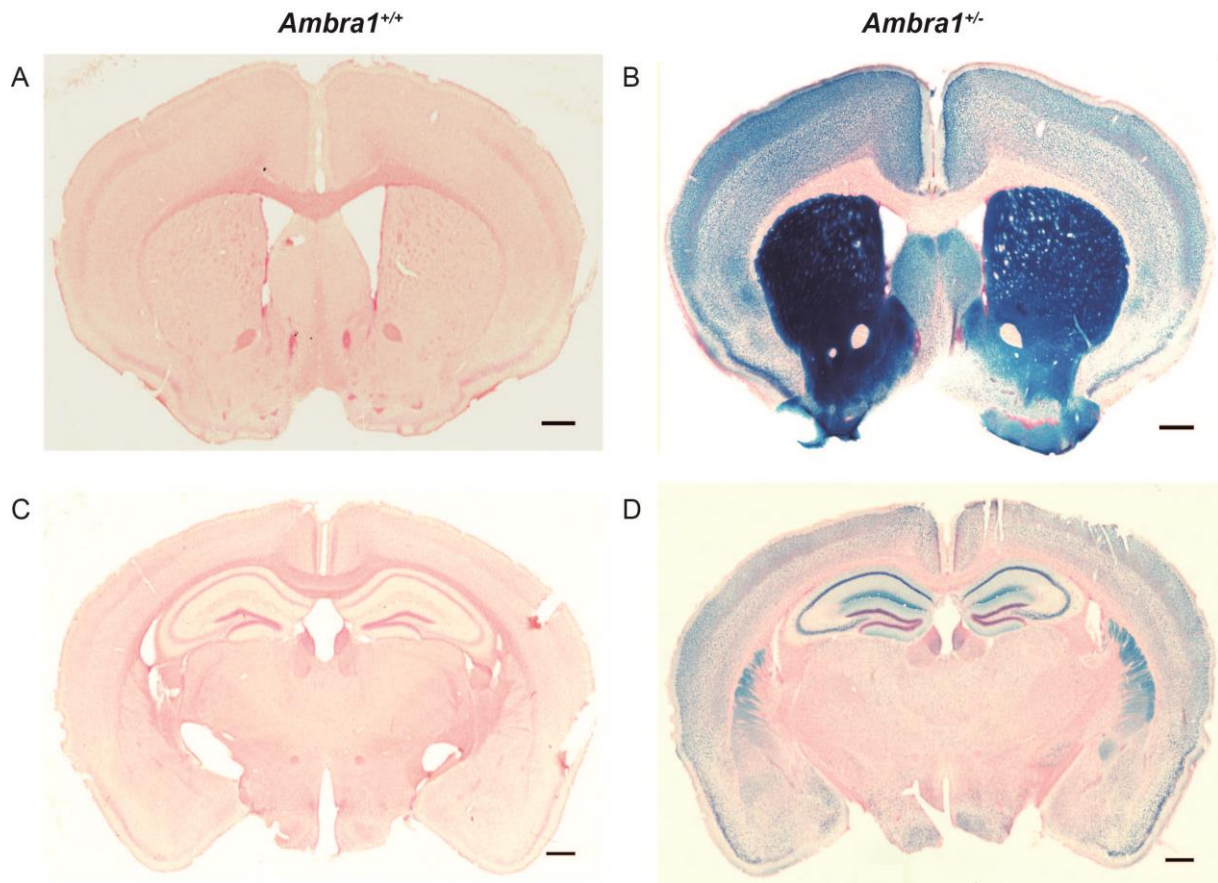


Figure 10. X-galactosidase staining in coronal brain sections of *Ambra1^{+/+}* and *Ambra1^{+/-}* mice. A,C: X-gal staining of same brain region in *Ambra1^{+/+}* mice was used as negative control. B,D: Coronal brain sections of X-gal staining in *Ambra1^{+/-}* mice. Scale bar: 100 μ m

X-gal staining is a rapid histochemical technique used to detect β -gal, reporter gene expression under the promoter of *Ambra1*. Notably, the *lacZ* gene encodes the bacterial (*E.coli*) enzyme β -gal and is commonly visualized as a blue intracellular precipitate following an oxidative reaction with substrate 'X-gal'. Coronal sections of anterior part with prefrontal cortex and striatum and posterior part with hippocampus part of mouse brain in *Ambra1^{+/+}* and *Ambra1^{+/-}* mice were selected for X-gal staining. Fig 10. A-D show the expression of β -gal in striatum, prefrontal cortex and hippocampus, especially, in pyramidal layers of the hippocampus in *Ambra1^{+/-}* postnatal brain, whereas control shows no signal.

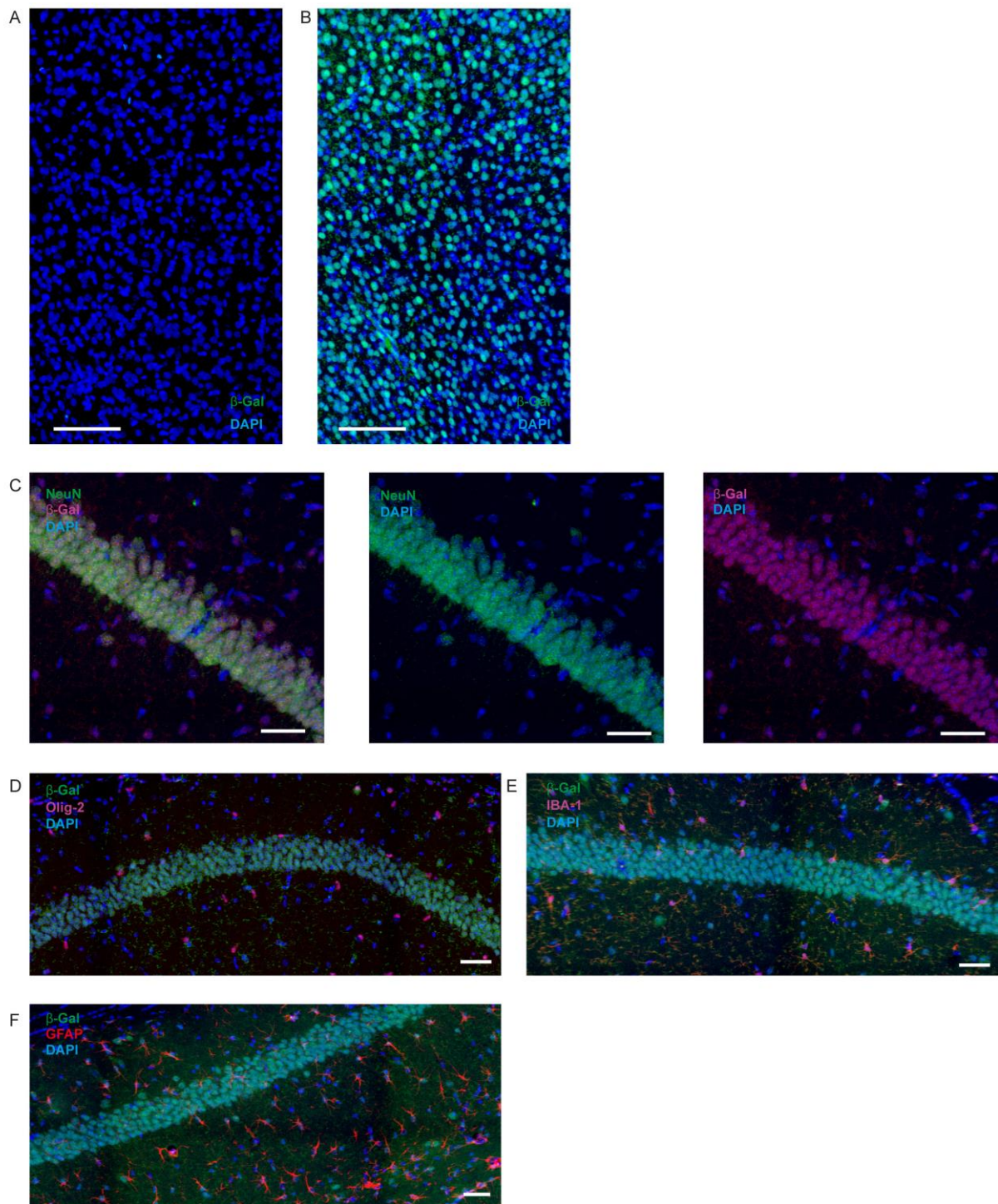


Figure 11. Immunofluorescence staining of β -gal and co-localization of β -gal with different cellular markers in CA1 region of hippocampus in *Ambra1*^{-/-} mouse

The staining of β -gal in the coronal brain sections of **A:** *Ambra1*^{+/+} and **B:** *Ambra1*^{-/-} mice, Scale bar: 100 μ m. The co-staining of β -gal with **C:** NeuN, neuronal marker, **D:** Olig-2, oligodendrocyte marker, **E:** IBA-1, microglial marker, and **F:** GFAP, astrocyte marker, in the hippocampal CA1 region of *Ambra1*^{-/-} mouse. Scale bar: 40 μ m

On the basis of this data, the expression of β -gal in specific cell types was explored by immunofluorescent staining of β -gal together with different cellular markers, such as prototypical markers of neurons, microglia, astrocytes and oligodendrocytes, in the brain. First of all, the immunofluorescent staining of β -gal was validated by comparing *Ambra1^{+/+}* and *Ambra1^{+/-}* sample (Fig 11. A and B). This staining protocol was combined with the immunofluorescence staining of NeuN, neuronal marker, Olig-2, oligodendrocyte marker, IBA-1, microglia-specific protein, and GFAP, astroglial marker. Fig 10. C shows clear co-localization between β -gal and NeuN which is also proved by separation of channels. However, Fig 11. D, E and F represent no co-localization of β -gal with Olig-2, IBA-1 and GFAP indicating that β -gal, which is a marker of *Ambra1* expression, shows neuron-specific expression.

3.5 Functional study of neuron

The neuron-specific expression of *Ambra1* gives a reason for neuronal characterization in *Ambra1^{+/-}*. Therefore, electrophysiological analysis of neuronal function was performed in the hippocampus comparing WT to *Ambra1^{+/-}*.

3.5.1 Synaptic plasticity

Synaptic plasticity is the activity-dependent modification of the strength or efficacy of synaptic transmission at preexisting synapses. It is also thought to play key roles in the early development of neural circuitry and evidence is accumulating that impairment in synaptic plasticity mechanisms contributes to several prominent neuropsychiatric disorders (Citri and Malenka, 2008).

The hippocampus is well known for the measurement of synaptic plasticity since its laminated structure enables extracellular recording by placing stimulating electrodes on the presynaptic fiber tracts and recording electrodes near the sites of synaptic termination. The information in the hippocampus flows through a "trisynaptic loop" as displayed in Fig 3. A-B. In this study, the Schaffer collateral (SC)-CA1 synapses where CA1 neurons are excited by the stimulation of SC axons from CA3 pyramidal neuron were analyzed by measuring field excitatory postsynaptic potential (fEPSP) in the CA1 *Stratum radiatum* applying the electric stimulation in the SC afferents (Citri and Malenka, 2008). Here, male and female *Ambra1^{+/+}* and *Ambra1^{+/-}* were used for analysis at the age of 3 and 4 weeks.

3.5.1.1 Input-Output relationship

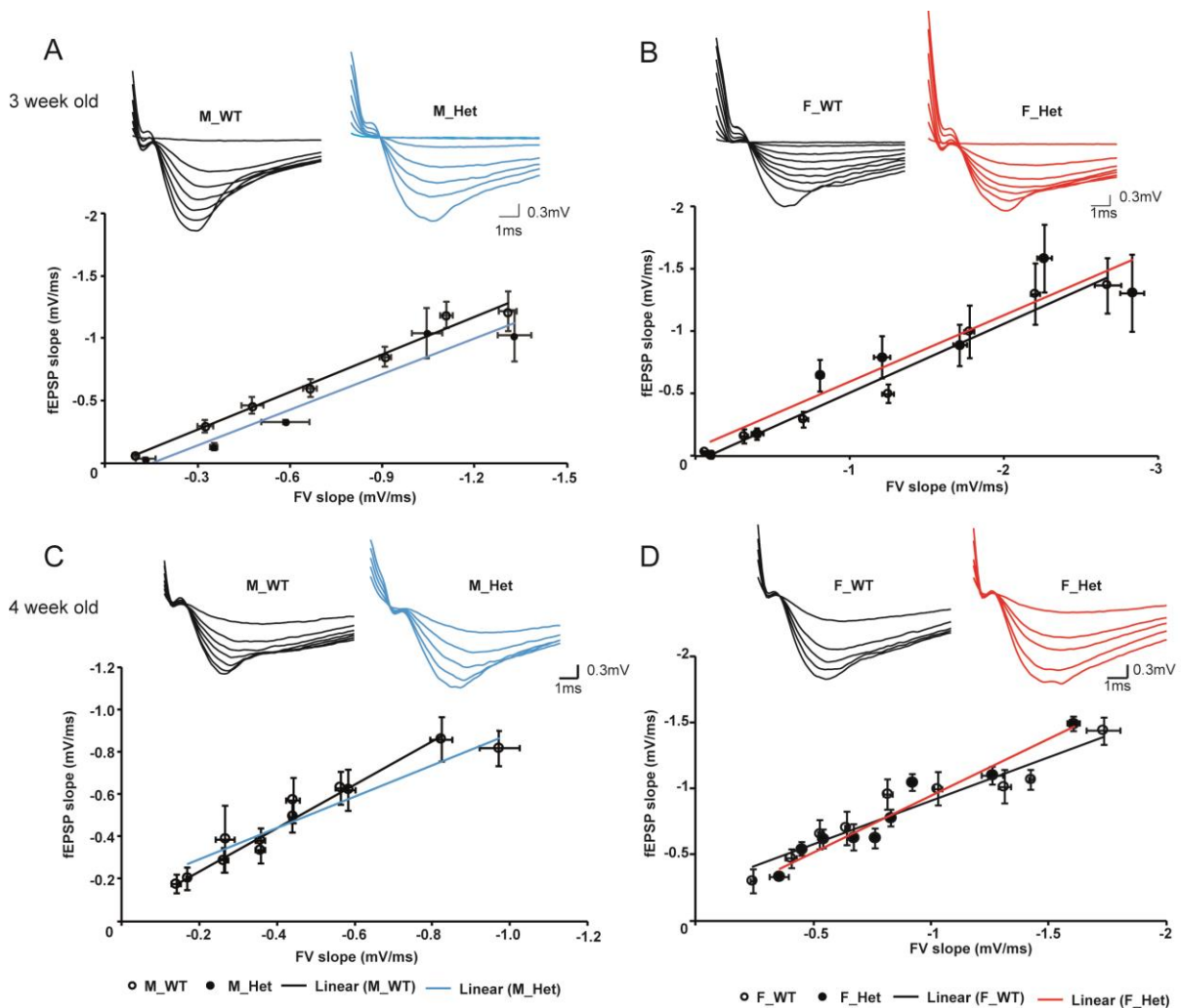


Figure 12. Input-output curve in *Ambra1*^{+/+} and *Ambra1*^{+/-} mice of both sexes in CA1 *Stratum radiatum* stimulated by Schaffer Collateral

Graphs of fEPSP slope as a function of FV slope in *Ambra1* WT and Het mice of male (M) and female (F) in **A, B**: 21-23 days (M_WT: 9/2, M_Het: 4/1, F_WT: 5/2, F_Het: 10/3, slice number/animal number) **C, D**: 4 weeks old (M_WT: 6/2, M_Het: 6/2, F_WT: 12/3, F_Het: 11/3, slice number/animal number); Each data point presents mean±SEM of both x and y values and linear regression was shown; Representative traces of input output curve are presented with each graph.

In order to determine whether *Ambra1*^{+/-} mice exhibited normal synaptic transmission, the evoked fEPSPs were measured by the application of different intensity of stimulus using extracellular field recording. The slope of fEPSP was plotted along with its FV slope and a trend line between two is depicted in each graph to see the input-output relationship in Fig 12. The input-output relationship was not significantly different between *Ambra1*^{+/-} and control mice, indicating that the loss of *Ambra1* does not affect the relationship between presynaptic inputs and postsynaptic response.

3.5.1.2 Paired-pulse ratio (PPR)

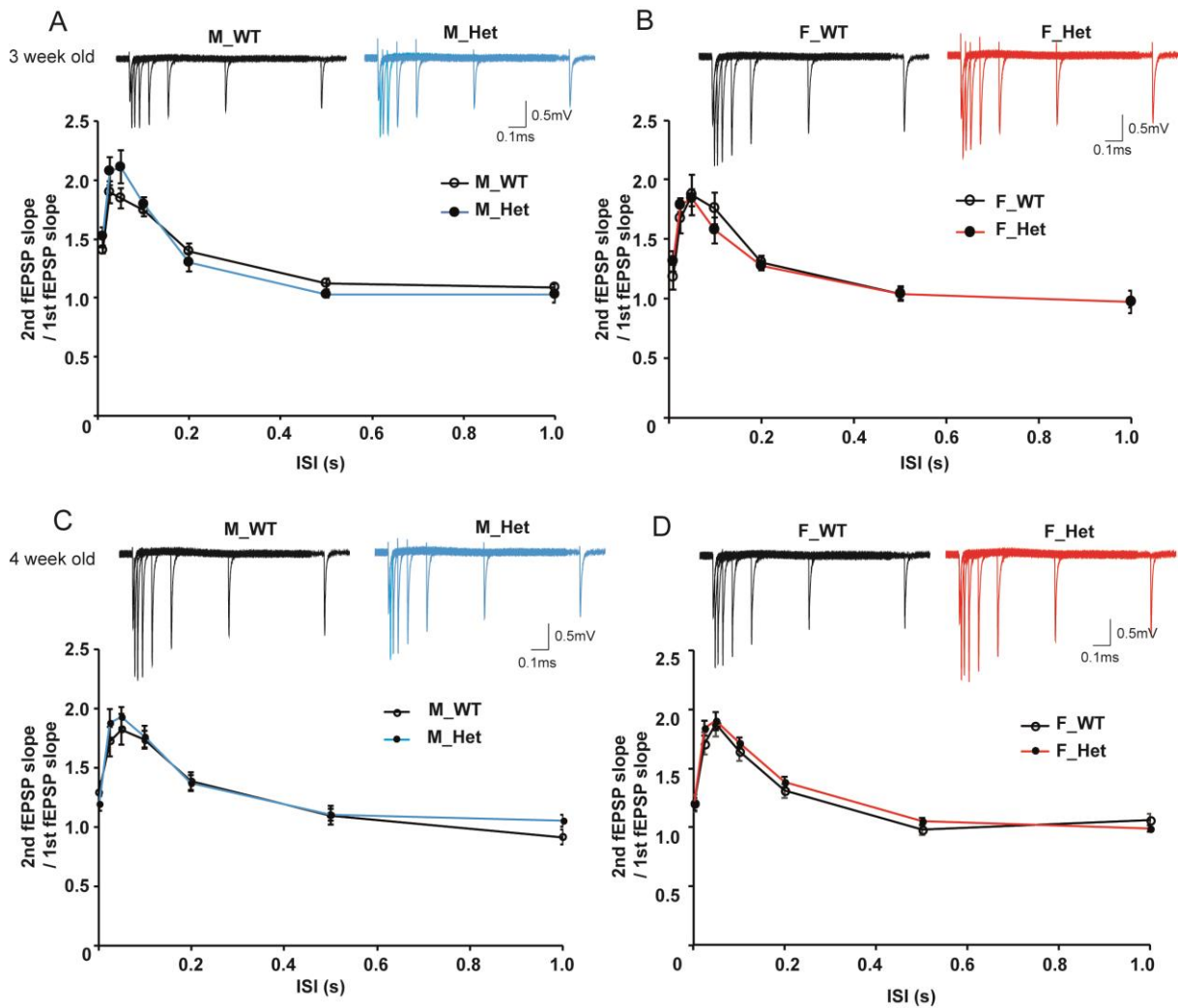


Figure 13. Paired pulse ratio (PPR) in *Ambra1*^{+/+} and *Ambra1*^{+/-} mice of both sexes in CA1 Stratum radiatum stimulated by Schaffer Collateral

Graphs of ratio between 2nd and 1st fEPSP slope with different interstimulus interval (ISI) (0.01, 0.025, 0.05, 0.1, 0.2, 0.5, 1 s) of both genotypes in male (M) and female (F) at **A, B**: 21-23 days (M_WT: 8/3, M_Het: 7/2, F_WT: 10/5, F_Het: 11/4, slice number/animal number) and **C, D**: 4 weeks old (M_WT: 6/2, M_Het: 6/2, F_WT: 10/3, F_Het: 11/3, slice number/animal number); Mean±SEM presented; Representative traces of PPR are shown with each graph.

Short-term synaptic plasticity, lasting milliseconds to several minutes, are thought to play important roles in short-term adaptations to sensory inputs, transient changes in behavioral states and short-lasting forms of memory. PPR, a form of short-term synaptic plasticity, is defined as the ratio of the post-synaptic second response to the first response when pair of stimuli is given at the same intensity in different time intervals. The maximum PPR in the SC-CA1 synapses generally occurs at short ISIs (e.g. 50 msec) and decreases exponentially with increased ISIs (up to 500 msec). This could be due to

residual calcium in the presynaptic bouton from the first action potential, but additional mechanisms are likely to be involved (Citri and Malenka, 2008).

Fig 13 includes the graphs of PPR versus different ISIs recorded in both sexes and genotypes from 3 (Fig 13. A, B) and 4 week-old mice (Fig 13. C, D). Both males and females in both ages didn't show any significant difference in PPR between genotypes over a range of the ISIs from 10ms to 1000ms, indicating that short-term synaptic plasticity is intact in the heterozygosity of *Ambra1*.

3.5.1.3 Early-phase LTP

In order to examine whether *Ambra1* is involved in LTP, SC afferents were stimulated by a single train of high frequency stimulation (HFS), consisting of 100 Hz for 1 sec. The slopes of fEPSPs were measured in the CA1 every 30 sec after electric stimulation in SC afferents before and after induction of LTP. As shown in Fig. 14, the magnitude of LTP at 40 min after the induction was not significantly different between the two genotypes tested ($p > 0.05$), showing that early-phase LTP was not affected by the loss of *Ambra1*.

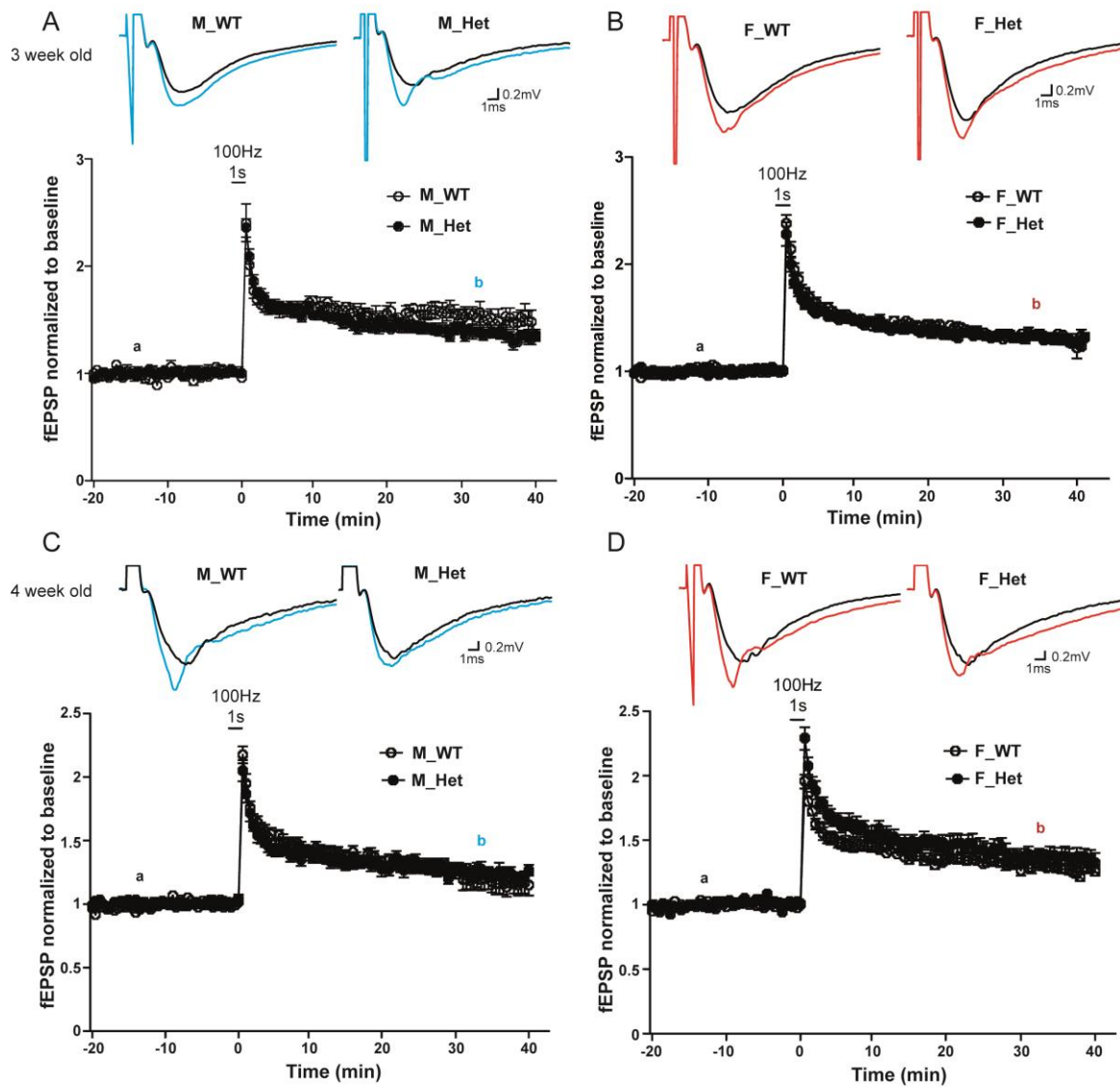


Figure 14. Early-phase long-term potentiation (E-LTP) in *Ambra1*^{+/+} and *Ambra1*^{+/-} mice of both sexes in CA1 *Stratum radiatum* stimulated by Schaffer Collateral

Graphs of fEPSP normalized to the average value of baseline before and after applying electronic shock, 100 Hz for 1 s in both genotypes in male (M) and female (F) at **A, B**: 21-23 days (M_{WT}: 5/2, M_{Het}: 12/3, F_{WT}: 16/5, F_{Het}: 16/5, slice number/animal number) and **C, D**: 4 weeks old (M_{WT}: 18/4, M_{Het}: 15/4, F_{WT}: 12/3, F_{Het}: 9/3, slice number/animal number); Mean±SEM presented; Representative traces of fEPSP in the baseline (a) and stable maintenance (b) of LTP are shown with each graph.

3.5.2 Gamma oscillation

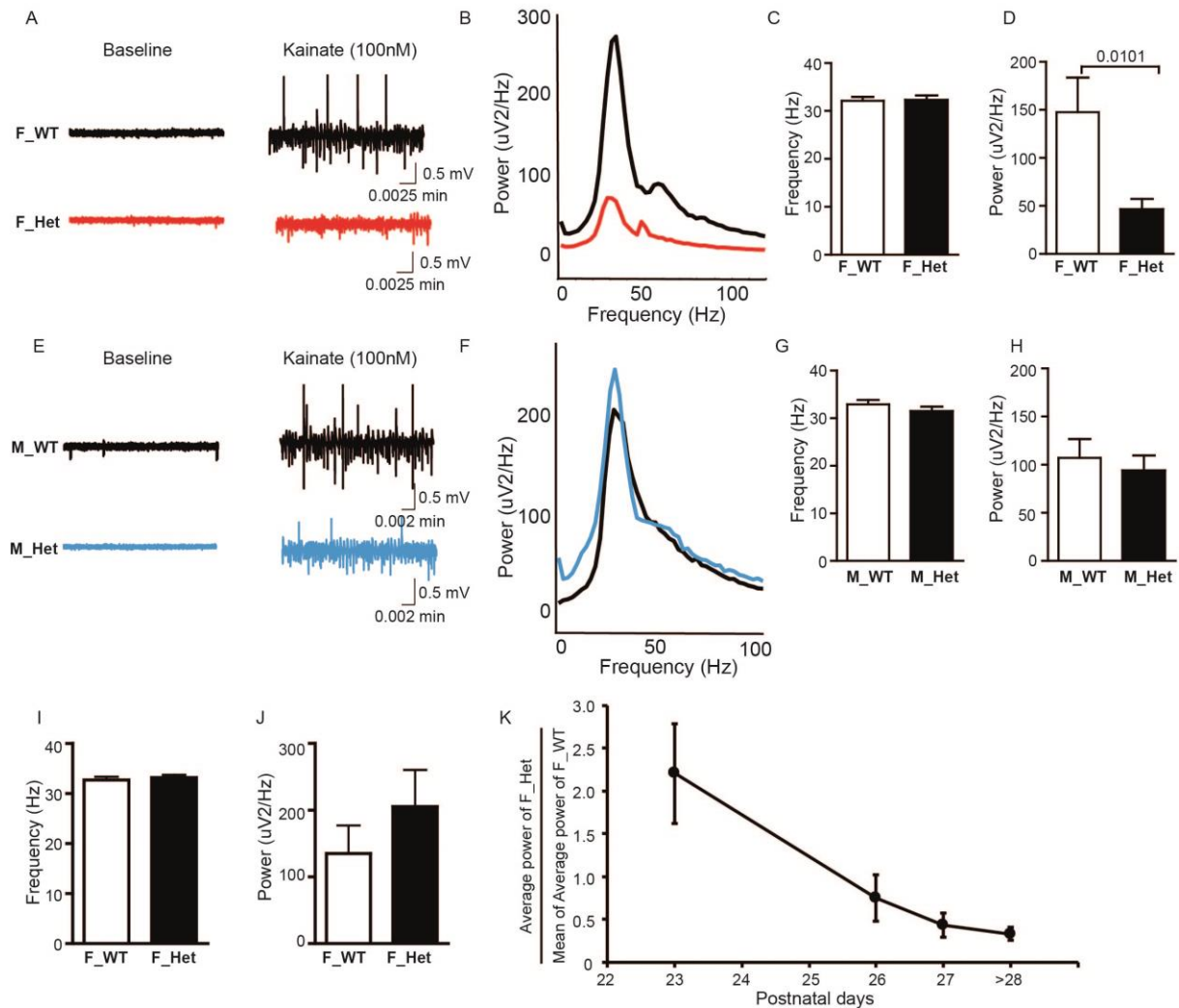


Figure 15. Kainate-induced gamma oscillation in the *Stratum pyramidale* of CA3 in hippocampus

A, E: Representative trace before and after application of kainate in the CA3 pyramidal layer of hippocampus in (A) *Ambra1*^{+/+} and (E) *Ambra1*^{+/-} mice in female (F) and male (M) at 4 weeks old. **B, F:** Representative power spectrum before and after induction in (B) *Ambra1*^{+/+} and (F) *Ambra1*^{+/-} mice in female and male at 4 weeks old. **C, D, G, H:** Peak frequency and average power of gamma oscillation within the range of 25-45 Hz of two genotypes in (C, D) female (F_WT: 28/4, F_Het: 27/4, slice number/animal number) and (G, H) male (M_WT: 12/3, M_Het: 12/3, slice number/animal number) at 4 weeks old. **I, J:** (I) Frequency and (J) average power of gamma oscillation in two genotypes of female at 3 weeks old (P21-27) (F_WT: 23/4, F_Het: 24/4, slice number/animal number). **H:** Graph of ratio between average power of *Ambra1*^{+/-} versus mean of average power of *Ambra1*^{+/+} littermate by date in female (F_WT; P23: 10/2, P26: 7/1, P27: 6/1, >P28: 28/4; F_Het; P23: 11/2, P26: 8/1, P27: 5/1, >P28: 27/4, slice number/animal number); Mean±SEM presented;

In the present study, kainate (100 nM)-induced gamma oscillation in the CA3 pyramidal layer of hippocampus in acute brain slice was measured in *Ambra1*^{+/+} and *Ambra1*^{+/-} littermates of both sexes.

The frequency of maximum power and the average power of gamma oscillation (gamma range is 25-

45 Hz) were calculated by subtraction between each 10 minute-epoch of long-lasting and stable gamma oscillation and baseline. In female mice of 3 weeks old (P23-P27), the frequency and power of gamma oscillation was no different between *Ambra1*^{+/-} and WT control (Frequency; F_WT: 32.69±0.6453 Hz, F_Het: 33.19±0.5442, p=0.5517; Power; F_WT: 135.1±42.11 μV²/Hz, F_Het: 205.5±54.68 μV²/Hz, p=0.3133). However, when analyzing the ratio between the power of *Ambra1*^{+/-} females and the mean of power in control by each day, it was dramatically reduced by day (Fig 15. I-K). As shown in Fig 15. H, the power of gamma oscillation in *Ambra1*^{+/-} females was two-times greater than control at age P23, but P27 it is reduced to approximately 1/3 of the control value (Fig 15. K). Therefore, the same experiment was carried out in 4 week-old (P28-34) females and males of both genotypes. There was no difference in frequency of gamma oscillation between genotypes (F_WT: 32.07±0.7874 Hz, F_Het: 32.27±0.7011 Hz, p=0.8626), while the power in *Ambra1*^{+/-} females was significantly lower compared to control littermates (F_WT: 147.5±35.84 μV²/Hz, F_Het: 46.35±10.42 μV²/Hz, p=0.0101) (Fig 15. A-D). In the 4 week-old males, both frequency and power of gamma oscillation were unchanged (Frequency; M_WT: 32.93±0.8300 Hz, M_Het: 31.50±0.8768 Hz, p=0.2481; Power; M_WT: 107.1±19.37 μV²/Hz, M_Het: 94.08±15.36 μV²/Hz, p=0.6052) (Fig 15. E-H). Taken together, our results indicate that *Ambra1* is involved in sex-specific neuronal network regulation, especially in the course of development.

3.6 Seizure propensity

For further characterization of *Ambra1*^{+/-} mice as mouse model of autism, we were interested in the comorbidity in ASD. The common comorbidity in patients with autism spectrum disorder (ASD) is epilepsy at 20 %. In the next experiment, we checked the seizure susceptibility in our animal model of ASD, *Ambra1*^{+/-} mice. The administration of PTZ, a GABA_A receptor antagonist, is routinely used to test seizure susceptibility (tonic-clonic seizures) in animal models. Low doses (e.g. 20-30 mg/kg) of PTZ in rodents cause episodes of generalized spike-and-wave discharge (SWD) on an EEG associated with behavioral arrest (MCLEAN et al., 2004; Tabuchi et al., 2007). Higher doses (i.g. 50-85 mg/kg) induce convulsive seizures with generalized tonic-clonic motor activity (Chiu et al., 2008; Harai et al., 2012).

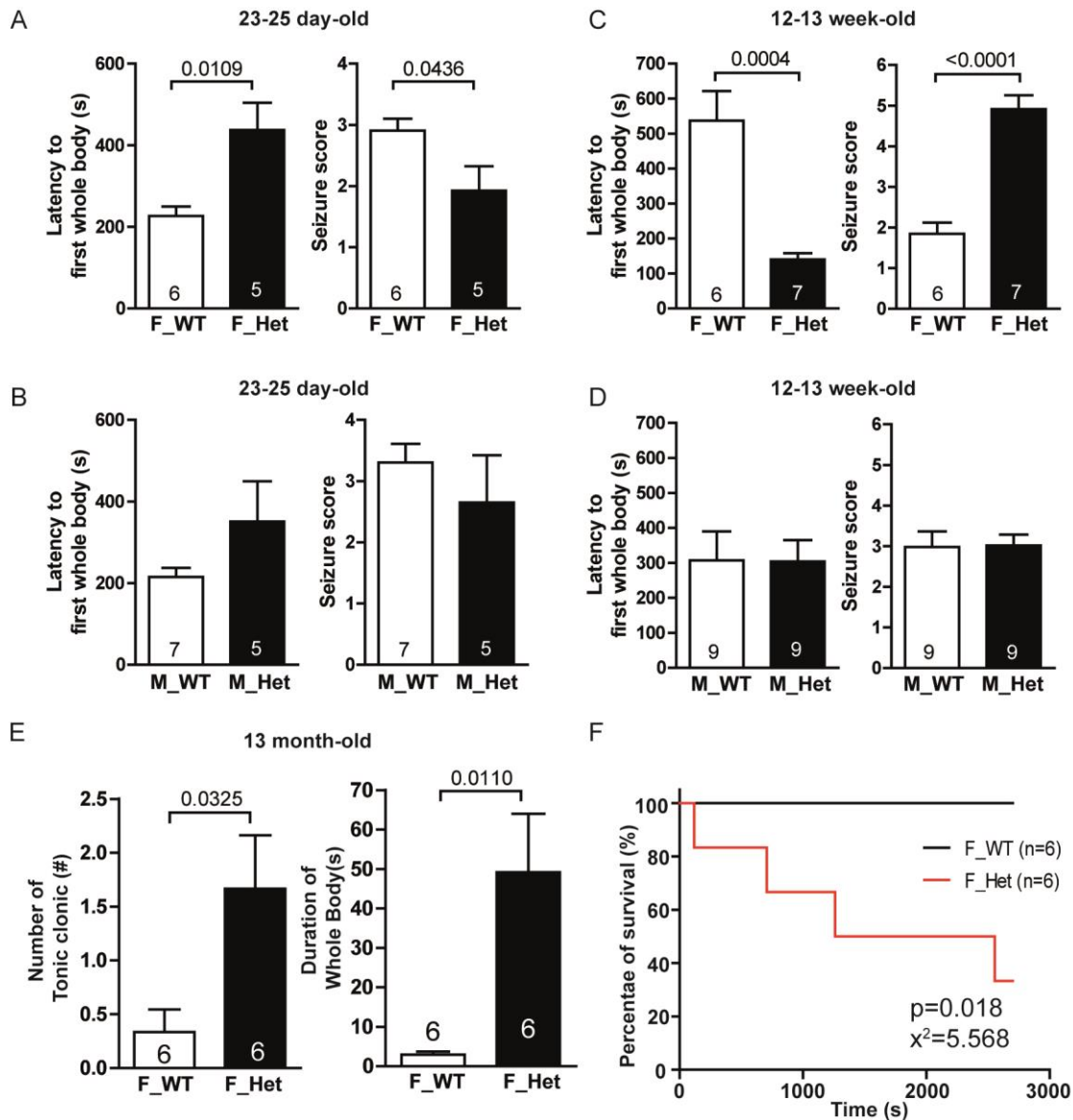


Figure 16. Seizure propensity induced by intraperitoneal injection of Pentylene-tetrazol (50mg/kg) in *Ambra1*^{+/+} and *Ambra1*^{+/-} mice of both sexes in different time point

Latency to first whole body and seizure score of 23-25 day-old **A:** female (F) and **C:** male (M) and 12-13 week-old **B:** female and **D:** male; **E:** Frequency of tonic-clonic, duration of whole body and **F:** percentage of survival in 13 month-old female. p-value and χ^2 were obtained from survival analysis; Mean \pm SEM presented; n numbers of each group are shown in the figures.

The susceptibility to PTZ-induced seizures in higher doses was evaluated in juvenile, adult and aged mice (P23-25, 12-13 weeks old and 13 months old, respectively) in males and females of both genotypes (50 mg/kg). In juvenile mice, before hitting puberty, *Ambra1*^{+/-} females showed resistance to PTZ-induced seizures compared to control females, measured by a slower latency to the first whole body episode of seizure (F_WT: 225.7 \pm 23.27 sec, F_Het: 437.2 \pm 67.20 sec, p=0.0109) and lower

seizure score (F_WT: 2.907 ± 0.1949 , F_Het: 1.924 ± 0.3980 , $p=0.0436$) (Fig 16. A), while no genotype difference was found in either male genotypes (Latency to first whole body; M_WT: 215.1 ± 21.70 sec, M_Het: 350.8 ± 98.54 sec, $p>0.05$; Seizure score; M_WT: 3.307 ± 0.3010 , M_Het: 2.650 ± 0.7724 , $p>0.05$) (Fig 16. B). This resistant phenotype in females completely reversed in adulthood (12-13 weeks old). The seizure response of *Ambra1*^{+/-} females was higher than that in WT animals, with a faster latency to the first whole body episode (F_WT: 537.0 ± 84.53 sec, F_Het: 140.3 ± 18.25 sec, $p=0.0004$) and higher seizure score (F_WT: 1.848 ± 0.2731 , F_Het: 4.915 ± 0.3412 , $p<0.0001$) (Fig 16. C). Like in the earlier developmental stage, adult males had not difference between two genotypes in both parameters (Latency to first whole body; M_WT: 307.0 ± 83.45 sec, M_Het: 304.1 ± 60.88 sec, $p>0.05$; Seizure score; M_WT: 2.979 ± 0.3841 , M_Het: 3.017 ± 0.2696 , $p>0.05$) (Fig 16. D). In aged mice, this seizure phenotype in *Ambra1*^{+/-} females became severe by an increase in the number of tonic-clonic episodes (F_WT: 2.944 ± 0.7351 , F_Het: 49.18 ± 14.82 , $p=0.0325$) and longer duration of whole body episodes (F_WT: 0.3333 ± 0.2108 sec, F_Het: 1.667 ± 0.4944 sec, $p=0.0110$) (Fig 16. E). Furthermore, 4 mice out of 6 female *Ambra1*^{+/-} died during the observation, shown in the survival analysis in Fig 16. E.

3.7 Neuronal number and morphology

Ambra1 does not play a role in regulating activity-dependent synaptic transmission. The difference in the power of gamma oscillation could be caused by an imbalance in excitation/inhibition of network activity. To test this, cell morphology and populations of different cell types were assessed. This imbalance can be explained by either the neuronal number or morphology.

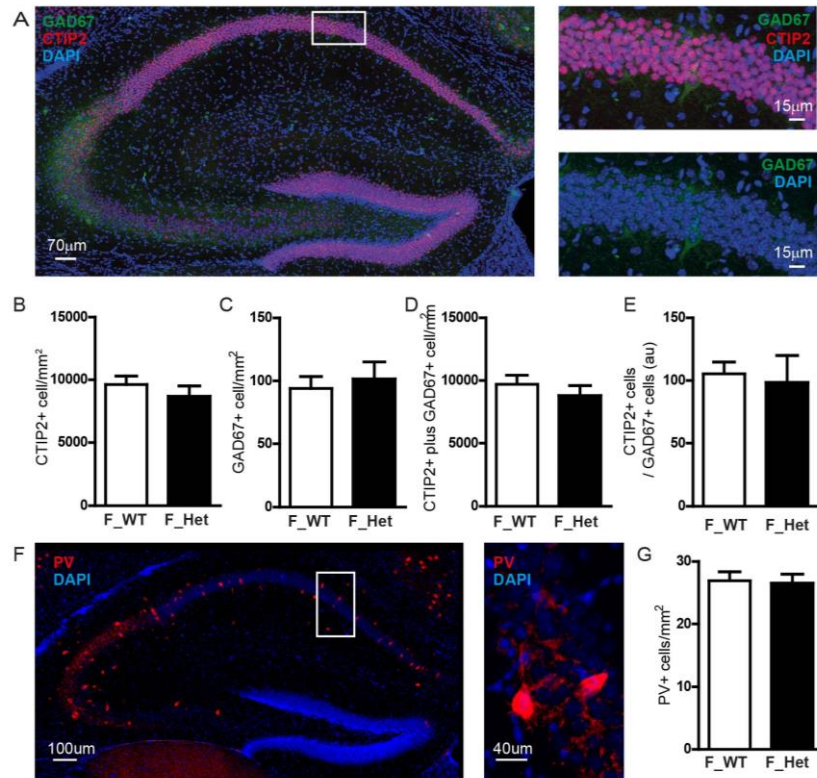


Figure 17. Counting excitatory and inhibitory neurons in the pyramidal layer of hippocampus

The coronal sections which contain hippocampus region were stained using CTIP2, GAD67 and PV antibodies. The representative staining pictures of **A**: co-staining of CTIP2+ and GAD67+ cells and **F**: single staining of PV+ interneurons in the pyramidal layer of hippocampus are shown with zoomed-in version. The densities of **B**: CTIP2+, **C**: GAD67+ and **G**: PV+ cells in the pyramidal layer of hippocampus were calculated in *Ambra1*^{+/+} and *Ambra1*^{+/-} female mice of 23 days old. The **D**: sum and **E**: ratio of CTIP2+ and GAD67+ cells, indicative of total number of neurons and ratio between excitation and inhibition, were calculated and compared. 6 animals with 3 sections each per group were used for analysis. Mean ± SEM presented.

3.7.1 Neuronal number (Counting of CTIP2+, GAD67 and PV+ cells)

The populations of neurons in 23-day old *Ambra1*^{+/+} and *Ambra1*^{+/-} female mice were counted using CTIP2 for glutamatergic neurons and GAD67 for GABAergic neurons in the CA1 region and PV for PV-positive neurons for the pyramidal layer of hippocampus. Fig 17. A and F show the representative images of CTIP2-, GAD67- and PV-expressing cells. The numbers of CTIP2+ and GAD67+ cells in CA1 were not different between two genotypes (CTIP2+; F_WT: 9619 ± 689.5 cells/mm², F_Het: 8680 ± 820.3 cells/mm², p=0.4015; GAD67+; F_WT: 93.87 ± 9.334 cells/mm², F_Het: 101.4 ± 13.52 cells/mm², p=0.6572) (Fig 17. B and C). Moreover, the sum and ratio of CTIP2+ and GAD67+ cells which might be indicators of the total number of neurons and the ratio between excitation and inhibition, respectively, are not different between genotypes (Sum; F_WT: 9713 ± 696 cells/mm²,

F_Het: 8781 ± 1068 cells/mm², $p=0.4037$; Ratio; F_WT: 105.4 ± 9.104 , F_Het: 98.54 ± 21.54 , $p=0.7766$) (Fig 17. D and E). PV+ cells, a subpopulation of interneurons, are well known to modulate gamma oscillation in hippocampus (Sohal et al., 2009). However, the number of PV+ cells did not differ between *Ambra1*^{+/+} and *Ambra1*^{+/-} females (F_WT: 26.90 ± 1.437 cells/mm², F_Het: 26.57 ± 1.415 cells/mm², $p=0.826$) (Fig 17. G).

3.7.2 Neuronal morphology

To study the properties of pyramidal neurons which induce the phenotype in gamma oscillations by reduction of Ambra1 protein, we investigated the neuronal morphology such as dendritic arborization and spine analysis. GFP construct was transfected into the pool of hippocampal progenitors at E14.5. Quantitative analysis of dendritic arborization and spine analysis was done with 3D reconstruction by NeuronStudio program which enables the analysis of neurons overlapping each other.

3.7.3 Dendritic arborization

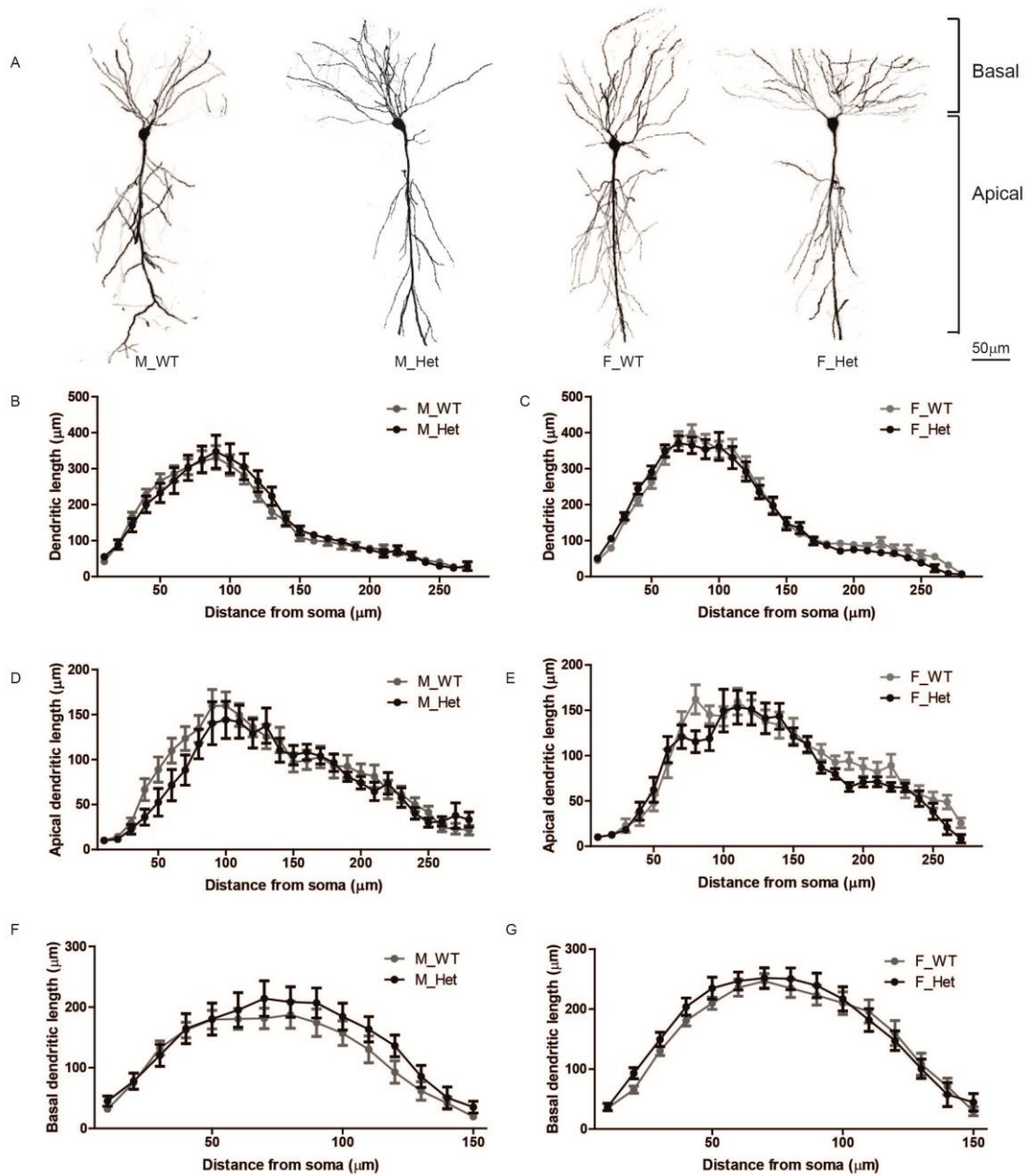


Figure 18. 3D sholl analysis of CA1 pyramidal neuron - I

A: Representative picture of CA1 pyramidal neuron in *Ambra1^{+/+}* and *Ambra1^{+/-}* mice in male and female at P28, **B-G:** Comparison of length of whole, apical or basal dendrites in every 10 μm between both genotypes in male (M) and female (F); Mean \pm SEM presented; (slice number/animal number; **B:** M_WT: 11/2, M_Het: 9/3; **C:** F_WT: 12/3, F_Het: 9/4; **D:** M_WT: 12/2, M_Het: 9/3; **E:** F_WT: 11/2, F_Het: 9/4; **F:** M_WT: 11/2, M_Het: 9/3; **G:** F_WT: 12/3, F_Het: 8/4)

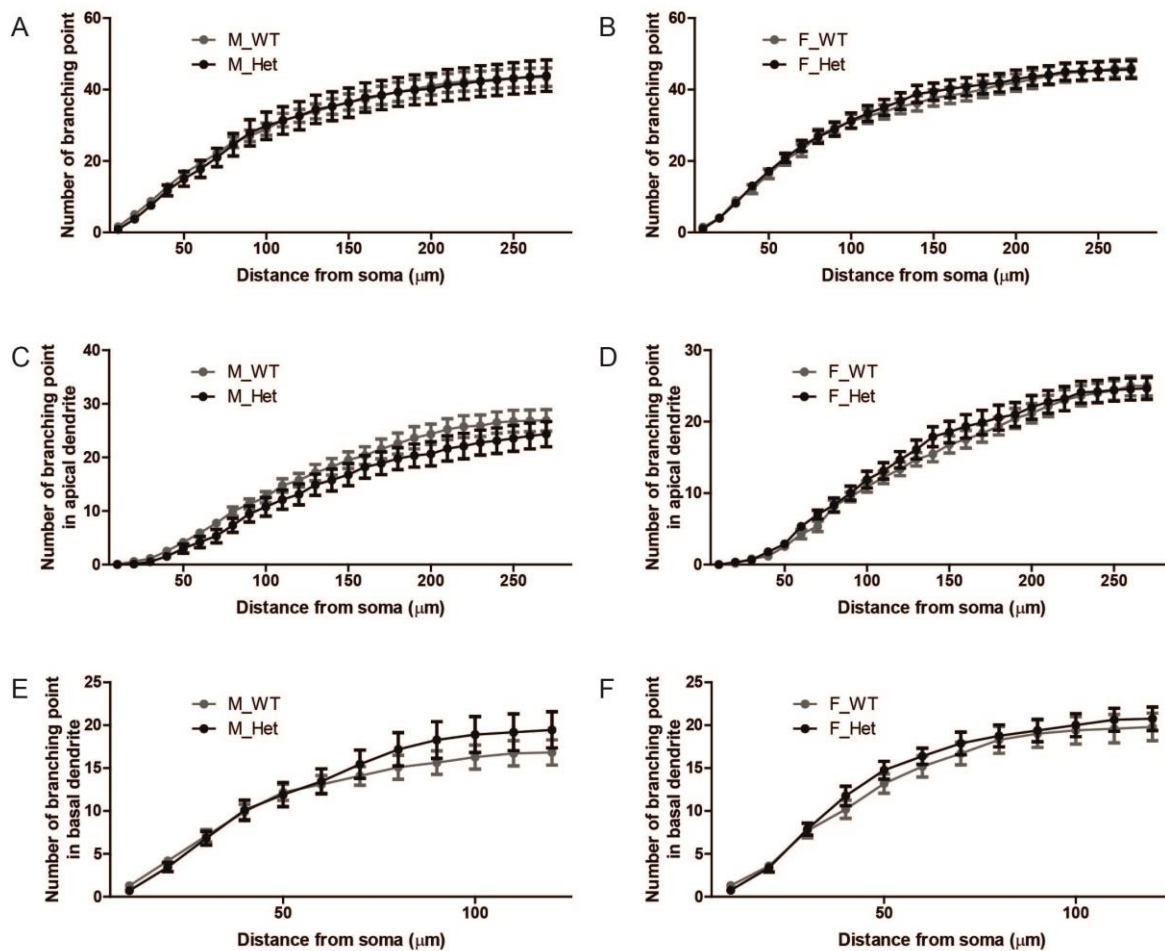


Figure 19. 3D sholl analysis of CA1 pyramidal neuron - II

A-F: Comparison of accumulative number of branching points in whole, apical or basal dendrites in every 10 μm between both genotypes in male (M) and female (F); **B-G:** Comparison of length of whole, apical or basal dendrites in every 10 μm between both genotypes in male (M) and female (F); Mean±SEM presented; (slice number/animal number; **A:** M_WT: 11/2, M_Het: 9/3; **B:** F_WT: 12/3, F_Het: 9/4; **C:** M_WT: 12/2, M_Het: 9/3; **D:** F_WT: 11/2, F_Het: 9/4; **E:** M_WT: 11/2, M_Het: 9/3; **F:** F_WT: 12/3, F_Het: 8/4)

The quantification of dendritic arborization in the CA1 pyramidal cells from 28 day-old mice from both genotypes and sexes was exploited by 3D Sholl analysis using NeuronStudio. Representative pictures of CA1 pyramidal neurons from both genotypes in male and female are displayed in Fig 18. A. The analysis of dendritic length (Fig 18. B-G) and number of branching points (Fig 19. A-F) was broken down into three parts: apical, basal, and whole cell, and was measured every 10 μm and plotted. There was no difference in any of these three regions in both sex and genotype, indicating that Ambra1 protein is not crucial for the neurite development.

4 Discussion

Autism or ASD is a heterogeneous disorder, as patients exhibit a wide range of symptoms, severity and prognosis, which is induced by hundreds of identified causes or potential causal genetic variants. Despite the unknown etiology of ASD, monogenic heritable forms of the disorder allowed to develop genetic mouse models with proven autism construct validity to investigate the mechanism of ASD (Tabuchi et al., 2007, Jamain et al., 2008, Etherton et al., 2009, Radyushkin et al., 2009, Berkel et al., 2010).

We detected an interesting mouse model of ASD, *Ambra1*^{+/-} mice. Although *Ambra1* was found to be essential for function of autophagy, unexpectedly, we found it associated with autism-like symptoms, including deficits in social interaction and communication, repetitive behaviors and cognitive rigidity. Most strikingly, this phenotype was restricted to females (Dere et al., 2014). However, a causal link between *Ambra1* protein and the development of ASD has remained obscure. Therefore, I further characterized *Ambra1*^{+/-} mice in order to better understand neural mechanisms of its phenotype at the circuitry and cellular level.

4.1 Neonatal development and communication function

Autism is diagnosed in children before the age of three in humans. Several studies have reported that autistic patients already showed sign of developmental abnormalities before diagnosis. For example, in ASD high-risk infants, subtle and repetitive movements or unusual sensory behaviors start earlier in development than impairments in social and communication skills (Rogers, 2009). Delay in early motor development such as gait abnormalities and difficulties with motor coordination have been consistently found as prominent neurological co-morbid conditions in autistic patients (Bhat et al., 2011; Maski et al., 2011; Provost et al., 2007). *Mecp2* mutant mice modelling Rett syndrome revealed abnormal neurodevelopment, such as delay of reflex maturation and of wire suspension performance as a neuromotor coordination readout (Bodda et al., 2013). Therefore, the observation of neonatal development, including physical development, reflex acquisition and fine-tuned neuro-motor coordination, was performed for further characterization of the *Ambra1*^{+/-} mice as a mouse model of autism. Indeed, the neonatal development of *Ambra1*^{+/-} mice in physical and neurological manners was normal in both male and female.

Isolation-induced USV of mouse pups by separation from their mothers are considered as a quantifiable behavior experiment relevant to ASD (Scattoni et al., 2009). For instance, pups of *Tsc2*^{+/-} and *Eif4ebp2* knockout mice, known genetic mouse model of ASD, displayed enhanced USV (Tsai et al., 2012; Young et al., 2010), while juveniles of *Nlgn4*^{-/-} mice produced less USV (Ju et al., 2014). Therefore, recording of isolation-induced USV was performed on male and female *Ambra1*^{+/+} and *Ambra1*^{+/-} pups to investigate the onset of communication deficits in early age. Interestingly, our data showed that at P8-9, *Ambra1*^{+/-} female pups had a reduction in the number of calls in comparison to WT (Fig 7. E, G), while male pups displayed WT USV behavior (Fig 7. F, H). This indicates that communication deficits phenotypically described in adulthood of *Ambra1*^{+/-} females have an earlier onset than previously thought.

4.2 mRNA and protein expression of Ambra1

In order to investigate the apparent sex-dependent ASD-like phenotype in *Ambra1* mutant mice, the mRNA and protein level of Ambra1 was extracted from cortical tissue and measured. There was a 50% reduction in *Ambra1* mRNA levels extracted from the cortices of both male and female *Ambra1*^{+/-} when compared to WT littermates (Fig 8. A). Between males and females, that was comparable in same genotype. Ambra1 protein levels were also reduced in *Ambra1*^{+/-} group compared to *Ambra1*^{+/+} but the reduction between two genotypes was relatively more in females compared to males (Fig 8. C). This difference might be due to substantially increased expression of Ambra1 protein in female WT mice compared to males, greater requirement of this protein in basal condition in females (Fig 8. D). Although the present study has not investigated the mechanism behind the different expression of Ambra1 between males and females, several proposals can be suggested to explain a sex-dependent expression of Ambra1 protein. The differences in protein expression levels may be due to two mechanisms, increase in synthesis and/or decrease in degradation of the protein. First of all, it is possible that the translational control of *Ambra1* mRNA might be sex-dependent according to its needs. Moreover, the translational pathway is known to be one of the mechanism for ASD etiology via eIF4E which is regulated by mTOR (Gkogkas et al., 2012; Santini et al., 2012). Ambra1 is able to bind directly to mTOR which is regulated by PTEN (Nazio et al., 2013). Since PTEN is able to bind to estrogen receptor α (ER α), mTOR-dependent protein synthesis might be affected by estrogen (Briz and Baudry, 2014; Yu and Henske, 2006).

Another possible explanation behind the increase of Ambra1 expression in female mice is the slower degradation of Ambra1 protein in female under certain physiological conditions. Studies on the degradation of Ambra1 revealed triggering by proteolytic degradation regulated by caspase and calpain under apoptotic stimuli (Pagliarini et al., 2012). Little research has been done showing sex-specific apoptosis, therefore it is difficult to find connection for the sex-dependent proteolysis of Ambra1 protein.

One of the main functions of Ambra1 is to stimulate autophagic process. Autophagy has been implicated in synaptic remodeling in *C.elegans* (Rowland et al., 2006) and *Drosophila* (Shen and Ganetzky, 2009). A postmortem study of brains from human autists revealed a reduced level of autophagic activity yielding markedly reduced synaptic pruning (Tang et al., 2014). However, Ambra1 might not be an important protein for regulating autophagic processes such as Atg proteins or Beclin1. LC3-II level in *Ambra1*^{-/-} embryonic brain at E14 was reduced by half compared to its WT control (Maria Fimia et al., 2007), whereas mutant mice of *Atg7*^{-/-} which is a key protein in the autophagic process had no LC3-II signal (Komatsu et al., 2006). Furthermore, in vitro experiments using GFP-fused-LC3, genotype-associated difference in LC3 signal was only detected under autophagic induction but not in basal condition, meaning that the autophagic process has not been ablated with the loss of Ambra1 and it is not a critical protein for autophagy but rather 'helper' for controlling autophagic process (Maria Fimia et al., 2007). This also provides us possibility that, in addition to autophagy, there is another function of Ambra1 in the brain, such as cell proliferation or apoptosis, as shown in previous research (Maria Fimia et al., 2007).

4.3 Very mild brain enlargement, neuronal expression & neuronal counting

Brain enlargement is a consistent finding from independent studies of human autistic children (Courchesne and Pierce, 2005; Courchesne et al., 2001, 2003; Fidler et al., 2007; Hazlett et al., 2011; Saitoh et al., 2001; Sparks et al., 2002). Increased volume in whole- or sub-region of autists' brains was mainly described in ASD patients aged two to three years (Courchesne et al., 2003; Hazlett et al., 2011), and after this age, the growth rate of brain slowed more than in clinically normal children, resulting in either average or reduced brain volume at an older age (Courchesne et al., 2004; Groen et al., 2010; Schumann et al., 2004). This enlargement was correlated with higher number of neurons

present in autistic children compared to control children (Courchesne et al., 2011). This exencephaly was also identified *Tsc2*^{+/-} mouse, one described mouse model of autism. Therefore, the brain size within different ROI, such as whole brain, hippocampus, cerebellum, olfactory bulb and ventricles, was assessed in the *Ambra1*^{+/-} mice in both male and female for additional characterization of this mouse line. *Ambra1*^{+/-} mice had larger whole brain and hippocampus compared to its respective WT control in 23 day-old males and females and 13 month-old females, while the difference between two genotypes was acquired in the ventricle size. The cerebellum was the only region where the enlarged size in *Ambra1*^{+/-} was assessed in females but not in males. Since this increase in the average size of *Ambra1*^{+/-} brain size was 103-110% of both male and female control brains, it can be deemed a 'mild enlargement' but not significantly increased as a pathological marker (Fig 9.). Given the fact that not only females but also males had enlarged brain in *Ambra1*^{+/-} compared to WT, brain enlargement has not been correlated with ASD but one of the features in *Ambra1*^{+/-} mice.

To understand the cellular substrate of brain enlargement, the next experiment was to investigate where this protein is expressed. Since β -gal was expressed under the promoter of *Ambra1* in mutant allele and mimic the expression of endogenous gene, it can be used as a reporter protein of *Ambra1* expression (Skarnes et al., 1995). By the X-gal staining, the expression of β -gal was detected in cortex, striatum and hippocampus of postnatal brain (Fig 10.). Since this experiment was previously performed in this mouse line (Maria Fimia et al., 2007), it was confirmation from previous paper. Intriguingly, in this staining, the expression of β -gal in the hippocampus seemed to be pyramidal neuron-specific. Therefore, I co-immunostained β -gal, combined and other cellular markers in the brain, was performed. The expression of β -gal was co-localized with NeuN, a marker for neuron, and not with markers for other cell types in the CNS such as astrocytes, microglia and oligodendrocytes, (Fig 11.). The specificity of the co-localization with neuronal markers leads me to conclude that *Ambra1* is expressed specifically neurons within the CNS. This data may suggest the possibility about a novel, neuron-specific function of *Ambra1*. Due to the fundamental importance of autophagy to be expressed in all cells, the molecular components important to this process should, therefore, to be expressed in every cell type in the brain. We speculate that *Ambra1* might have another role in neuron, which give a reason for the characterization of neuron in *Ambra1*^{+/-} mice.

Another function of Ambra1 protein was the regulation of cell proliferation and apoptosis to control their balance. *Ambra1*^{-/-} embryos showed not only incomplete closure of the neural tube, but also the absence of normal ventricular system due to the extensive overgrowth of the proliferative neuroepithelium. Analysis of cell proliferation by 5-bromodeoxyuridine (BrdU)-uptake experiment revealed a significant increase in the number of proliferating cells at E8.5 but not later developmental timepoints, indicating the hyper-proliferation phenotype at the onset of neurulation. Thus, excessive apoptosis was present in selected areas of the mutant nervous system from E9.0 onwards (Maria Fimia et al., 2007). PP2A, a regulator of cell cycle and mitochondrial Bcl-2, an anti-apoptotic factor, are direct binding partners of Ambra1 giving evidence that Ambra1 controls cellular proliferation and apoptosis (Cianfanelli et al., 2014; Strappazzon et al., 2011). Based on previous findings, we considered that malfunction of Ambra1 to regulate the balance between cellular proliferation and apoptosis might affect different neuronal number and/or composition of excitatory and inhibitory synaptic inputs, consequently changing the function of neuronal networks.

Therefore, the number of neuron was counted in the hippocampus where the brain volume size had the greatest increase between mutant and WT. However, there was no difference in the number of excitatory and inhibitory neurons in the pyramidal layer of hippocampus between two genotypes (Fig 17. B, C). I found no change in the balance of excitation and inhibition based on cell counts in mutant hippocampi (Fig 17. D, E). Additionally, the number of PV+ neurons that initiate and regulate gamma oscillations remained unchanged in the mutants (Fig 17. G) (Sohal et al., 2009). In conclusion, Ambra1 might not disturb the balance of proliferation and apoptosis in the brain of *Ambra1*^{+/-}. Also, such subtle increase in brain size in *Ambra1*^{+/-} could not reflect the change in neuronal number and composition.

4.4 The effect of Ambra1 on synaptic plasticity

Synaptic plasticity is the activity-dependent modification of strength and efficacy of synaptic transmission. It mainly explains sensory adaptation, learning and memory but the real meaning is the neuro-adaptations such as enhanced or depressed synaptic transmission that result from a wide range of environmental stimuli. As described previously, synaptic plasticity can be categorized by the duration of enduring the activity-dependent change; short-term plasticity and long-term plasticity. Short-term facilitation is due to residual Ca²⁺ from the first stimulus which contributes to a second, more robust response. So far, strengthening of synaptic connections through LTP in animals and LTP-

like plasticity in humans has been shown. It has been reported that several genetic mouse models of ASD, such as *Tsc1/2*, *Mecp2*, *Shank2* and *Shank3* mutants, display deficits in paired-pulse ratio or LTP, suggesting that impairment in synaptic plasticity property may be a milestone to explain their autism-like behaviors (Bateup et al., 2013; Bozdagi et al., 2010; Kirschstein, 2012; Na et al., 2013; Schmeisser et al., 2012; Wang et al., 2011). *Mecp2* mutant mouse is very exemplar mouse model of ASD which exhibited disruption in the synaptic plasticity in both forms. For instance, loss-of-*Mecp2* function showed reduced paired pulse ratios, while gain-of-*Mecp2* function augmented paired pulse responses (Asaka et al., 2006; Collins et al., 2004; Moretti et al., 2006; Na et al., 2012; Nelson et al., 2006). Moreover, the profound attenuation of Schaffer-collateral LTP and LTD are displayed in symptomatic *Mecp2* null mice, whereas *Mecp2* overexpression mouse lines showed enhanced hippocampal LTP (Asaka et al., 2006; Moretti et al., 2006; Weng et al., 2011). Taken together, it was suggested that *Mecp2* might either affect or be affected by Ca^{2+} in the presynaptic terminal or perhaps may alter proteins involved in neurotransmitter release (Na et al., 2013). *Tsc2*^{+/-} rats showed impaired LTP and LTD, implying that the protein synthesis in the mTOR signaling which is regulated by *Tsc2*, will control synaptic plasticity (Kirschstein, 2012). Different mutant mouse of *Shank2* and *Shank3* showed impairment in NMDAR-dependent LTP and LTD, which can be explained by the effect of Ca^{2+} -mediated calpain signaling on the Shank-actin connection, important in NMDAR-LTP (Yoo et al., 2014). Therefore, we studied the activity-dependent synaptic plasticity in *Ambra1*^{+/+} and *Ambra1*^{+/-} mice in both male and female of 3 and 4 weeks old. Surprisingly, the short-term and the long-term synaptic plasticity in *Ambra1*^{+/-} didn't change compared to its WT in both sexes of 3 and 4 weeks old (Fig 13, Fig 14). This is in line with normal learning and memory behavior test in this mouse line (Dere et al., 2014). Therefore, autistic phenotypes shown in *Ambra1*^{+/-} have no relationship with synaptic plasticity, activity-dependent modification of synaptic strength, suggesting that Ca^{2+} -dependent signaling and the AMPA/NMDA receptors is not related with *Ambra1* and not involved in ASD.

4.5 Seizure phenotype, gamma oscillations and E/I balance

Psychiatric disorders are mostly caused by the abnormal functions of neurons which mainly originate from two main reasons: neuronal degeneration and network disturbance. The effect of neuronal degeneration on psychiatric disorders is well studied, especially in Alzheimer's disease (Cárdenas et al., 2012; Kowall and McKee, 1993). Additionally, increasing number of research suggests that

disturbance of neural network might induce psychiatric disorders, including ASD. Although the neurophysiological substrates of ASD are poorly understood, several studies with different monogenic mouse models proposed different speculations to explain the etiology of ASD in terms of disturbance in neural network (O'Donovan et al., 2009; Pardo and Eberhart, 2007; Patterson, 2011; Südhof, 2008). One emerging hypothesis is that imbalance between excitation and inhibition (E/I) could affect the deficit in the social and cognitive functions which are important features in autism (Kehrer et al., 2008; Lee et al., 2016; Markram and Markram, 2010). Recording gamma oscillation and induction of seizure are two appropriate tools to study the alteration of E/I balance in neural network.

Firstly, gamma oscillation was induced by the application of kainate in the acute brain slice of *Ambra1^{+/+}* and *Ambra1^{+/-}* mice of male and female in 3 or 4 weeks old. Our data showed that the power of gamma oscillation (γ -power) in *Ambra1^{+/-}* females was lower than that in *Ambra1^{+/+}* female at the age of 4 weeks (Fig 15. D), whereas this reduction was not detected in 3 week-old female mice (Fig 15. J). By calculating the ratio of γ -power between *Ambra1^{+/-}* and *Ambra1^{+/+}* by date, it was revealed that γ -power of *Ambra1^{+/-}* was approximately two times more than that of *Ambra1^{+/+}* at P23, and this ratio was decreased until P27 when this power was less than *Ambra1^{+/+}* γ -power (Fig 15. K). However, the male mice showed similar γ -power between two genotypes in 4 weeks old (Fig 15. H), meaning that gamma oscillation might be indicative for ASD. Opposite pattern of data in female of 3 and 4 weeks old might provide evidence of *Ambra1* function, since the period of 3 weeks is very critical point for synaptic pruning or sexual maturation in mice.

Since this E/I imbalance is correlated with the seizure phenotype, which is one of the co-morbid conditions of ASD, the measurement of seizure propensity in mouse model is another tool to study this imbalance. Moreover, a recent study using neuron-specific *Ube3a* mutant mouse demonstrated the association between neural oscillations measured by EEG and seizure susceptibility (Judson et al., 2016). Therefore, the seizure propensity was assessed in *Ambra1^{+/+}* and *Ambra1^{+/-}* mice of male and female by i.p. injection of PTZ, agonist of GABA_A receptor, in different ages. In the present study, *Ambra1^{+/-}* females at P23-25 showed the later onset of whole body seizure and lower seizure score compared to control, indicating less seizure propensity (Fig 16. A), whereas at 12-13 weeks old, these mice exhibited significantly faster onset of whole body seizure and higher seizure score than control animals (Fig 16. C), indicating that *Ambra1^{+/-}* female mice are more prone to seizure at later ages. At

these two-time periods, male mice didn't show any difference between both genotypes (Fig 16. B, D). This is correlated with higher incidence of the later seizure onset in human ASD, approximately after 10 years old (Volkmar and Nelson, 1990). Furthermore, in very old age, 13 months old, the genotype-associated difference of seizure propensity in female developed more severe by more number of tonic and clonic episodes and longer duration of whole body seizure (Fig 16. E). Even, 4 out of 6 *Ambra1*^{+/-} females died during this experiment, showing severe seizure propensity (Fig 16. F). In the end, our data of gamma oscillation and seizure phenotype are correlated with each other, pointing to the E/I imbalance in *Ambra1*^{+/-} females. In detail, these data provide three points to discuss about; 1) genotype-associated difference, 2) sex-dependent difference, 3) age-dependent difference of E/I balance.

The causal factors of E/I imbalance should be considered for the etiology of these differences. This E/I imbalance, an indicative of change in excitatory and inhibitory inputs, can be caused by alteration either in the neuronal cell number or in neuronal morphology, such as dendritic morphology or spine numbers. Our previous data already showed no difference of excitatory and inhibitory cell numbers in hippocampus between two genotypes. Moreover, the number of PV+ neuron, the main cause of synchronized oscillation, (Sohal et al., 2009) was not altered. Therefore, the etiology of E/I balance by the functional deficiency of *Ambra1* should be studied for the next step. Sex- and age-dependent differences of E/I balance will be explained in detail in Section 4.7.

4.6 Dendritic arborization & spine number

The genetic factors of ASD involve the genes encoding postsynaptic regulatory proteins, as well as scaffolding proteins and synaptic receptors (Muhle et al., 2004). The activity of these regulatory proteins can be triggered by external stimuli or controlled by intrinsic factors. Since there was no change in synaptic plasticity in *Ambra1*^{+/-} compared to control animals, change in the E/I balance in *Ambra1*^{+/-} mice is likely to result from independent factors of external stimuli. The morphological change in the neuron, such as dendritic arborization or spine number, will affect the entire synaptic input.

Dendrite morphology is a hallmark of the neuron and it has important functions in defining which sort of signals one neuron will receive and how these signals will be integrated. During the past two

decades, transcription factors, local translational machinery, regulation of cytoskeletal elements, vesicle trafficking and various signaling pathways have been identified to regulate dendritic arborization of individual neurons and the integration of these dendrites into the neuronal circuitry. The dendritic arborization has been investigated in the ASD (Ramocki and Zoghbi, 2008). The genetic mouse model of *Mecp2* overexpression exhibited dendritic overgrowth in cortical pyramidal neurons (Jiang et al., 2013). Additionally, *Pten*, deletion of which produced autism-like behavior, is known to regulate neurite growth (Hsia et al., 2014; Lugo et al., 2014). The major structural components that underlie dendritic morphology are actin and microtubule. Any factors which modulate the actin and microtubule dynamics or the transport of building elements and organelles to the dendrites play important roles in the dendritic morphogenesis. Given that *Ambra1* is binding to the microtubule in the basal condition via its dynein binding domain (Di Bartolomeo et al., 2010), it is possible to hypothesize that *Ambra1* might be involved in the dendritic morphogenesis. Therefore, the quantification of dendritic arborization was performed in the CA1 pyramidal neurons of hippocampus in *Ambra1^{+/+}* and *Ambra1^{+/-}* at P28, when the reduced γ -power was detected. GFP construct was sparsely electroporated at E14.5 into the hippocampal precursor cells, which allowed us to analyze single pyramidal neuron by the reconstruction of dendrite and sholl analysis in Neuronstudio program. However, there was no significant difference in dendritic length and branching point in apical, basal and total dendrites of CA1 pyramidal neurons between two genotypes, suggesting that *Ambra1* might not regulate the dendritic growth (Fig 18, Fig 19). Therefore, the number of spines or electrophysiological recording of single pyramidal neuron should be considered in order to measure excitation and inhibition for the next step. As increased synaptic density in the cortical pyramidal neurons was reported the postmortem brain of human autists, it is important to study the synaptic or dendritic spine number in *Ambra1^{+/-}* to study neural mechanism of gamma oscillation. Currently, single cell patch-clamp recording of hippocampal pyramidal neurons is on-going both in acute brain slice and in autaptic culture in order to compare the number of functional excitatory and inhibitory synapses between genotypes. The culture of autaptic neurons in this study was established at E14 to enable to study *Ambra1* null mutation. In this culture system, the neuron of *Ambra1^{-/-}* was able to survive and grow normally, meaning that *Ambra1* might not critically regulate on the neuronal development. In acute brain slice, CA1 and CA3 pyramidal neurons will be filled with biocytin during patch-clamp recording for quantification of different spine types in whole neurons.

4.7 Female-specific ASD

So far, it is still unclear why *Ambra1*^{+/-} shows genotype-associated phenotype, such as autism-like behavior, gamma oscillation and seizure, only in female. However, as I mentioned before, our data and other previous literature provides evidence to discuss in several ways.

One possible mechanism for sex-dependent phenotype in *Ambra1*^{+/-} is the relationship between *Ambra1* and estrogen which was mentioned previously. Different pattern of mRNA and protein expression in the present study gave possible explanation that the sex-dependent control of *Ambra1* translation is able to exist. The relationship PTEN and estrogen might regulate mTOR, which is an upstream regulator of *Ambra1* and involved in regulating local protein synthesis and cytoskeletal reorganization via eukaryotic translation initiation factor 4E (eIF4E), in sex-dependent manner (Briz and Baudry, 2014; Yu and Henske, 2006). Moreover, the translational pathway through eIF4E is known to be one of the mechanisms for ASD etiology (Gkogkas et al., 2012; Santini et al., 2012). However, this eIF4E translational machinery plays an important role in the process of sex determination in *Drosophila melanogaster*, which is not controlled by sex hormone, by regulating *Sex lethal* (*Sxl*)-dependent female-specific alternative splicing of the male specific lethal-2 (*msl-2*) and *Sxl* translation, without any effect of sex hormones (Graham et al., 2011). Therefore, *Ambra1* translation from mRNA to protein might be regulated in sex-specific manner dependent or independent of sex hormone.

Another genetic mouse model of autism which shows sex-dependent autism-like behavior is Activity-dependent neuroprotective protein (*ADNP*) haploinsufficient males, while its females showed cognitive decline in later age like Alzheimer's disease (Malishkevich et al., 2015). It is consistent with our mouse model because their sex-specific phenotype was coming from different expression of protein between males and females. *ADNP* is part of SWI/SNF chromatin remodeling complex including BAF57 that specifically regulates ER α -mediated transcription. Interestingly, this protein was able to bind to eIF4E which regulate protein translation and is one of the candidate proteins for ASD by regulating the synaptic protein expression, such as neuroligin.

Intriguingly, our data about the higher propensity of seizure and reduced γ -power in *Ambra1*^{+/-} females is in line with the later onset of seizure in human autists (Volkmar and Nelson, 1990). Moreover, there

is a puberty period when the sexual maturation starts and the synaptic pruning takes place. This enables us to speculate that the number of excitatory or inhibitory synapses was altered in *Ambra1*^{+/-} mice which could cause the difference in gamma oscillations. A number of studies showed the mechanism of pubertal synaptic pruning dependent or independent of sexual hormones, such as estradiol or testosterone (Afroz et al., 2016; Oren-Suissa et al., 2016; Yildirim et al., 2008).

One recent study using diffusion tensor imaging in human brains showed different neural networks between males and females as well as sex-dependent development of brain connectivity during pubertal period. For example, during development, male brains are structured to facilitate within-lobe and within-hemisphere connectivity, whereas female brains have greater inter-hemispheric connectivity and greater cross-hemispheric participation (Ingalhalikar et al., 2014). This might explain the sex- and age-dependent difference of γ -power in females of our mouse line. I speculate that certain genetic mutation might help exceeding a threshold to induce psychiatric disorders in one sex, whereas in the other sex, this mutation is not effective due to different brain connectivity. Similarly, *Ambra1* haploinsufficiency is enough to trigger ASD, seizure propensity and reduced γ -power only in female animals, but not in males.

Surprisingly, a recent research has revealed sex-specific pruning of neuronal synapses in *C.elegans*. The nervous system of *C.elegans* containing sex-specific neurons and sex-shared neurons found in both hermaphrodite and male organisms gave a crucial evidence of sex-dimorphic regulation of neurons independently of sexual hormones. It is shown that sex-shared synaptic wiring patterns were utilized in sex-shared neurons in neuron-type specific manner. Moreover, the formation of sex-specific synapse arises prior to sexual maturation in the animal which was regulated by sex-specifically expressed transcriptional factors, indicating that there is an intrinsic, sex-specific mechanism controlling the synaptic pruning independent of sexual hormones (Oren-Suissa et al., 2016). Other causal factor for the etiology of sex difference can be considered, such as fT and XY chromosomes.

Taken together, based on the comprehensive behavioral analysis, the present study characterized the brain of *Ambra1*^{+/-} mice as the genetic mouse model of female-specific ASD in cellular and circuitry approach. *Ambra1*^{+/-} female mice showed phenotype not only in autism-like behavior but also in seizure propensity and gamma oscillation compared to its control. Further study should be needed to investigate the mechanistic insight of female-specific autism.

5 References

- Afroz, S., Parato, J., Shen, H., and Smith, S.S. (2016). Synaptic pruning in the female hippocampus is triggered at puberty by extrasynaptic GABAA receptors on dendritic spines. *Elife* 5, e15106.
- Asaka, Y., Jugloff, D.G.M., Zhang, L., Eubanks, J.H., and Fitzsimonds, R.M. (2006). Hippocampal synaptic plasticity is impaired in the *Mecp2*-null mouse model of Rett syndrome. *Neurobiol. Dis.* 21, 217–227.
- Association, A.P. (2013). *DSM-5 Diagnostic Classification* (American Psychiatric Association).
- Auyeung, B., Lombardo, M. V, Heinrichs, M., Chakrabarti, B., Sule, A., Deakin, J.B., Bethlehem, R.A.I., Dickens, L., Mooney, N., Sipple, J.A.N., et al. (2015). Oxytocin increases eye contact during a real-time, naturalistic social interaction in males with and without autism. *Transl. Psychiatry* 5, e507.
- Bailey, A., Le Couteur, A., Gottesman, I., Bolton, P., Simonoff, E., Yuzda, E., and Rutter, M. (1995). Autism as a strongly genetic disorder: evidence from a British twin study. *Psychol. Med.* 25, 63–77.
- Bailey, D.B., Raspa, M., Olmsted, M., and Holiday, D.B. (2008). Co-occurring conditions associated with *FMR1* gene variations: Findings from a national parent survey. *Am. J. Med. Genet. Part A* 146A, 2060–2069.
- Barbaresi, W.J., Katusic, S.K., Colligan, R.C., Pankratz, V.S., Weaver, A.L., Weber, K.J., Mrazek, D.A., Jacobsen, S.J., RA, B., LJ, M., et al. (2002). How Common Is Attention-Deficit/Hyperactivity Disorder? *Arch. Pediatr. Adolesc. Med.* 156, 217.
- Baron-Cohen, S., Lutchmaya, S., and Knickmeyer, R. (2004). *Prenatal testosterone in mind : amniotic fluid studies* (MIT Press).
- Baron-Cohen, S., Lombardo, M. V., Auyeung, B., Ashwin, E., Chakrabarti, B., and Knickmeyer, R. (2011). Why Are Autism Spectrum Conditions More Prevalent in Males? *PLoS Biol.* 9, e1001081.
- Di Bartolomeo, S., Corazzari, M., Nazio, F., Oliverio, S., Lisi, G., Antonioli, M., Pagliarini, V., Matteoni, S., Fuoco, C., Giunta, L., et al. (2010). The dynamic interaction of *AMBRA1* with the dynein motor complex regulates mammalian autophagy. *J. Cell Biol.* 191, 155–168.
- Bartos, M., Vida, I., and Jonas, P. (2007). Synaptic mechanisms of synchronized gamma oscillations in inhibitory interneuron networks. *Nat. Rev. Neurosci.* 8, 45–56.
- Bateup, H.S., Johnson, C.A., Deneffrio, C.L., Saulnier, J.L., Kornacker, K., and Sabatini, B.L. (2013). Excitatory/Inhibitory Synaptic Imbalance Leads to Hippocampal Hyperexcitability in Mouse Models of Tuberous Sclerosis. *Neuron* 78, 510–522.
- Berke, J.D., Okatan, M., Skurski, J., Eichenbaum, H.B., Albin, R.L., Young, A.B., Penney, J.B., Alonso, A., Garcia-Austt, E., Apicella, P., et al. (2004). Oscillatory Entrainment of Striatal Neurons in Freely Moving Rats. *Neuron* 43, 883–896.
- Betancur, C., Sakurai, T., Buxbaum, J.D., Fombonne, E., Abrahams, B.S., Geschwind, D.H., Sebat, J., al., et, Marshall, C.R., al., et, et al. (2009). The emerging role of synaptic cell-adhesion pathways in the pathogenesis of autism spectrum disorders. *Trends Neurosci.* 32, 402–412.
- Bhat, A.N., Landa, R.J., Galloway, J.C., Ganz, M., Ghaziuddin, M., Butler, E., Green, D., Baird, G., Barnett, A., Miyahara, M., et al. (2011). Current perspectives on motor functioning in infants, children, and adults with autism spectrum disorders. *Phys. Ther.* 91, 1116–1129.
- Bigler, E.D., Tate, D.F., Neeley, E.S., Wolfson, L.J., Miller, M.J., Rice, S.A., Cleavinger, H., Anderson, C., Coon, H., Ozonoff, S., et al. (2003). Temporal lobe, autism, and macrocephaly. *AJNR. Am. J. Neuroradiol.* 24, 2066–2076.
- Bodda, C., Tantra, M., Mollajew, R., Arunachalam, J.P., Laccone, F.A., Can, K., Rosenberger, A., Mironov, S.L., Ehrenreich, H., and Mannan, A.U. (2013). Mild Overexpression of *Mecp2* in Mice

Causes a Higher Susceptibility toward Seizures. *Am. J. Pathol.* 183, 195–210.

Bortolotto, Z.A., Amici, M., Anderson, W.W., Isaac, J.T.R., Collingridge, G.L., Bortolotto, Z.A., Amici, M., Anderson, W.W., Isaac, J.T.R., and Collingridge, G.L. (2011). Synaptic Plasticity in the Hippocampal Slice Preparation. In *Current Protocols in Neuroscience*, (Hoboken, NJ, USA: John Wiley & Sons, Inc.), p. 6.13.1-6.13.26.

Bozdagi, O., Sakurai, T., Papapetrou, D., Wang, X., Dickstein, D.L., Takahashi, N., Kajiwara, Y., Yang, M., Katz, A.M., Scattoni, M., et al. (2010). Haploinsufficiency of the autism-associated Shank3 gene leads to deficits in synaptic function, social interaction, and social communication. *Mol. Autism* 1, 15.

Bragin, A., Jandó, G., Nádasdy, Z., Hetke, J., Wise, K., and Buzsáki, G. (1995). Gamma (40-100 Hz) oscillation in the hippocampus of the behaving rat. *J. Neurosci.* 15, 47–60.

Briz, V., and Baudry, M. (2014). Estrogen Regulates Protein Synthesis and Actin Polymerization in Hippocampal Neurons through Different Molecular Mechanisms. *Front. Endocrinol. (Lausanne)*. 5, 1–14.

Bruining, H., Swaab, H., Kas, M., and van Engeland, H. (2009). Psychiatric characteristics in a self-selected sample of boys with Klinefelter syndrome. *Pediatrics* 123, e865-70.

Buzsáki, G., Leung, L.W., and Vanderwolf, C.H. (1983). Cellular bases of hippocampal EEG in the behaving rat. *Brain Res.* 287, 139–171.

Buzsáki, G., Anastassiou, C.A., and Koch, C. (2012). The origin of extracellular fields and currents — EEG, ECoG, LFP and spikes. *Nat. Rev. Neurosci.* 13, 407–420.

Cárdenas, A.M., Ardiles, A.O., Barraza, N., Baéz-Matus, X., and Caviedes, P. (2012). Role of Tau Protein in Neuronal Damage in Alzheimer's Disease and Down Syndrome. *Arch. Med. Res.* 43, 645–654.

Chen, C., Van Horn, J.D., and Consortium, G.R. (2016). Developmental neurogenetics and multimodal neuroimaging of sex differences in autism. *Brain Imaging Behav.* 1–24.

Chez, M.G., Buchanan, T., Aimonovitch, M., Mrazek, S., Krasne, V., Langburt, W., and Memon, S. (2004). Frequency of EEG abnormalities in age-matched siblings of autistic children with abnormal sleep EEG patterns. *Epilepsy Behav.* 5, 159–162.

Chiu, C., Reid, C.A., Tan, H.O., Davies, P.J., Single, F.N., Koukoulas, I., Berkovic, S.F., Tan, S.-S., Sprengel, R., Jones, M. V., et al. (2008). Developmental impact of a familial GABA_A receptor epilepsy mutation. *Ann. Neurol.* 64, 284–293.

Christensen, D.L., Baio, J., Braun, K.V.N., Bilder, D., Charles, J., Constantino, J.N., Daniels, J., Durkin, M.S., Fitzgerald, R.T., Kurzius-Spencer, M., et al. (2016). Prevalence and Characteristics of Autism Spectrum Disorder Among Children Aged 8 Years - Autism and Developmental Disabilities Monitoring Network, 11 Sites, United States, 2012. *MMWR. Surveill. Summ.* 65, 1–23.

Chrobak, J.J., and Buzsáki, G. (1998). Gamma oscillations in the entorhinal cortex of the freely behaving rat. *J. Neurosci.* 18, 388–398.

Cianfanelli, V., Fuoco, C., Lorente, M., Salazar, M., Quondamatteo, F., Gherardini, P.F., De Zio, D., Nazio, F., Antonioli, M., D'Orazio, M., et al. (2014). AMBRA1 links autophagy to cell proliferation and tumorigenesis by promoting c-Myc dephosphorylation and degradation. *Nat. Cell Biol.* 17, 20–30.

Cianfanelli, V., De Zio, D., Di Bartolomeo, S., Nazio, F., Strappazzon, F., and Cecconi, F. (2015a). Ambra1 at a glance. *J. Cell Sci.* 128, 2003–2008.

Cianfanelli, V., D'Orazio, M., and Cecconi, F. (2015b). AMBRA1 and BECLIN 1 interplay in the crosstalk between autophagy and cell proliferation. *Cell Cycle* 14, 959–963.

Citri, A., and Malenka, R.C. (2008). Synaptic Plasticity: Multiple Forms, Functions, and Mechanisms.

Neuropsychopharmacology 33, 18–41.

Collins, A.L., Levenson, J.M., Vilaythong, A.P., Richman, R., Armstrong, D.L., Noebels, J.L., Sweatt, J.D., and Zoghbi, H.Y. (2004). Mild overexpression of MeCP2 causes a progressive neurological disorder in mice. *Hum. Mol. Genet.* 13, 2679–2689.

Colvert, E., Tick, B., McEwen, F., Stewart, C., Curran, S.R., Woodhouse, E., Gillan, N., Hallett, V., Lietz, S., Garnett, T., et al. (2015). Heritability of Autism Spectrum Disorder in a UK Population-Based Twin Sample. *JAMA Psychiatry* 72, 415–423.

Courchesne, E., and Pierce, K. (2005). Brain overgrowth in autism during a critical time in development: implications for frontal pyramidal neuron and interneuron development and connectivity. *Int. J. Dev. Neurosci.* 23, 153–170.

Courchesne, E., Karns, C.M., Davis, H.R., Ziccardi, R., Carper, R.A., Tigue, Z.D., Chisum, H.J., Moses, P., Pierce, K., Lord, C., et al. (2001). Unusual brain growth patterns in early life in patients with autistic disorder: An MRI study. *Neurology* 57, 245–254.

Courchesne, E., Carper, R., Akshoomoff, N., E, C., G, A., D, W., EM, M., TN, W., O, D., SJ, R., et al. (2003). Evidence of Brain Overgrowth in the First Year of Life in Autism. *JAMA* 290, 337–344.

Courchesne, E., Redcay, E., and Kennedy, D.P. (2004). The autistic brain: birth through adulthood. *Curr. Opin. Neurol.* 17, 489–496.

Courchesne, E., Mouton, P.R., Calhoun, M.E., Semendeferi, K., Ahrens-Barbeau, C., Hallett, M.J., Barnes, C.C., Pierce, K., PR, M., PC, B., et al. (2011). Neuron Number and Size in Prefrontal Cortex of Children With Autism. *JAMA* 306, 2001–2010.

Crider, A., Thakkar, R., Ahmed, A.O., Pillai, A., Gillberg, C., Cederlund, M., Lamberg, K., Zeijlon, L., Auyeung, B., Knickmeyer, R., et al. (2014). Dysregulation of estrogen receptor beta (ER β), aromatase (CYP19A1), and ER co-activators in the middle frontal gyrus of autism spectrum disorder subjects. *Mol. Autism* 5, 46.

dal Maschio, M., Ghezzi, D., Bony, G., Alabastri, A., Deidda, G., Brondi, M., Sato, S.S., Zaccaria, R.P., Di Fabrizio, E., Ratto, G.M., et al. (2012). High-performance and site-directed in utero electroporation by a triple-electrode probe. *Nat. Commun.* 3, 960.

D V Madison, R C Malenka, A., and Nicoll, R.A. (2003). Mechanisms Underlying Long-Term Potentiation of Synaptic Transmission. *Annu. Rev. Neurosci.* 14, 379–397.

Deng, W., Aimone, J.B., and Gage, F.H. (2010). New neurons and new memories: how does adult hippocampal neurogenesis affect learning and memory? *Nat. Rev. Neurosci.* 11, 339–350.

Dere, E., Dahm, L., Lu, D., Hammerschmidt, K., Ju, A., Tantra, M., KÄstner, A., Chowdhury, K., and Ehrenreich, H. (2014). Heterozygous Ambra1 Deficiency in Mice: A Genetic Trait with Autism-Like Behavior Restricted to the Female Gender. *Front. Behav. Neurosci.* 8, 181.

Durand, C.M., Betancur, C., Boeckers, T.M., Bockmann, J., Chaste, P., Fauchereau, F., Nygren, G., Rastam, M., Gillberg, I.C., Anckarsäter, H., et al. (2007). Mutations in the gene encoding the synaptic scaffolding protein SHANK3 are associated with autism spectrum disorders. *Nat. Genet.* 39, 25–27.

Elia, M., Musumeci, S.A., Ferri, R., and Bergonzi, P. (1995). Clinical and neurophysiological aspects of epilepsy in subjects with autism and mental retardation. *Am. J. Ment. Retard.* 100, 6–16.

Elsabbagh, M., Divan, G., Koh, Y.-J., Kim, Y.S., Kauchali, S., Marcín, C., Montiel-Nava, C., Patel, V., Paula, C.S., Wang, C., et al. (2012). Global prevalence of autism and other pervasive developmental disorders. *Autism Res.* 5, 160–179.

Fassio, A., Patry, L., Congia, S., Onofri, F., Piton, A., Gauthier, J., Pozzi, D., Messa, M., Defranchi, E., Fadda, M., et al. (2011). SYN1 loss-of-function mutations in autism and partial epilepsy cause impaired synaptic function. *Hum. Mol. Genet.* 20, 2297–2307.

- Fattal-Valevski, A., Kramer, U., Leitner, Y., Nevo, Y., Greenstein, Y., and Harel, S. (2007). Characterization and comparison of autistic subgroups: 10 years' experience with autistic children. *Dev. Med. Child Neurol.* *41*, 21–25.
- Ferraro, T.N., Golden, G.T., Smith, G.G., St Jean, P., Schork, N.J., Mulholland, N., Ballas, C., Schill, J., Buono, R.J., and Berrettini, W.H. (1999). Mapping loci for pentylenetetrazol-induced seizure susceptibility in mice. *J. Neurosci.* *19*, 6733–6739.
- Fidler, D.J., Bailey, J.N., and Smalley, S.L. (2007). Macrocephaly in autism and other pervasive developmental disorders. *Dev. Med. Child Neurol.* *42*, 737–740.
- Fisahn, A., Pike, F.G., Buhl, E.H., and Paulsen, O. (1998). Cholinergic induction of network oscillations at 40 Hz in the hippocampus in vitro. *Nature* *394*, 186–189.
- Fisahn, A., Contractor, A., Traub, R.D., Buhl, E.H., Heinemann, S.F., and McBain, C.J. (2004). Distinct Roles for the Kainate Receptor Subunits GluR5 and GluR6 in Kainate-Induced Hippocampal Gamma Oscillations. *J. Neurosci.* *24*, 9658–9668.
- Fisher, R.S., van Emde Boas, W., Blume, W., Elger, C., Genton, P., Lee, P., and Engel, J. (2005). Epileptic seizures and epilepsy: definitions proposed by the International League Against Epilepsy (ILAE) and the International Bureau for Epilepsy (IBE). *Epilepsia* *46*, 470–472.
- Frazier, T.W., Thompson, L., Youngstrom, E.A., Law, P., Hardan, A.Y., Eng, C., and Morris, N. (2014). A Twin Study of Heritable and Shared Environmental Contributions to Autism. *J. Autism Dev. Disord.* *44*, 2013–2025.
- Freund, T.F. (2003). Interneuron Diversity series: Rhythm and mood in perisomatic inhibition. *Trends Neurosci.* *26*, 489–495.
- Fries, P., Reynolds, J.H., Rorie, A.E., Desimone, R., Desimone, R., Duncan, J., Chelazzi, L., Miller, E.K., Duncan, J., Desimone, R., et al. (2001). Modulation of Oscillatory Neuronal Synchronization by Selective Visual Attention. *Science* (80-.). *291*, 1560–1563.
- Geerts, M., Steyaert, J., and Fryns, J.P. (2003). The XYY syndrome: a follow-up study on 38 boys. *Genet. Couns.* *14*, 267–279.
- Giovanardi Rossi, P., Posar, A., and Parmeggiani, A. (2000). Epilepsy in adolescents and young adults with autistic disorder. *Brain Dev.* *22*, 102–106.
- Gkogkas, C.G., Khoutorsky, A., Ran, I., Rampakakis, E., Nevarko, T., Weatherill, D.B., Vasuta, C., Yee, S., Truitt, M., Dallaire, P., et al. (2012). Autism-related deficits via dysregulated eIF4E-dependent translational control. *Nature* *493*, 371–377.
- Goffin, A., Hoefsloot, L.H., Bosgoed, E., Swillen, A., and Fryns, J.-P. (2001). PTEN mutation in a family with Cowden syndrome and autism. *Am. J. Med. Genet.* *105*, 521–524.
- Graham, P.L., Yanowitz, J.L., Penn, J.K.M., Deshpande, G., and Schedl, P. (2011). The Translation Initiation Factor eIF4E Regulates the Sex-Specific Expression of the Master Switch Gene *Sxl* in *Drosophila melanogaster*. *PLoS Genet.* *7*, e1002185.
- Gray, C.M., König, P., Engel, A.K., and Singer, W. (1989). Oscillatory responses in cat visual cortex exhibit inter-columnar synchronization which reflects global stimulus properties. *Nature* *338*, 334–337.
- Groen, W., Teluij, M., Buitelaar, J., and Tendolkar, I. (2010). Amygdala and Hippocampus Enlargement During Adolescence in Autism. *J. Am. Acad. Child Adolesc. Psychiatry* *49*, 552–560.
- Gutierrez, G.C., Smalley, S.L., and Tanguay, P.E. (1998). Autism in tuberous sclerosis complex. *J. Autism Dev. Disord.* *28*, 97–103.
- Halgren, E., Babb, T.L., and Crandall, P.H. (1977). Responses of human limbic neurons to induced changes in blood gases. *Brain Res.* *132*, 43–63.

- Hallmayer, J., Cleveland, S., Torres, A., Phillips, J., Cohen, B., Torigoe, T., Miller, J., Fedele, A., Collins, J., Smith, K., et al. (2011). Genetic Heritability and Shared Environmental Factors Among Twin Pairs With Autism. *Arch. Gen. Psychiatry* 68, 1095.
- Harai, T., Inoue, R., Fujita, Y., Tanaka, A., Horio, M., Hashimoto, K., Hongou, K., Miyawaki, T., Mori, H., Benediktsson, A.M., et al. (2012). Decreased susceptibility to seizures induced by pentylenetetrazole in serine racemase knockout mice. *Epilepsy Res.* 102, 180–187.
- Hazlett, H.C., Poe, M.D., Gerig, G., Styner, M., Chappell, C., Smith, R.G., Vachet, C., Piven, J., E, F., EM, M., et al. (2011). Early Brain Overgrowth in Autism Associated With an Increase in Cortical Surface Area Before Age 2 Years. *Arch. Gen. Psychiatry* 68, 467.
- Haznedar, M.M., Buchsbaum, M.S., Wei, T.C., Hof, P.R., Cartwright, C., Bienstock, C.A., and Hollander, E. (2000). Limbic circuitry in patients with autism spectrum disorders studied with positron emission tomography and magnetic resonance imaging. *Am. J. Psychiatry* 157, 1994–2001.
- Heinrich, A., Nees, F., Lourdasamy, A., Tzschoppe, J., Meier, S., Vollstädt-Klein, S., Fauth-Bühler, M., Steiner, S., Bach, C., Poustka, L., et al. (2013). From gene to brain to behavior: schizophrenia-associated variation in *AMBRA1* alters impulsivity-related traits. *Eur. J. Neurosci.* 38, 2941–2945.
- Herbert, M.R., Ziegler, D.A., Deutsch, C.K., O'Brien, L.M., Lange, N., Bakardjiev, A., Hodgson, J., Adrien, K.T., Steele, S., Makris, N., et al. (2003). Dissociations of cerebral cortex, subcortical and cerebral white matter volumes in autistic boys. *Brain* 126, 1182–1192.
- Hoffman, E.J., Turner, K.J., Fernandez, J.M., Cifuentes, D., Ghosh, M., Ijaz, S., Jain, R.A., Kubo, F., Bill, B.R., Baier, H., et al. (2016). Estrogens Suppress a Behavioral Phenotype in Zebrafish Mutants of the Autism Risk Gene, *CNTNAP2*. *Neuron* 89, 725–733.
- Hoshino, Y., Kaneko, M., Yashima, Y., Kumashiro, H., Volkmar, F.R., and Cohen, D.J. (1987). Clinical features of autistic children with setback course in their infancy. *Jpn. J. Psychiatry Neurol.* 41, 237–245.
- Hsia, H.-E., Kumar, R., Luca, R., Takeda, M., Courchet, J., Nakashima, J., Wu, S., Goebbels, S., An, W., Eickholt, B.J., et al. (2014). Ubiquitin E3 ligase *Nedd4-1* acts as a downstream target of PI3K/PTEN-mTORC1 signaling to promote neurite growth. *Proc. Natl. Acad. Sci.* 111, 13205–13210.
- Hulbert, S.W., and Jiang, Y.-H. (2016). Monogenic mouse models of autism spectrum disorders: Common mechanisms and missing links. *Neuroscience* 321, 3–23.
- Ingalhalikar, M., Smith, A., Parker, D., Satterthwaite, T.D., Elliott, M.A., Ruparel, K., Hakonarson, H., Gur, R.E., Gur, R.C., and Verma, R. (2014). Sex differences in the structural connectome of the human brain. *Proc. Natl. Acad. Sci.* 111, 823–828.
- Jamain, S., Quach, H., Betancur, C., Råstam, M., Colineaux, C., Gillberg, I.C., Soderstrom, H., Giros, B., Leboyer, M., Gillberg, C., et al. (2003). Mutations of the X-linked genes encoding neuroligins *NLGN3* and *NLGN4* are associated with autism. *Nat. Genet.* 34, 27–29.
- Jamain, S., Radyushkin, K., Hammerschmidt, K., Granon, S., Boretius, S., Varoqueaux, F., Ramanantsoa, N., Gallego, J., Ronnenberg, A., Winter, D., et al. (2008). Reduced social interaction and ultrasonic communication in a mouse model of monogenic heritable autism. *Proc. Natl. Acad. Sci. U. S. A.* 105, 1710–1715.
- Jiang, M., Ash, R.T., Baker, S.A., Suter, B., Ferguson, A., Park, J., Rudy, J., Torsky, S.P., Chao, H.-T., Zoghbi, H.Y., et al. (2013). Dendritic arborization and spine dynamics are abnormal in the mouse model of *MECP2* duplication syndrome. *J. Neurosci.* 33, 19518–19533.
- Jonas, P., Bischofberger, J., Fricker, D., Miles, R., Cobb, S., al., et, Pouille, F., Scanziani, M., Miles, R., al., et, et al. (2004). Interneuron Diversity series: Fast in, fast out – temporal and spatial signal processing in hippocampal interneurons. *Trends Neurosci.* 27, 30–40.
- Jones, M.C., and Okere, K. (2008). Treatment of Hypersexual Behavior with Oral Estrogen in an

Autistic Male. *South. Med. J.* 101, 959–960.

Ju, A., Hammerschmidt, K., Tantra, M., Krueger, D., Brose, N., and Ehrenreich, H. (2014). Juvenile manifestation of ultrasound communication deficits in the neurologin-4 null mutant mouse model of autism. *Behav. Brain Res.* 270, 159–164.

Judson, M.C., Wallace, M.L., Sidorov, M.S., Burette, A.C., Gu, B., van Woerden, G.M., King, I.F., Han, J.E., Zylka, M.J., Elgersma, Y., et al. (2016). GABAergic Neuron-Specific Loss of Ube3a Causes Angelman Syndrome-Like EEG Abnormalities and Enhances Seizure Susceptibility. *Neuron* 90, 56–69.

Kates, W.R., Burnette, C.P., Eliez, S., Strunge, L.A., Kaplan, D., Landa, R., Reiss, A.L., and Pearlson, G.D. (2004). Neuroanatomic Variation in Monozygotic Twin Pairs Discordant for the Narrow Phenotype for Autism. *Am. J. Psychiatry* 161, 539–546.

Kawasaki, Y., Yokota, K., Shinomiya, M., Shimizu, Y., and Niwa, S. (1997). Brief report: electroencephalographic paroxysmal activities in the frontal area emerged in middle childhood and during adolescence in a follow-up study of autism. *J. Autism Dev. Disord.* 27, 605–620.

Kehrer, C., Maziashvili, N., Dugladze, T., and Gloveli, T. (2008). Altered Excitatory-Inhibitory Balance in the NMDA-Hypofunction Model of Schizophrenia. *Front. Mol. Neurosci.* 1, 6.

Kirschstein, T. (2012). Synaptic Plasticity and Learning in Animal Models of Tuberous Sclerosis Complex. *Neural Plast.* 2012, 1–8.

Knickmeyer, R., Baron-Cohen, S., Raggatt, P., and Taylor, K. (2005). Foetal testosterone, social relationships, and restricted interests in children. *J. Child Psychol. Psychiatry* 46, 198–210.

Knickmeyer, R., Baron-Cohen, S., Raggatt, P., Taylor, K., and Hackett, G. (2006). Fetal testosterone and empathy. *Horm. Behav.* 49, 282–292.

Kolk, S.M., de Mooij-Malsen, A.J., and Martens, G.J.M. (2011). Spatiotemporal Molecular Approach of in utero Electroporation to Functionally Decipher Endophenotypes in Neurodevelopmental Disorders. *Front. Mol. Neurosci.* 4, 1–7.

Komatsu, M., Waguri, S., Chiba, T., Murata, S., Iwata, J., Tanida, I., Ueno, T., Koike, M., Uchiyama, Y., Kominami, E., et al. (2006). Loss of autophagy in the central nervous system causes neurodegeneration in mice. *Nature* 441, 880–884.

Kopp, S., and Gillberg, C. (2011). The Autism Spectrum Screening Questionnaire (ASSQ)-Revised Extended Version (ASSQ-REV): An instrument for better capturing the autism phenotype in girls? A preliminary study involving 191 clinical cases and community controls. *Res. Dev. Disabil.* 32, 2875–2888.

Kowall, N.W., and McKee, A.C. (1993). The histopathology of neuronal degeneration and plasticity in Alzheimer disease. *Adv. Neurol.* 59, 5–33.

Lai, D.-C., Tseng, Y.-C., Hou, Y.-M., and Guo, H.-R. (2012). Gender and geographic differences in the prevalence of autism spectrum disorders in children: Analysis of data from the national disability registry of Taiwan. *Res. Dev. Disabil.* 33, 909–915.

Lai, M.-C., Lombardo, M. V., Pasco, G., Ruigrok, A.N. V., Wheelwright, S.J., Sadek, S.A., Chakrabarti, B., Baron-Cohen, S., and Baron-Cohen, S. (2011). A Behavioral Comparison of Male and Female Adults with High Functioning Autism Spectrum Conditions. *PLoS One* 6, e20835.

Lee, E., Lee, J., and Kim, E. (2016). Excitation/inhibition Imbalance in Animal Models of ASDs. *Biol. Psychiatry In Press*.

Liu, X., Kawashima, M., Miyagawa, T., Otowa, T., Latt, K.Z., Thiri, M., Nishida, H., Sugiyama, T., Tsurusaki, Y., Matsumoto, N., et al. (2015). Novel rare variations of the oxytocin receptor (OXTR) gene in autism spectrum disorder individuals. *Hum. Genome Var.* 2, 1–5.

- Lois, C., Hong, E.J., Pease, S., Brown, E.J., and Baltimore, D. (2002). Germline transmission and tissue-specific expression of transgenes delivered by lentiviral vectors. *Science* 295, 868–872.
- Lotspeich, L.J., Kwon, H., Schumann, C.M., Fryer, S.L., Goodlin-Jones, B.L., Buonocore, M.H., Lammers, C.R., Amaral, D.G., Reiss, A.L., L, K., et al. (2004). Investigation of Neuroanatomical Differences Between Autism and Asperger Syndrome. *Arch. Gen. Psychiatry* 61, 291–298.
- Lugo, J.N., Smith, G.D., Arbuckle, E.P., White, J., Holley, A.J., Floruta, C.M., Ahmed, N., Gomez, M.C., and Okonkwo, O. (2014). Deletion of PTEN produces autism-like behavioral deficits and alterations in synaptic proteins. *Front. Mol. Neurosci.* 7, 27.
- Lutchmaya, S., Baron-Cohen, S., and Raggatt, P. (2001). Foetal testosterone and vocabulary size in 18- and 24-month-old infants. *Infant Behav. Dev.* 24, 418–424.
- Lutchmaya, S., Baron-Cohen, S., and Raggatt, P. (2002). Foetal testosterone and eye contact in 12-month-old human infants. *Infant Behav. Dev.* 25, 327–335.
- Malishkevich, A., Amram, N., Hacoheh-Kleiman, G., Magen, I., Giladi, E., and Gozes, I. (2015). Activity-dependent neuroprotective protein (ADNP) exhibits striking sexual dichotomy impacting on autistic and Alzheimer's pathologies. *Transl. Psychiatry* 5, e501.
- Mann, E.O., and Paulsen, O. (2007). Role of GABAergic inhibition in hippocampal network oscillations. *Trends Neurosci.* 30, 343–349.
- Mann, E.O., Suckling, J.M., Hajos, N., Greenfield, S.A., Paulsen, O., Batschelet, E., Bleakman, D., Ballyk, B.A., Schoepp, D.D., Palmer, A.J., et al. (2005). Perisomatic Feedback Inhibition Underlies Cholinergically Induced Fast Network Oscillations in the Rat Hippocampus In Vitro. *Neuron* 45, 105–117.
- Maria Fimia, G., Stoykova, A., Romagnoli, A., Giunta, L., Di Bartolomeo, S., Nardacci, R., Corazzari, M., Fuoco, C., Ucar, A., Schwartz, P., et al. (2007). Ambra1 regulates autophagy and development of the nervous system. *Nature* 447, 1121–1125.
- Markram, K., and Markram, H. (2010). The Intense World Theory – A Unifying Theory of the Neurobiology of Autism. *Front. Hum. Neurosci.* 4, 224.
- Maski, K.P., Jeste, S.S., and Spence, S.J. (2011). Common neurological co-morbidities in autism spectrum disorders. *Curr. Opin. Pediatr.* 23, 609–615.
- Mathalon, D.H., Sohal, V.S., G, B., BJ, R., RT, C., J, N., CA, B., P, T., and Y, H. (2015). Neural Oscillations and Synchrony in Brain Dysfunction and Neuropsychiatric Disorders. *JAMA Psychiatry* 72, 840–844.
- Matsui, A., Yoshida, A.C., Kubota, M., Ogawa, M., and Shimogori, T. (2011). Mouse &em>in Utero&em>; Electroporation: Controlled Spatiotemporal Gene Transfection. *J. Vis. Exp.* e3024–e3024.
- MCLEAN, K.J., O'BRIEN, T.J., COOK, M.J., VAJDA, F.J., Bauer, J., Gram, L., Dulac, O., Lerman, P., Perucca, E., Gram, L., et al. (2004). The influence of gender on the aggravation of absence seizures by carbamazepine in the low-dose pentylenetetrazol rat model. *Seizure* 13, 208–216.
- Miles, R., Tóth, K., Gulyás, A.I., Hájos, N., Freund, T.F., Alger, B., Nicoll, R., Atwood, H., Marin, L., Baude, A., et al. (1996). Differences between Somatic and Dendritic Inhibition in the Hippocampus. *Neuron* 16, 815–823.
- Moretti, P., Levenson, J.M., Battaglia, F., Atkinson, R., Teague, R., Antalffy, B., Armstrong, D., Arancio, O., Sweatt, J.D., and Zoghbi, H.Y. (2006). Learning and Memory and Synaptic Plasticity Are Impaired in a Mouse Model of Rett Syndrome. *J. Neurosci.* 26, 319–327.
- Muhle, R., Trentacoste, S. V, and Rapin, I. (2004). The genetics of autism. *Pediatrics* 113, e472-86.

- Murthy, V.N., and Fetz, E.E. (1992). Coherent 25-to 35-Hz oscillations in the sensorimotor cortex of awake behaving monkeys. *Neurobiology* 89, 5670–5674.
- Na, E.S., Nelson, E.D., Adachi, M., Autry, A.E., Mahgoub, M.A., Kavalali, E.T., and Monteggia, L.M. (2012). A Mouse Model for MeCP2 Duplication Syndrome: MeCP2 Overexpression Impairs Learning and Memory and Synaptic Transmission. *J. Neurosci.* 32, 3109–3117.
- Na, E.S., Nelson, E.D., Kavalali, E.T., and Monteggia, L.M. (2013). The impact of MeCP2 loss- or gain-of-function on synaptic plasticity. *Neuropsychopharmacology* 38, 212–219.
- Nazio, F., Strappazzon, F., Antonioli, M., Bielli, P., Cianfanelli, V., Bordi, M., Gretzmeier, C., Dengjel, J., Piacentini, M., Fimia, G.M., et al. (2013). mTOR inhibits autophagy by controlling ULK1 ubiquitylation, self-association and function through AMBRA1 and TRAF6. *Nat. Cell Biol.* 15, 406–416.
- Nelson, E.D., Kavalali, E.T., and Monteggia, L.M. (2006). MeCP2-Dependent Transcriptional Repression Regulates Excitatory Neurotransmission. *Curr. Biol.* 16, 710–716.
- Neves, G., Cooke, S.F., and Bliss, T.V.P. (2008). Synaptic plasticity, memory and the hippocampus: a neural network approach to causality. *Nat. Rev. Neurosci.* 9, 65–75.
- O'Donovan, M.C., Craddock, N.J., and Owen, M.J. (2009). Genetics of psychosis; insights from views across the genome. *Hum. Genet.* 126, 3–12.
- Oren-Suissa, M., Bayer, E.A., and Hobert, O. (2016). Sex-specific pruning of neuronal synapses in *Caenorhabditis elegans*. *Nature* 533, 206–211.
- Ozonoff, S., Young, G.S., Carter, A., Messinger, D., Yirmiya, N., Zwaigenbaum, L., Bryson, S., Carver, L.J., Constantino, J.N., Dobkins, K., et al. (2011). Recurrence risk for autism spectrum disorders: a Baby Siblings Research Consortium study. *Pediatrics* 128, e488-95.
- Pagliarini, V., Wirawan, E., Romagnoli, A., Ciccocanti, F., Lisi, G., Lippens, S., Cecconi, F., Fimia, G.M., Vandenabeele, P., Corazzari, M., et al. (2012). Proteolysis of Ambra1 during apoptosis has a role in the inhibition of the autophagic pro-survival response. *Cell Death Differ.* 19, 1495–1504.
- Pardo, C.A., and Eberhart, C.G. (2007). The Neurobiology of Autism. *Brain Pathol.* 17, 434–447.
- Patterson, P.H. (2011). Modeling Autistic Features in Animals. *Pediatr. Res.* 69, 34R–40R.
- Pieretti, M., Zhang, F., Fu, Y.-H., Warren, S.T., Oostra, B.A., Caskey, C.T., and Nelson, D.L. (1991). Absence of expression of the FMR-1 gene in fragile X syndrome. *Cell* 66, 817–822.
- Pinault, D., and Descheˆnes, M. (1992). Voltage-dependent 40-Hz oscillations in rat reticular thalamic neurons in vivo. *Neuroscience* 51, 245–258.
- Piven, J., Bailey, J., Ranson, B.J., and Arndt, S. (1998). No difference in hippocampus volume detected on magnetic resonance imaging in autistic individuals. *J. Autism Dev. Disord.* 28, 105–110.
- Popescu, A.T., Popa, D., and Paré, D. (2009). Coherent gamma oscillations couple the amygdala and striatum during learning. *Nat. Neurosci.* 12, 801–807.
- Provost, B., Lopez, B.R., and Heimerl, S. (2007). A Comparison of Motor Delays in Young Children: Autism Spectrum Disorder, Developmental Delay, and Developmental Concerns. *J. Autism Dev. Disord.* 37, 321–328.
- Ramocki, M.B., and Zoghbi, H.Y. (2008). Failure of neuronal homeostasis results in common neuropsychiatric phenotypes. *Nature* 455, 912–918.
- Raymond, C.R. (2007). LTP forms 1, 2 and 3: different mechanisms for the “long” in long-term potentiation. *Trends Neurosci.* 30, 167–175.
- Rhee, J.M., Pirity, M.K., Lackan, C.S., Long, J.Z., Kondoh, G., Takeda, J., and Hadjantonakis, A.-K. (2006). In vivo imaging and differential localization of lipid-modified GFP-variant fusions in embryonic

stem cells and mice. *Genesis* 44, 202–218.

Rietschel, M., Mattheisen, M., Degenhardt, F., Kahn, R.S., Linszen, D.H., Os, J. van, Wiersma, D., Bruggeman, R., Cahn, W., de Haan, L., et al. (2012). Association between genetic variation in a region on chromosome 11 and schizophrenia in large samples from Europe. *Mol. Psychiatry* 17, 906–917.

Rodriguez, A., Ehlenberger, D.B., Dickstein, D.L., Hof, P.R., and Wearne, S.L. (2008). Automated Three-Dimensional Detection and Shape Classification of Dendritic Spines from Fluorescence Microscopy Images. *PLoS One* 3, e1997.

Rogers, S.J. (2009). What are infant siblings teaching us about autism in infancy? *Autism Res.* 2, 125–137.

Rowland, A.M., Richmond, J.E., Olsen, J.G., Hall, D.H., and Bamber, B.A. (2006). Presynaptic Terminals Independently Regulate Synaptic Clustering and Autophagy of GABAA Receptors in *Caenorhabditis elegans*. *J. Neurosci.* 26, 1711–1720.

Sacktor, T.C. (2008). Chapter 2 PKM ζ , LTP maintenance, and the dynamic molecular biology of memory storage. *Prog. Brain Res.* 169, 27–40.

Saitoh, O., Courchesne, E., Egaas, B., Lincoln, A.J., and Schreibman, L. (1995). Cross-sectional area of the posterior hippocampus in autistic patients with cerebellar and corpus callosum abnormalities. *Neurology* 45, 317–324.

Saitoh, O., Karns, C.M., and Courchesne, E. (2001). Development of the hippocampal formation from 2 to 42 years MRI evidence of smaller area dentata in autism. *Brain* 124, 1317–1324.

Santini, E., Huynh, T.N., MacAskill, A.F., Carter, A.G., Pierre, P., Ruggero, D., Kaphzan, H., and Klann, E. (2012). Exaggerated translation causes synaptic and behavioural aberrations associated with autism. *Nature* 493, 411–415.

Sarachana, T., Xu, M., Wu, R.-C., and Hu, V.W. (2011). Sex Hormones in Autism: Androgens and Estrogens Differentially and Reciprocally Regulate RORA, a Novel Candidate Gene for Autism. *PLoS One* 6, e17116.

Scattoni, M.L., Crawley, J., and Ricceri, L. (2009). Ultrasonic vocalizations: a tool for behavioural phenotyping of mouse models of neurodevelopmental disorders. *Neurosci. Biobehav. Rev.* 33, 508–515.

Schendel, D.E., Grønborg, T.K., Parner, E.T., M, E., YS, K., J, S., H, T., RE, R., P, L., J, H., et al. (2014). The Genetic and Environmental Contributions to Autism. *JAMA* 311, 1738–1739.

Schmeisser, M.J., Ey, E., Wegener, S., Bockmann, J., Stempel, A.V., Kuebler, A., Janssen, A.-L., Udvardi, P.T., Shiban, E., Spilker, C., et al. (2012). Autistic-like behaviours and hyperactivity in mice lacking ProSAP1/Shank2. *Nature* 486, 256–260.

Schumann, C.M., Hamstra, J., Goodlin-Jones, B.L., Lotspeich, L.J., Kwon, H., Buonocore, M.H., Lammers, C.R., Reiss, A.L., and Amaral, D.G. (2004). The Amygdala Is Enlarged in Children But Not Adolescents with Autism; the Hippocampus Is Enlarged at All Ages. *J. Neurosci.* 24, 6392–6401.

Sharpe, M.A., Gist, T.L., Baskin, D.S., Sharpe, M.A., Gist, T.L., and Baskin, D.S. (2013). Alterations in sensitivity to estrogen, dihydrotestosterone, and xenogens in B-lymphocytes from children with autism spectrum disorder and their unaffected twins/siblings. *J. Toxicol.* 2013, 1–11.

Shen, W., and Ganetzky, B. (2009). Autophagy promotes synapse development in *Drosophila*. *J. Cell Biol.* 187, 71–79.

Sirota, A., Montgomery, S., Fujisawa, S., Isomura, Y., Zugaro, M., Buzsáki, G., Abeles, M., Alonso, A., Garcia-Austt, E., Anderson, M.I., et al. (2008). Entrainment of Neocortical Neurons and Gamma Oscillations by the Hippocampal Theta Rhythm. *Neuron* 60, 683–697.

- Skarnes, W.C., Moss, J.E., Hurlley, S.M., Beddington, R.S.P., and Rubin, G.M. (1995). Capturing genes encoding membrane and secreted proteins important for mouse development (mouse embryonic stem cells/gene trap/insertional mutation). *Dev. Biol.* 92, 6592–6596.
- Sohal, V.S., Zhang, F., Yizhar, O., and Deisseroth, K. (2009). Parvalbumin neurons and gamma rhythms enhance cortical circuit performance. *Nature* 459, 698–702.
- Sparks, B.F., Friedman, S.D., Shaw, D.W., Aylward, E.H., Echelard, D., Artru, A.A., Maravilla, K.R., Giedd, J.N., Munson, J., Dawson, G., et al. (2002). Brain structural abnormalities in young children with autism spectrum disorder. *Neurology* 59, 184–192.
- Spruston, N. (2008). Pyramidal neurons: dendritic structure and synaptic integration. *Nat. Rev. Neurosci.* 9, 206–221.
- Strappazon, F., Vietri-Rudan, M., Campello, S., Nazio, F., Florenzano, F., Fimia, G.M., Piacentini, M., Levine, B., and Cecconi, F. (2011). Mitochondrial BCL-2 inhibits AMBRA1-induced autophagy. *EMBO J.* 30, 1195–1208.
- Strappazon, F., Nazio, F., Corrado, M., Cianfanelli, V., Romagnoli, A., Fimia, G.M., Campello, S., Nardacci, R., Piacentini, M., Campanella, M., et al. (2015). AMBRA1 is able to induce mitophagy via LC3 binding, regardless of PARKIN and p62/SQSTM1. *Cell Death Differ.* 22, 419–432.
- Südhof, T.C. (2008). Neuroligins and neuroligins link synaptic function to cognitive disease. *Nature* 455, 903–911.
- Szatmari, P., Offord, D.R., and Boyle, M.H. (1989). Ontario Child Health Study: Prevalence of Attention Deficit Disorder with Hyperactivity. *J. Child Psychol. Psychiatry* 30, 219–223.
- Szatmari, P., Paterson, A.D., Zwaigenbaum, L., Roberts, W., Brian, J., Liu, X.-Q., Vincent, J.B., Skaug, J.L., Thompson, A.P., Senman, L., et al. (2007). Mapping autism risk loci using genetic linkage and chromosomal rearrangements. *Nat. Genet.* 39, 319–328.
- Tabuchi, K., Blundell, J., Etherton, M.R., Hammer, R.E., Liu, X., Powell, C.M., and Südhof, T.C. (2007). A neuroligin-3 mutation implicated in autism increases inhibitory synaptic transmission in mice. *Science* 318, 71–76.
- Tang, G., Gudsnek, K., Kuo, S.-H., Cotrina, M.L., Rosoklija, G., Sosunov, A., Sonders, M.S., Kanter, E., Castagna, C., Yamamoto, A., et al. (2014). Loss of mTOR-Dependent Macroautophagy Causes Autistic-like Synaptic Pruning Deficits. *Neuron* 83, 1131–1143.
- Tartaglia, N., Davis, S., Hench, A., Nimishakavi, S., Beauregard, R., Reynolds, A., Fenton, L., Albrecht, L., Ross, J., Visootsak, J., et al. (2008). A new look at XYY syndrome: Medical and psychological features. *Am. J. Med. Genet. Part A* 146A, 1509–1522.
- Tartaglia NR, Hansen RL, Reynolds A, Hessel D, B. (2006). Attentional deficit hyperactivity disorder and autism spectrum disorders in males with XXY, XYY and XYYX syndromes. *J. Intellect. Disabil. Res.* 50, 783–790.
- Tsai, P.T., Hull, C., Chu, Y., Greene-Colozzi, E., Sadowski, A.R., Leech, J.M., Steinberg, J., Crawley, J.N., Regehr, W.G., and Sahin, M. (2012). Autistic-like behaviour and cerebellar dysfunction in Purkinje cell Tsc1 mutant mice. *Nature* 488, 647–651.
- Viding, E., Spinath, F.M., Price, T.S., Bishop, D.V.M., Dale, P.S., and Plomin, R. (2004). Genetic and environmental influence on language impairment in 4-year-old same-sex and opposite-sex twins. *J. Child Psychol. Psychiatry* 45, 315–325.
- Voigt, R.G., Dickerson, C.L., Reynolds, A.M., Childers, D.O., Rodriguez, D.L., and Brown, F.R. (2000). Laboratory evaluation of children with autistic spectrum disorders: a guide for primary care pediatricians. *Clin. Pediatr. (Phila.)* 39, 669–671.
- Volkmar, F.R., and Nelson, D.S. (1990). Seizure Disorders in Autism. *J. Am. Acad. Child Adolesc.*

Psychiatry 29, 127–129.

Vorstman, J.A.S., Staal, W.G., van Daalen, E., van Engeland, H., Hochstenbach, P.F.R., and Franke, L. (2006). Identification of novel autism candidate regions through analysis of reported cytogenetic abnormalities associated with autism. *Mol. Psychiatry* 11, 18–28.

Wang, X., McCoy, P.A., Rodriguiz, R.M., Pan, Y., Je, H.S., Roberts, A.C., Kim, C.J., Berrios, J., Colvin, J.S., Bousquet-Moore, D., et al. (2011). Synaptic dysfunction and abnormal behaviors in mice lacking major isoforms of Shank3. *Hum. Mol. Genet.* 20, 3093–3108.

Weng, S.-M., McLeod, F., Bailey, M.E.S., and Cobb, S.R. (2011). Synaptic plasticity deficits in an experimental model of rett syndrome: long-term potentiation saturation and its pharmacological reversal. *Neuroscience* 180, 314–321.

Whitacre, C.C. (2001). Sex differences in autoimmune disease. *Nat. Immunol.* 2, 777–780.

Whittington, M.A., Traub, R.D., and Jefferys, J.G.R. (1995). Synchronized oscillations in interneuron networks driven by metabotropic glutamate receptor activation. *Nature* 373, 612–615.

Wojcik, S.M., Tantra, M., Stepniak, B., Man, K.-N.M., Muller-Ribbe, K., Begemann, M., Ju, A., Papiol, S., Ronnenberg, A., Gurvich, A., et al. (2013). Genetic markers of a Munc13 protein family member, BAIAP3, are gender specifically associated with anxiety and benzodiazepine abuse in mice and humans. *Mol. Med.* 19, 135–148.

Yatawara, C.J., Einfeld, S.L., Hickie, I.B., Davenport, T.A., and Guastella, A.J. (2015). The effect of oxytocin nasal spray on social interaction deficits observed in young children with autism: a randomized clinical crossover trial. *Mol. Psychiatry* 1–7.

Yazdankhah, M., Farioli-Vecchioli, S., Tonchev, A.B., Stoykova, A., and Cecconi, F. (2014). The autophagy regulators Ambra1 and Beclin 1 are required for adult neurogenesis in the brain subventricular zone. *Cell Death Dis.* 5, e1403.

Yildirim, M., Mapp, O.M., Janssen, W.G.M., Yin, W., Morrison, J.H., and Gore, A.C. (2008). Postpubertal decrease in hippocampal dendritic spines of female rats. *Exp. Neurol.* 210, 339–348.

Yoo, J., Bakes, J., Bradley, C., Collingridge, G.L., Kaang, B.-K., Kanner, L., Asperger, H., Frith, U., Association, A.P., Organization, W.H., et al. (2014). Shank mutant mice as an animal model of autism. *Philos. Trans. R. Soc. Lond. B. Biol. Sci.* 369, 20130143.

Young, D.M., Schenk, A.K., Yang, S.-B., Jan, Y.N., and Jan, L.Y. (2010). Altered ultrasonic vocalizations in a tuberous sclerosis mouse model of autism. *Proc. Natl. Acad. Sci.* 107, 11074–11079.

Yu, J., and Henske, E.P. (2006). Estrogen-induced activation of mammalian target of rapamycin is mediated via tuberin and the small GTPase Ras homologue enriched in brain. *Cancer Res.* 66, 9461–9466.

Zoghbi, H.Y., Amir, R.E., Van den Veyver, I.B., Wan, M., Tran, C.Q., and Francke, U. (1999). Rett syndrome is caused by mutations in X-linked MECP2, encoding methyl-CpG-binding protein 2. *Nat. Genet.* 23, 185–188.

Zucker, R.S., and Regehr, W.G. (2002). SHORT-TERM SYNAPTIC PLASTICITY. *Annu. Rev. Physiol.* 64, 355–405.

6 List of Abbreviations

-/-	Knockout
+/-	Heterozygous
+/+	Wild type
°C	Degrees Celsius
2D	2-dimension(al)
3D	3-dimension(al)
ACSF	Artificial cerebrospinal fluid
ADNP	Activity-dependent neuroprotective protein
Ambra1	Activating molecule in Beclin-1-regulated autophagy (murine)
AMBRA1	Activating molecule in Beclin-1-regulated autophagy (human)
<i>Ambra1</i> ^{-/-}	Ambra1 knock-out
<i>Ambra1</i> ^{+/-}	Ambra1 heterozygous
<i>Ambra1</i> ^{+/+}	Ambra1 wild-type
AMPA	α-amino-3-hydroxy-5-methyl-4-isoxazolepropionic acid
AMPA	AMPA Receptor
ARR	Air righting reflex
ASD	Autism spectrum disorder
Atg7	Autophagy related 7
BAF57	Brahma-related gene 1-associated factor 57
Bcl-2	B-cell lymphoma 2
Beclin1	Coiled-coil myosin-like BCL2-interacting protein
bp	Basepair
BrdU	Bromodeoxyuridine
BSA	Bovine serum albumin
<i>C.elegans</i>	Caenorhabditis elegans
CA	Cliff avoidance
CA1	Cornu Ammonis 1
CA3	Cornu Ammonis 3
cm	Centimeter
c-Myc	Myc proto-oncogene protein
CNS	Central nervous system
CTIP2	COUP-TF-interacting protein 2
DAPI	4',6-diamidino-2-phenylindole
DHPG	3,5-dihydroxyphenylglycine
Di	Diencephalon
DLC1/2	Dynein light chains 1/2
DNA	Deoxyribonucleic acid
dNTP	Desoxyribonucleoside triphosphate
DSM-V	Diagnostic and Statistical Manual of Mental Disorders, fifth edition
DTT	Dithiothreitol
<i>E.Coli</i>	Escherichia coli
E/I	Excitation/Inhibition
E8 ,9,---	Embryonic day 8, 9, ...

EC	Entorhinal cortex
ECL	Enhanced chemiluminescence
EEG	Electroencephalogram
eIF4E	Eukaryotic translation initiation factor 4E
Eif4ebp2	Eukaryotic Translation Initiation Factor 4E Binding Protein 2
E-LTP	Early-phase long-term potentiation
ER	Endoplasmic reticulum
Er α	Estrogen receptor α
ET	Ear twitch
Ex	Exencephaly
F	Female
F_Het	Female <i>Ambra1</i> heterozygous
F_WT	Female <i>Ambra1</i> wild type
fEPSP	field excitatory postsynaptic potential
FMR1	Fragile X mental retardation 1
fT	Fetal testosterone
FV	Fiber volley
g	Gram
GABA	Gamma-Aminobutyric acid
GABA _A receptor	GABA A Receptor
GAD67	Glutamate decarboxylase 67
GC	Generalized clonus
GFAP	Glial fibrillary acidic protein
GFP	Green fluorescent protein
GWAS	Genome-wide association study
Het	Heterozygous
HFS	High frequency stimulation
hr	Hour(s)
HRP	Horseradish peroxidase
Hz	Herz
i.p.	Interaperitoneally
IBA-1	Ionized calcium binding adaptor molecule-1
IL-2	Interleukin-2
ISI	Interstimulus interval
kb	Kilo basepair
kg	Kilogram
KO	Knockout
lacZ	Bacterial β -galactosidase gene
LC3	Light chain 3
LIR	LC3-interacting region
LPP	Lateral perforant pathway
LTD	Long-term depression
LTP	Long-term potentiation
Lys	Lysine
M	Male

M	Male
M	Molar
M_Het	Male Ambra1 heterozygous
M_WT	Male Ambra1 wild type
mAChRs	Muscarinic acetylcholine receptors
mBcl-2	Mitochondrial B-cell lymphoma 2
Mecp2	Methyl-CpG binding protein 2 (Murine)
MeCP2	Methyl-CpG binding protein 2 (Human)
mg	Milligram
mg	Milligram
mGluRs	Metabotropic glutamate receptors
min	Minute(s)
ml	Milliliter
mm	Millimeter
mM	Millimolar
MPP	Medial perforant pathway
MRI	Magnetic resonance imaging
mRNA	Messenger ribonucleic acid
msec	Millisecond
msl	Male specific lethal-2
mTOR	Mammalian target of rapamycin
mTORC1	Mammalian target of rapamycin complex 1
MΩ	Mega Ohm
NeuN	Neuronal nuclei
NF1	Neurofibromin 1
NGF	Negative geotaxis reflex
NHS	Normal horse serum
NLGN3	Neuroigin 3
NLGN4X	Neuroigin 4 X-linked
NLGN4Y	Neuroigin 3 Y-linked
nm	Nanometer
NMDA	N-methyl-D-aspartate
NMDAR	NMDA receptor
NRX1	Neurexin 1
OF	Open field traversal
Olig-2	Oligodendrocyte transcription factor
P	Postnatal day
PBS	Phosphate buffered saline
PC	Partial clonus
PCR	Polymerase chain reaction
PI3KIII	Class III Phosphoinositol-3-kinase complex
pmol	Picomol
PP	Perforant pathway
PP2A	Serine/threonine protein phosphatase 2A
PPR	Paired-pulse ratio

PR	Placing response
Pten	Phosphatase and tensin homolog
PTZ	Pentylentetrazol
PV	Parvalbumin
PXP	PxPxxxR motif in AMBRA1 protein
qPCR	Quantitative polymerase chain reaction
REM	Rapid eye movement
RNA	Ribonucleic acid
ROI	Region of interest
rpm	Revolution per minute
RT	Room temperature
RT-qPCR	Quantitative reverse transcription-polymerase chain reaction
Sb	Spina bifida
SC	Schaffer collateral
Sc	Spinal cord
SDS-PAGE	Sodium dodecyl sulfate-Polyacrylamide gel electrophoresis
sec	Second(s)
SEM	Standard error of means
Shank2	SH3 and multiple ankyrin repeat domains protein 2 (Murine)
SHANK3	SH3 and multiple ankyrin repeat domains protein 3 (Human)
Shank3	SH3 and multiple ankyrin repeat domains protein 3 (Murine)
SRR	Surface righting reflex
SVZ	Sub-ventricular zone
SWD	Spike-and-wave discharge
SWI/SNF	SWItch/Sucrose Non-Fermentable complex
<i>sxl</i>	<i>Sex lethal</i>
SYN1	Synapsin 1 (Human)
T	Tesla
T	Telencephalon
TA	Temporoammonic pathway
TAE	Tris/acetate/EDTA
TBST	Tris buffered saline/Tween20
TC	Tonic-Clonic
TEMED	N,N,N',N'-Tetramethylethylenediamine
TS	Tactile startle
TSC1	Tuberous sclerosis 1 (Human)
TSC2	Tuberous sclerosis 2 (Human)
Tsc2	Tuberous sclerosis 2 (Murine)
Tween20	Polyethylene glycol (20) sorbitan monolaurate
U	Unit
Ube3a	Ubiquitin protein ligase E3A
ULK1	Unc-51-like kinase 1
USV	Ultrasound vocalization
V	Volt
VG	Fifth ganglia

WD40	Beta-transducin repeats
WS	Wire suspension
WT	Wild type
X-gal	X-galactosidase
β -gal	β -galactosidase
γ -power	Average power of gamma oscillations
μ g	Microgram
μ g	Microgram
μ m	Micrometer

7 Acknowledgement

I would like to express my thanks to all the people who made my project done successfully. First of all, I would like to express my sincere gratitude to my supervisor, Prof. Dr. Dr. Hannelore Ehrenreich for integrating me as a member of her group and giving me the opportunity to work on very interesting projects. Due to her constant support and guidance, I have developed a lot as a scientist during my PhD period.

I am sincerely grateful to my thesis committee members, Prof. Thomas Bayer, Dr. Oliver Schlüter and Dr. Kamal Chowdhury for their valuable scientific input during my progress report. I sincerely thank to Dr. Kamal Chowdhury for providing the *Ambra1* mutant mice and his support in my project.

This work would not be accomplished without the collaborators. First, and foremost, I would like to acknowledge the support of all the members in Clinical Neuroscience in MPIEM throughout the course of my PhD. I am particularly grateful to Dr. Imam Hassouna and Barbara Oliveira for cell counting in my thesis. I would like to thank to Behavior team, Dr. Ekrem Dere, Dr. Martesa Tantra, Dr. Daniela, and Anja Ronnenberg, for helping my behavior experiments.

Many amazing collaborators within MPIEM have supported my work. I sincerely thank Dr. Jeong Seop Rhee for his supervision and scientific input about electrophysiology, without which this project would be totally incomplete. I would specially like to thank to Dr. Bekir Altas, Dr. Hong Jun Rhee and Anja Günther for slice and autaptic patching which are laborious works in this project. I am grateful to Dr. Hiroshi Kawabe and Manuela Schwark who performed *in utero* electroporation in my project. Moreover, I would like to thank Albrecht Sigler who helped me establishing the conditions of spine scanning and providing me macros for analysis and supervising data analysis. I am also grateful to Dr. Dilja Krüger-Burg and Prof. Nils Brose for providing me *Nlgn4* mutant mouse line for the other project.

I also would like to express my gratitude to Prof. Jens Frahm in MPIBPC and Prof. Susann Boretius in DPZ who participated in MRI part in my thesis. Especially, I am grateful to Susann since she had to carry my mice from Göttingen to Kiel for scanning. I would like to thank Dr. Kurt Hammerschmidt in DPZ for recoding USV in my thesis.

I want to thank my friends in Göttingen for their emotional support which made my life in this city so colorful and gave me amazing memories. Last, I would like to express my deepest gratitude to my family. Without constant support and trust of my parents, I couldn't continue my academic carrier. I am also grateful to my sister, Yoanna and my brother, Yohan. I want to dedicate this work to my grandmother who loved me unconditionally and always pray for me.

8 Curriculum Vitae

Anes Ju

E-mail Ju@em.mpg.de
Address Clinical Neuroscience, Max Planck Institute of Experimental Medicine
Hermann-Rein-Straße 3, 37075, Göttingen, Germany
Date of birth 28th.Feb.1986
Place of birth Seoul, Republic of Korea
Nationality Korean

Education

2012-2016 **Ph.D.** at Georg-August-Universität Göttingen, Göttingen, Germany
Max Planck Institute of Experimental Medicine, Clinical Neuroscience
Academic Advisor : Prof. Dr. Dr. Hannelore Ehrenreich
Thesis: Characterization of *Ambra1* heterozygous mice as genetic mouse model of female-specific autism

2009-2011 **M.S.** at Catholic University of Korea, Graduate school, Seoul, South Korea
Department of Biomedical Science (Neurobiology)
Academic Advisor: Prof. Dai Jin Kim, M.D, Ph.D. (Laboratory of Addiction)
Thesis: The change of plasma ghrelin and leptin levels by the development of type 2 diabetes mellitus in the patients with alcohol dependence

2004-2009 **B.S.** in Chemistry at Seoul National University, Seoul, South Korea
Academic Advisor: Prof. Jwa-Min Nam, Ph.D.
Thesis: Eximer Formation Reaction of Pyrene

Work experience

2011-2012 Research assistant at Catholic University of Korea, Graduate school, Seoul
Department of Biomedical Science (Neurobiology)
Academic Advisor: Prof. Dai Jin Kim, M.D, Ph.D. (Laboratory of Addiction)

2008 (Jan-Feb) Intern in Seoul National University, College of Medicine, Seoul
Physiology Office
Recognition: Fourth prize for the poster presentation by Seoul National University, College of Medicine
Academic Advisor: Prof. Won Kyoung Ho, M.D, Ph.D. (Cell Signal Lab)

Awards and Honors

- 2010** Second prize for the poster presentation
The Korean Society for Research on Nicotine and Tobacco 2010
- 2008** Fourth prize for the poster presentation
Seoul National University College of Medicine 2008

Publications

Lee SS, Hong OK, **Ju A**, Kim MJ, Kim BJ, Kim SR, Kim WH, Cho NH, Kang MI, Kang SK, Kim DJ, Yoo SJ. Chronic Alcohol Consumption Results in Greater Damage to the Pancreas Than to the Liver in the Rats. *Korean J Physiol Pharmacol*. 2015 Jul;19(4):309-18.

Ju A, Hammerschmidt K, Tantra M, Krueger D, Brose N, Ehrenreich H. Juvenile manifestation of ultrasound communication deficits in the neuroligin-4 null mutant mouse model of autism. *Behav Brain Res*. 2014 Aug 15;270:159-64.

Dere E, Dahm L, Lu D, Hammerschmidt K, **Ju A**, Tantra M, Kästner A, Chowdhury K, Ehrenreich H. Heterozygous *ambra1* deficiency in mice: a genetic trait with autism-like behavior restricted to the female gender. *Front Behav Neurosci*. 2014 May 16;8:181.

Kim SJ, **Ju A**, Lim SG, Kim DJ. Chronic alcohol consumption, type 2 diabetes mellitus, insulin-like growth factor-I (IGF-I), and growth hormone (GH) in ethanol-treated diabetic rats. *Life Sci*. 2013 Nov 13;93(21):778-82.

Wojcik SM, Tantra M, Stepniak B, Man KN, Müller-Ribbe K, Begemann M, **Ju A**, Papiol S, Ronnenberg A, Gurvich A, Shin Y, Augustin I, Brose N, Ehrenreich H. Genetic markers of a Munc13 protein family member, *BAIAP3*, are gender specifically associated with anxiety and benzodiazepine abuse in mice and humans. *Mol Med*. 2013 Jul 24;19:135-48.

Lee DW, Kim SY, Lee T, Nam YK, **Ju A**, Woo DC, You SJ, Han JS, Lee SH, Choi CB, Kim SS, Shin HC, Kim HY, Kim DJ, Rhim HS, Choe BY. Ex vivo detection for chronic ethanol consumption-induced neurochemical changes in rats. *Brain Res*. 2012 Jan 6;1429:134-44.

Min JA, Lee HR, Kim JI, **Ju A**, Kim DJ, Kaang BK. Impairment of long-term potentiation in the hippocampus of alcohol-treated OLETF rats. *Neurosci Lett*. 2011 Aug 1;500(1):52-6.

Ju A, Cheon YH, Lee KS, Lee SS, Lee WY, Won WY, Park SI, Kim WH, Kim DJ. The change of plasma ghrelin and leptin levels by the development of type 2 diabetes mellitus in patients with alcohol dependence. *Alcohol Clin Exp Res*. 2011 May;35(5):905-11.

Jung KI, **Ju A**, Lee HM, Lee SS, Song CH, Won WY, Jeong JS, Hong OK, Kim JH, Kim DJ. Chronic ethanol ingestion, type 2 diabetes mellitus, and brain-derived neurotrophic factor (BDNF) in rats. *Neurosci Lett*. 2011 Jan 7;487(2):149-52.

Presentations

- Jul. 2015** 8th Euro-Korean conference on Science and Technology, Strasbourg, France
(Oral presentation)
- Nov. 2010** Korean Academy of Addiction Psychiatry, Seoul, South Korea (Poster presentation)
- Oct. 2010** Korean Biological Psychiatry, Seoul, South Korea (Poster presentation)

- Jun. 2010** Korean Society for Research on Nicotine and Tobacco, Seoul, South Korea
(Poster presentation)
- Apr. 2010** 2010 Annual Spring Meeting Korean Neuropsychiatric Association, Seoul, South Korea (Poster presentation)
- Nov. 2009** 1st Congress of Asia-Pacific Society for Alcohol and Addiction Research, Seoul, South Korea (Poster presentation)
- Nov. 2009** SfN Neuroscience 2009, Chicago, IL, USA (Poster presentation)

Teaching

- 2013/2014/2015/2016** Junior lecture at the annual interdisciplinary workshop
Translational Neuroscience, Block: Schizophrenia
- 2013** Junior lecture at the annual interdisciplinary workshop
Translational Neuroscience, Block: Multiple Sclerosis

Research Experience

- 2010-2012** Researcher position in a project supported by National Research Foundation of Korea
Title of project: Exploring the molecular targets for the treatment of nicotine dependence from the changes of neuropsychological tests and neuroendocrinal substances after smoking cessation
- 2009-2010** Researcher position in a project supported by Korea Center for Disease Control and Prevention
Title of project: Cohort Study on HCV patients with IV drug abuse
- 2009-2009** Researcher position in a project supported by Ministry of Health and Welfare, Korea
Title of project: Classification of Internet Addiction according to the behavior patterns of internet use and psychiatric comorbidity and optimization of treatment for internet addiction
- 2008-2009** Researcher position in a project supported by Korea Center for Disease Control and Prevention
Title of project: Study of the association between the alcohol and diabetes through the evaluation for the effects of diabetes incidence in alcohol-dependent patient in Korea
- Sep.2008 - Feb. 2009** Lab rotation, Seoul National University
Nanostructure Fabrication Laboratory; Prof. Doo Jeon Jang , Ph.D.
- Mar. 2008-Oct. 2008** Lab rotation, Seoul National University
Biopolymer & Medical Nanomaterials Laboratory; Prof. Jong Sang Park , Ph.D.
- Sep. 2007- Feb. 2007** Lab rotation, Seoul National University
Molecule Optics & Bioanalytical Chemistry Laboratory; Prof. Doo Soo Jung , Ph.D.

9 List of Publications

Lee SS, Hong OK, **Ju A**, Kim MJ, Kim BJ, Kim SR, Kim WH, Cho NH, Kang MI, Kang SK, Kim DJ, Yoo SJ. Chronic Alcohol Consumption Results in Greater Damage to the Pancreas Than to the Liver in the Rats. *Korean J Physiol Pharmacol*. 2015 Jul;19(4):309-18.

Ju A, Hammerschmidt K, Tantra M, Krueger D, Brose N, Ehrenreich H. Juvenile manifestation of ultrasound communication deficits in the neuroligin-4 null mutant mouse model of autism. *Behav Brain Res*. 2014 Aug 15;270:159-64.

Dere E, Dahm L, Lu D, Hammerschmidt K, **Ju A**, Tantra M, Kästner A, Chowdhury K, Ehrenreich H. Heterozygous *ambra1* deficiency in mice: a genetic trait with autism-like behavior restricted to the female gender. *Front Behav Neurosci*. 2014 May 16;8:181.

Kim SJ, **Ju A**, Lim SG, Kim DJ. Chronic alcohol consumption, type 2 diabetes mellitus, insulin-like growth factor-I (IGF-I), and growth hormone (GH) in ethanol-treated diabetic rats. *Life Sci*. 2013 Nov 13;93(21):778-82.

Wojcik SM, Tantra M, Stepniak B, Man KN, Müller-Ribbe K, Begemann M, **Ju A**, Papiol S, Ronnenberg A, Gurvich A, Shin Y, Augustin I, Brose N, Ehrenreich H. Genetic markers of a Munc13 protein family member, *BAIAP3*, are gender specifically associated with anxiety and benzodiazepine abuse in mice and humans. *Mol Med*. 2013 Jul 24;19:135-48.

Lee DW, Kim SY, Lee T, Nam YK, **Ju A**, Woo DC, You SJ, Han JS, Lee SH, Choi CB, Kim SS, Shin HC, Kim HY, Kim DJ, Rhim HS, Choe BY. Ex vivo detection for chronic ethanol consumption-induced neurochemical changes in rats. *Brain Res*. 2012 Jan 6;1429:134-44.

Min JA, Lee HR, Kim JI, **Ju A**, Kim DJ, Kaang BK. Impairment of long-term potentiation in the hippocampus of alcohol-treated OLETF rats. *Neurosci Lett*. 2011 Aug 1;500(1):52-6.

Ju A, Cheon YH, Lee KS, Lee SS, Lee WY, Won WY, Park SI, Kim WH, Kim DJ. The change of plasma ghrelin and leptin levels by the development of type 2 diabetes mellitus in patients with alcohol dependence. *Alcohol Clin Exp Res*. 2011 May;35(5):905-11.

Jung KI, **Ju A**, Lee HM, Lee SS, Song CH, Won WY, Jeong JS, Hong OK, Kim JH, Kim DJ. Chronic ethanol ingestion, type 2 diabetes mellitus, and brain-derived neurotrophic factor (BDNF) in rats. *Neurosci Lett*. 2011 Jan 7;487(2):149-52.